Title (117 characters): **Transmission of West Nile and other temperate mosquito-borne viruses peaks at intermediate environmental temperatures**

Marta S. Shocket[1,2*] (mshocket@stanford.edu), Anna B. Verwillow[1] (anna19@stanford.edu), Mailo G. Numazu[1] (mnumazu@stanford.edu), Hani Slamani[3] (hanis1@vt.edu), Jeremy M. Cohen[4,5] (jcohen39@wisc.edu), Fadoua El Moustaid[6] (fadoua@vt.edu), Jason Rohr[4,7] (jasonrohr@gmail.com), Leah R. Johnson[3,6] (lrjohn@vt.edu), and Erin A. Mordecai[1] (emordeca@stanford.edu)

[1]Department of Biology, Stanford University, Stanford, CA, USA

[2]Department of Ecology and Evolutionary Biology, University of California Los Angeles, Los Angeles, CA, USA

[3]Department of Statistics, Virginia Polytechnic Institute and State University (Virginia Tech), Blacksburg, Virginia, USA

[4]Department of Integrative Biology, University of South Florida, Tampa, FL, USA

[5]Department of Forest and Wildlife Ecology, University of Wisconsin, Madison, WI, USA

[6]Department of Biological Sciences, Virginia Polytechnic Institute and State University (Virginia Tech), Blacksburg, Virginia, USA

[7]Department of Biological Sciences, Eck Institute of Global Health, Environmental Change Initiative, University of Notre Dame, South Bend, IN, USA

Keywords: *Culex pipiens*, *Culex tarsalis*, *Culex quinquefasciatus*, West Nile virus, Western Equine Encephalitis virus, Eastern Equine encephalitis virus, St. Louis Encephalitis virus, Rift Valley Fever virus, Sindbis virus, Ockelbo disease, mosquito-borne disease, infectious disease,

temperature

* Corresponding Author: Marta S. Shocket, mshocket@stanford.edu, phone: 650-723-5923

Availability of data and material: Upon acceptance, all data and code will be submitted to Dryad repository and the appropriate web link will be listed here for publication.

Authors' contributions: EAM, LRJ, and MSS conceived of and designed the study. MN, AV, HS, FEM, and MSS collected trait data. MN and MSS fit models. JC compiled West Nile virus case data and climate data. JC and MSS analyzed West Nile virus case data. MSS wrote the first draft of the manuscript. All authors revised and approved the manuscript.

ABSTRACT (150 WORDS = LIMIT)

The temperature-dependence of many important mosquito-borne diseases has never been quantified. These relationships are critical for understanding current distributions and predicting future shifts from climate change. We used trait-based models to characterize temperature-dependent transmission of 10 vector–pathogen pairs of mosquitoes (*Culex pipiens*, *Cx. quinquefascsiatus*, *Cx. tarsalis*, and others) and viruses (West Nile, Eastern and Western Equine Encephalitis, St. Louis Encephalitis, Sindbis, and Rift Valley Fever viruses), most with substantial transmission in temperate regions. Transmission is optimized at intermediate temperatures (23–26ºC) and often has wider thermal breadths (due to cooler lower thermal limits) compared to pathogens with predominately tropical distributions (in previous studies). The incidence of human West Nile virus cases across US counties responded unimodally to average summer temperature and peaked at 24ºC, matching model-predicted optima (24–25ºC). Climate warming will likely shift transmission of these diseases, increasing it in cooler locations while decreasing it in warmer locations.

INTRODUCTION

Temperature is a key driver of transmission of mosquito-borne diseases because the mosquitoes and pathogens are ectotherms whose physiology and life histories depend strongly on environmental temperature [1–8]. These temperature-dependent traits drive the biological processes required for transmission. For example, temperature-dependent fecundity, development, and mortality of mosquitoes determine whether vectors are present in sufficient numbers for transmission. Temperature also affects the mosquito biting rate on hosts and probability of becoming infectious.

Mechanistic models based on these traits and guided by principles of thermal biology predict that the thermal response of transmission is unimodal: transmission peaks at intermediate temperatures and declines at extreme cold and hot temperatures [2–12]. This unimodal response is predicted consistently across mosquito-borne diseases [2–8] and supported by independent empirical evidence for positive relationships between temperature and human cases in many settings [5,13–16], but negative relationships at extremely high temperatures in other studies [2,16–19]. Accordingly, we expect increasing temperatures due to climate change to shift disease distributions geographically and seasonally, as warming increases transmission in cooler settings but decreases it in settings near or above the optimal temperature for transmission [20–23]. Thus, mechanistic models have provided a powerful and general rule describing how temperature affects the transmission of mosquito-borne disease. However, thermal responses vary among mosquito and pathogen species and drive important differences in how predicted transmission responds to temperature, including the specific temperatures of the optimum and thermal limits for each vector–pathogen pair [2–7]. We currently lack a framework to describe or predict this variation among vectors and pathogens.

70 Filling this gap requires comparing mechanistic, temperature-dependent transmission
71 models for many vector–pathogen pairs. However, models that incorporate all relevant traits are
72 not yet available for many important pairs for several reasons. First, the number of relevant
73 vector–pathogen pairs is large because many mosquitoes transmit multiple pathogens and many
74 pathogens are transmitted by multiple vectors. Second, empirical data are costly to produce, and
75 existing data are often insufficient because experiments or data reporting were not designed for
76 this purpose. Here, we address these challenges by systematically compiling data and building
77 models for understudied mosquito-borne disease systems, including important pathogens with
78 substantial transmission in temperate areas like West Nile virus (WNV) and Eastern Equine
79 Encephalitis virus (EEEV). Accurately characterizing the thermal limits and optima for these
80 systems is critical for understanding where and when temperature currently promotes or
81 suppresses transmission and where and when climate change will increase, decrease, or have
82 minimal effects on transmission.
83 In this study, we model the effects of temperature on an overlapping suite of widespread,
84 important mosquito vectors and viruses that currently lack complete temperature-dependent
85 models. These viruses include: West Nile virus (WNV), St. Louis Encephalitis virus (SLEV),
86 Eastern and Western Equine Encephalitis viruses (EEEV and WEEV), Sindbis virus (SINV), and
87 Rift Valley fever virus (RVFV) [24–28] (summarized in Table 1). All but RVFV sustain
88 substantial transmission in temperate regions [24–28]. We selected this group because many of
89 the viruses share common vector species and several vector species transmit multiple viruses
90 (Table 1, Fig 1). All the viruses cause febrile illness and severe disease symptoms, including
91 long-term arthralgia and neuroinvasive syndromes with a substantial risk of mortality in severe
92 cases [24–28]. Since invading North America in 1999, WNV is now distributed worldwide

93 [21,24] and is the most common mosquito-borne disease in the US, Canada, and Europe. SLEV,
94 EEEV, and WEEV occur in the Western hemisphere (Table 1), with cases in North, Central, and
95 South America [28–30]. For EEEV, the North American strains are genetically distinct and more
96 virulent than the Central and South American strains [28]. An unusually large outbreak of EEEV
97 in the United States last year (2019) has yielded incidence four times higher than average (31
98 cases, resulting in 9 fatalities) and brought renewed attention to this disease [31]. SINV occurs
99 across Europe, Africa, Asia, and Australia, with substantial transmission in northern Europe and
100 southern Africa [26,28]. RVFV originated in eastern Africa and now also occurs across Africa
101 and the Middle East [27]. These pathogens primarily circulate and amplify in wild bird reservoir
102 hosts (except RVFV, which primarily circulates in livestock). For all six viruses, humans are
103 dead-end or unimportant reservoir hosts [28,32], in contrast to pathogens like malaria, dengue
104 virus, yellow fever virus, and Ross River virus, which sustain infection cycles between humans
105 and mosquitoes [28,33,34]. Most transmission of RVFV to humans occurs through direct contact
106 with infected livestock (that are infected by mosquitoes), and to a lesser extent via the mosquito-
107 borne transmission from infected vectors [32].

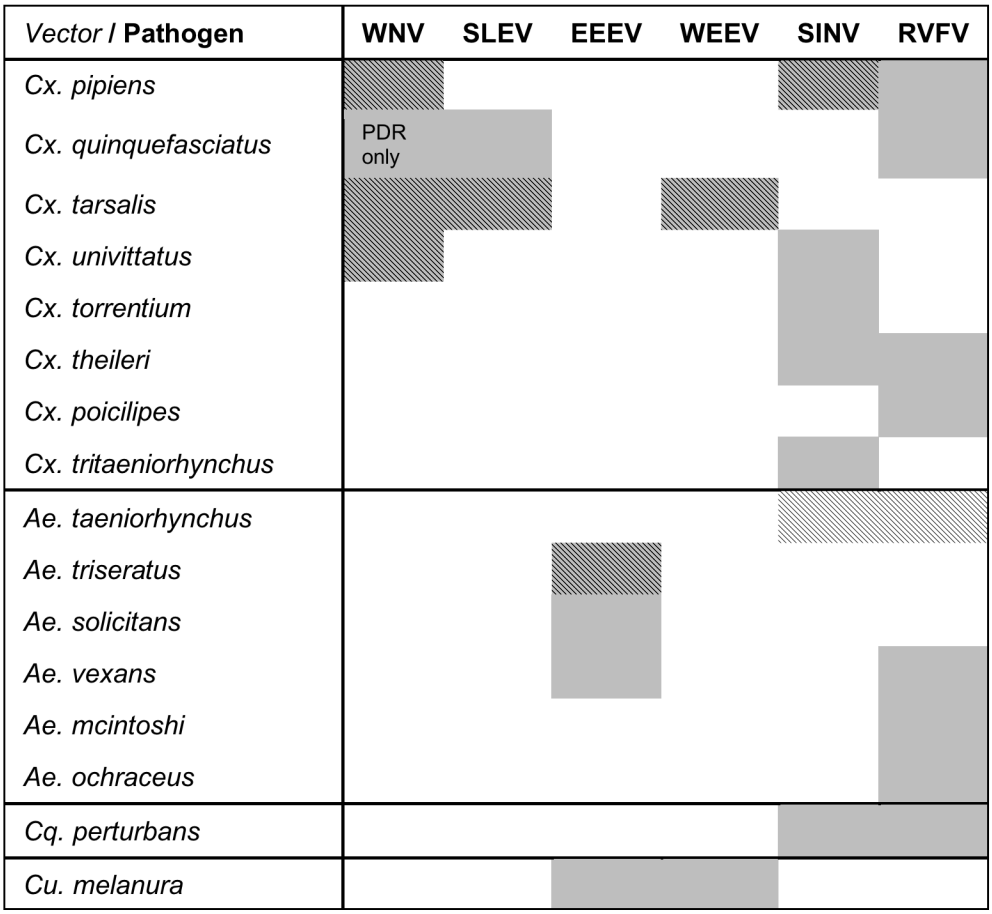

Figure 1: Viruses transmitted by a community of vectors. The six viruses in this study (WNV = West Nile virus, SLEV = St. Louis Encephalitis virus, EEEV = Eastern Equine Encephalitis virus, WEEV = Western Equine Encephalitis virus, SINV = Sindbis virus, RVFV = Rift Valley Fever virus) and the *Culex* (*Cx.*), *Aedes* (*Ae.*), *Coquillettidia* (*Cq.*), and *Culiseta* (*Cs.*) vectors that are important for sustaining transmission to humans. Grey shading indicates an important vector-virus pair; hatching indicates available temperature-dependent data for infection traits (parasite development rate [*PDR*] and vector competence [*bc* or *b* and *c*]). The importance of each vector for transmission may vary over the geographic range of the virus. Infection data were available for SINV and RVFV in *Ae. taeniorhynchus*, although this North American mosquito does not occur in the endemic range of these pathogens. Data sources: [25–27,32,76].

TABLE 1:

Virus (*genus*)	Primary vector spp.	Geographic range	Presentation & mortality	Epidemiology & Ecology
West Nile virus (WNV, *Flavivirus*)	*Cx. pipiens*, *Cx. quinquefasciatus*, *Cx. tarsalis*	Globally distributed	Febrile illness and encephalitis. 10% mortality in neuro-invasive cases. Long-term physical & cognitive disabilities.	The most common mosquito-borne disease in North America. Since invading in 1999, 7 million estimated infections, 22,999 neuro-invasive cases, and 2,163 deaths in US; 5,614 reported cases in Canada. Typically 100-300 cases annually in Europe, but over 1500 in 2018. Poor surveillance in Africa, but seroprevalence ~80% in some areas. Birds are main reservoir/amplification hosts.
St. Louis Encephalitis virus (SLEV, *Flavivirus*)	*Cx. quinquefasciatus*, *Cx. tarsalis*	Western hemisphere; western, midwestern, & southern US	Encephalitis. 5-15% mortality in diagnosed cases.	92 cases and 6 deaths recorded in US from 2009-2018. Birds are main reservoir/amplification hosts.
Eastern Equine Encephalitis virus (EEEV, *Alphavirus*)	*Ae. triseriatus*, *Cs. melanura*	Western hemisphere; eastern & midwestern US	Febrile illness and encephalitis. 33% mortality in diagnosed cases. Long-term cognitive disabilities.	73 cases and 30 deaths recorded in US from 2009-2018. Birds are main reservoir/amplification hosts.
Western Equine Encephalitis virus (WEEV, *Alphavirus*)	*Cx. tarsalis*	Western hemisphere; western & midwestern US	Febrile illness and encephalitis. Low mortality, except in infants.	The CDC does not report WEEV infection. Birds are main reservoir/amplification hosts. WEEV is derived from a recombinant event between the ancestors of EEEV and SINV.
Sindbis virus (SINV, *Alphavirus*), also called Pogosta, Ockelbo, & Karelian Fever	*Cx. torrentium*, *Cx. pipiens, Cx. univittatus*	Europe, Africa, Asia & Australia, primarily northern Europe & southern Africa	Febrile illness, rash, and joint pain. No mortality, but long-term disability.	Poor surveillance except in Finland, where annual incidence is 2–26 per 100,000 people and seroprevalence can reach ~40%. Birds are main reservoir/amplification hosts. Long-distance migratory birds may spread the virus between temperate zones in Northern and Southern hemispheres.
Rift Valley Fever virus (RVFV, *Phlebovirus*)	*Ae. mcintoshi, Ae. ochraceus, Ae. vexans, Cx. pipiens, Cx. poicilipes, Cx. theileri* and many more	Africa & the Middle East	Febrile illness and encephalitis. <1% mortality in total cases. 50% mortality in hemorrhagic cases, permanent blindness in 50% of ocular cases (<2% of cases).	Livestock are main reservoir/amplification hosts, and suffer mortality and abortion after being infected by mosquitoes. Most transmission to humans occurs via direct contact with infected livestock. Vertical transmission in vectors (via dormant eggs) can initiate epidemics. In eastern and southern Africa, there are large epidemics every 5-15 years driven by rainfall and blooms of *Ae. spp*. from low-lying flooded areas known as *dambos*.

Table 1: Properties of six viruses transmitted by an overlapping network of mosquito vectors. Sources: WNV [24,25,140,147–150]; SLEV [25,29]; EEEV [25,30]; WEEV [25]; SINV [26]; RVFV [27,32,76,151].

We primarily focus on *Culex pipiens*, *Cx. quinquefasciatus*, and *Cx. tarsalis*, well-studied species that are important vectors for many of the viruses and for which appropriate temperature-dependent data exist for nearly all traits relevant to transmission. Although the closely-related *Cx. pipiens* and *Cx. quinquefasciatus* overlap in their home ranges in Africa, they have expanded into distinct regions globally (Fig 2) [35]. *Cx. pipiens* occurs in higher-latitude temperate areas in the Northern and Southern hemisphere, while *Cx. quinquefasciatus* occurs in lower-latitude temperate and tropical areas (Fig 2A). By contrast, *Cx. tarsalis* is limited to North America but spans the tropical-temperate gradient (Fig 2B). In this system of shared pathogens and vectors with distinct geographical distributions, we also test the hypothesis that differences in thermal performance underlie variation in vector and pathogen geographic distributions, since temperate environments have cooler temperatures and a broader range of temperatures than tropical environments. We also include thermal responses from other relevant vector or laboratory model species in some models: *Aedes taeniorhynchus* (SINV and RVFV), *Ae. triseriatus* (EEEV), *Ae. vexans* (RVFV), *Cx. theileri* (RVFV), and *Culiseta melanura* (EEEV). Additionally, we compare our results to previously published models [2–4,6,7] for transmission of more tropical diseases by the following vectors: *Ae. aegypti*, *Ae. albopictus*, *Anopheles* spp., and *Cx. annulirostris*.

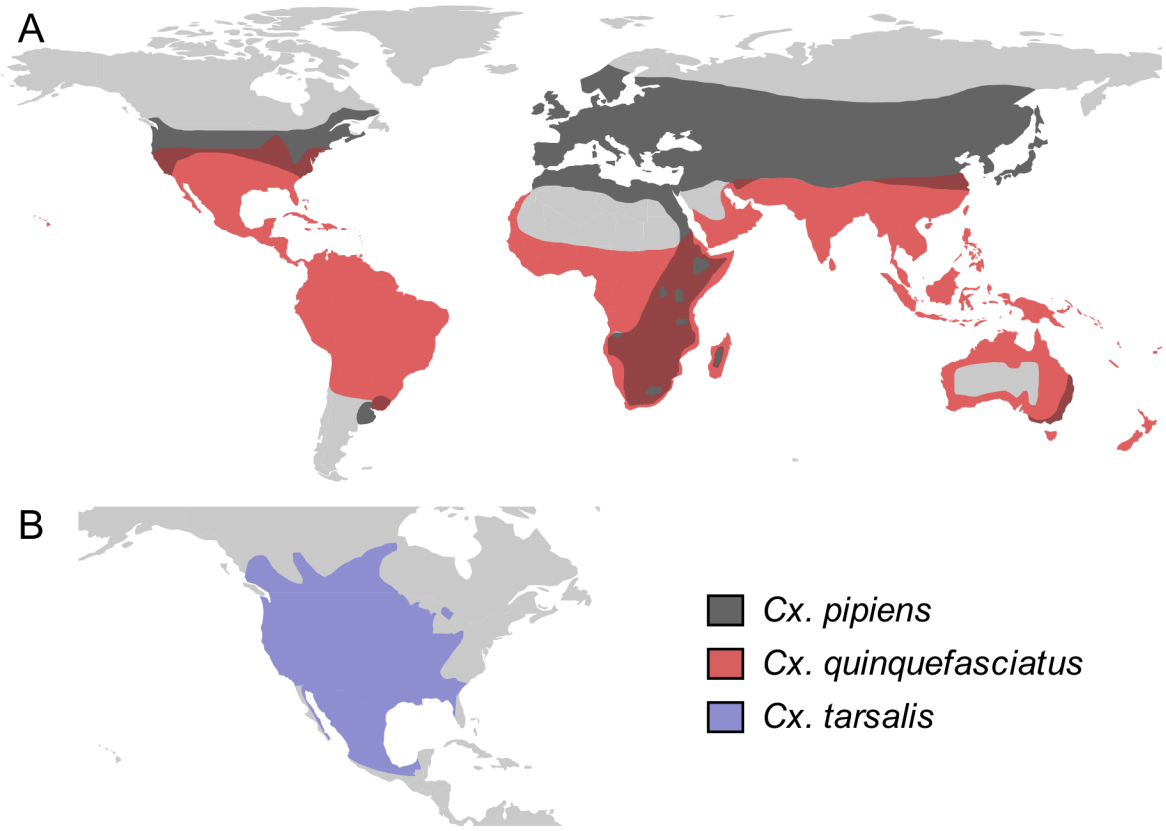

139

140 **Figure 2: *Culex* spp. vectors of West Nile and other viruses have distinct but overlapping**
141 **geographic distributions.** The geographic distribution of the primary vectors of West Nile
142 virus: (A) *Culex pipiens* (dark grey) and *Cx. quinquefasciatus* (red), adapted from [35,83]; (B)
143 *Cx. tarsalis* (blue), northern boundary from [84], southern boundary based on data from the
144 Global Biodiversity Information Facility. Figure created by Michelle Evans for this paper.
145

146 We use a mechanistic approach to characterize the effects of temperature on vector–virus
147 pairs in this network using the thermal responses of traits that drive transmission. Specifically,
148 we use experimental data to measure the thermal responses of the following traits: vector
149 survival, biting rate, fecundity, development rate, competence for acquiring and transmitting
150 each virus, and the extrinsic incubation rate of the virus within the vector. We ask: (1) Do these
151 vectors have qualitatively similar trait thermal responses to each other, and to vectors from

152 previous studies? (2) Is transmission of disease by these vectors predicted to be optimized and
153 limited at similar temperatures, compared to each other and to other mosquito-borne diseases in
154 previous studies? (3) How do the thermal responses of transmission vary across vectors that
155 transmit the same virus and across viruses that share a vector? (4) Which traits limit transmission
156 at low, intermediate, and high temperatures? Broadly, we hypothesize that variation in thermal
157 responses is predictable based on vectors' and viruses' geographic ranges.

158 Mechanistic models allow us to incorporate nonlinear effects of temperature on multiple
159 traits, measured in controlled laboratory experiments across a wide thermal gradient, to
160 understand their combined effect on disease transmission. This approach is critical when making
161 predictions for future climate regimes because thermal responses are almost always nonlinear,
162 and therefore current temperature–transmission relationships may not extend into temperatures
163 beyond those currently observed in the field. We use Bayesian inference to quantify uncertainty
164 and to rigorously incorporate prior knowledge of mosquito thermal physiology to constrain
165 uncertainty when data are sparse [3]. The mechanistic modeling approach also provides an
166 independently-generated, *a priori* prediction for the relationship between temperature and
167 transmission to test with observational field data on human cases, allowing us to connect data
168 across scales, from individual-level laboratory experiments, to population-level patterns of
169 disease transmission, to climate-driven geographic variation across populations. Using this
170 approach, we build mechanistic models for 10 vector–virus pairs by estimating thermal
171 responses of the traits that drive transmission. We validate the models using observations of
172 human cases in the US over space (county-level) and time (month-of-onset). The validation
173 focuses on WNV because it is the most common of the diseases we investigated and has the most
174 complete temperature-dependent trait data.

175 **MODEL OVERVIEW**

176 To understand the effect of temperature on transmission and to compare the responses
177 across vector and virus species, we used R_0—the basic reproduction number [36]. We use R_0 as a
178 static, relative metric of temperature suitability for transmission that incorporates the nonlinear
179 effects of temperature on multiple traits [1,8,37] and is comparable across systems, rather than
180 focusing on its more traditional interpretation as a threshold for disease invasion into a
181 susceptible population. Temperature variation creates additional nonlinear effects on
182 transmission [38–41] that are not well-captured by R_0, [10,36,42–44] but could be incorporated
183 in future work by integrating the thermal performance curves fit here over the observed
184 temperature regime.

185 The basic R_0 model (eq. 1) [37] includes the following traits that depend on temperature
186 (T): adult mosquito mortality (μ, the inverse of lifespan [*lf*]), biting rate (a, proportional to the
187 inverse of the gonotrophic [oviposition] cycle duration), pathogen development rate (PDR, the
188 inverse of the extrinsic incubation period: the time required for exposed mosquitoes to become
189 infectious), and vector competence (bc, the proportion of exposed mosquitoes that become
190 infectious). Vector competence is the product of infection efficiency (c, the proportion of
191 exposed mosquitoes that develop a disseminated infection) and transmission efficiency (b, the
192 proportion of infected mosquitoes that become infectious, with virus present in saliva). Three
193 parameters do not depend on temperature: mosquito density (M), human density (N), the rate at
194 which infected hosts recover and become immune (r).

195 Basic R_0: $$R_0(T) = \left(\frac{a(T)^2 bc(T) e^{-\frac{\mu(T)}{PDR(T)}} M}{N\, r\, \mu(T)} \right)^{1/2} \quad \text{eq. 1}$$

196 As in previous work [2–4,6–8,10], we extend the basic R_0 model to account for the effects of
197 temperature on mosquito density (*M*) via additional temperature-sensitive life history traits (eq.
198 2): fecundity (as eggs per female per day, *EFD*), egg viability (proportion of eggs hatching into
199 larvae, *EV*), proportion of larvae surviving to adulthood (*pLA*), and mosquito development rate
200 (*MDR*, the inverse of the development period).

201 Full R_0: $$R_0(T) = \left(\frac{a(T)^2 bc(T) e^{-\frac{\mu(T)}{PDR(T)}} EFD(T) EV(T) pLA(T) MDR(T)}{N\, r\, \mu(T)^3} \right)^{1/2} \quad \text{eq. 2}$$

202 Fecundity data were only available as eggs per female per gonotrophic cycle (*EFGC*; for Cx.
203 *pipiens*) or eggs per raft (*ER*; for Cx. *quinquefasciatus*). Thus, we further modified the model to
204 obtain the appropriate units for fecundity: we added an additional biting rate term to the model
205 (to divide by the length of the gonotrophic cycle, eqs. S1 and S2) and for *Cx. quinquefasciatus*
206 we also added a term for the proportion of females ovipositing (*pO*; eq. S2).

207 We parameterized a temperature-dependent R_0 model for each relevant vector–virus pair
208 using previously published data. We conducted a literature survey to identify studies that
209 measured the focal traits at three or more constant temperatures in a controlled laboratory
210 experiment. From these data, we fit thermal responses for each trait using Bayesian inference.
211 This approach allowed us to quantify uncertainty and formally incorporate prior data [3] to
212 constrain fits when data for the focal species were sparse or only measured on a limited portion
213 of the temperature range (see *Material and Methods* for details).

214 For each combination of trait and species, we selected the most appropriate of three
215 functional forms for the thermal response. As in previous work [2–4,6–8], we fit traits with a
216 symmetrical unimodal thermal response with a quadratic function (eq. 3) and traits with an
217 asymmetrical unimodal thermal response with a Briére function [45] (eq. 4). For some

218 asymmetrical responses (e.g., *PDR* for most vector–virus pairs), we did not directly observe a
219 decrease in trait values at high temperatures due to a limited temperature range. In these cases,
220 we chose to fit a Briére function based on previous studies with wider temperature ranges [2,4–6]
221 and thermal biology theory [46]; the upper thermal limit for these fits did not limit transmission
222 in the R_0 models, and therefore did not impact the results. Unlike in previous work, lifespan data
223 for all vectors here exhibited a monotonically decreasing thermal response over the range of
224 experimental temperatures available. We fit these data using a linear function (eq. 5) that
225 plateaued at coldest observed data point to be conservative. To overwinter, *Cx. pipiens* and *Cx.*
226 *tarsalis* enter reproductive diapause and hibernate [47,48], and *Cx. pipiens* can survive
227 temperatures at or near freezing (0ºC) for several months [47]. *Cx. quinquefasciatus* enters a
228 non-diapause quiescent state [48,49] and is likely less tolerant of cold stress, but we wanted a
229 consistent approach across models and other traits constrained the lower thermal limit of the *Cx.*
230 *quinquefasciatus* R_0 model to realistic temperatures.

231 Quadratic function: $f(T) = -q(T - T_{min})(T - T_{max})$ eq. 3

232 Briére function: $f(T) = q \cdot T(T - T_{min})\sqrt{(T_{max} - T)}$ eq. 4

233 Linear function: $f(T) = -mT + \mathrm{z}$ eq. 5

234 In the quadratic and Briére functions of temperature (T), the trait values depend on a lower
235 thermal limit (T_{min}), an upper thermal limit (T_{max}), and a scaling coefficient (q). In the linear
236 function, the trait values depend on a slope (m) and intercept (z).

237 The fitting via Bayesian inference produced posterior distributions for each parameter in
238 the thermal response functions (eqs. 3–5) for each trait-species combination. These posterior
239 distributions represent the estimated uncertainty in the parameters. We used these parameter
240 distributions to calculate distributions of expected mean functions for each trait over a

241 temperature gradient (from 1–45ºC by 0.1ºC increments). Then we substituted these samples
242 from the distributions of the mean thermal responses for each trait into eq. 2 to calculate the
243 posterior distributions of predicted R_0 over this same temperature gradient for each vector–virus
244 pair (see *Material and Methods* and S1 Text for details). Thus, the estimated uncertainty in the
245 thermal response of each trait is propagated through to R_0 and combined to produce the estimated
246 response of R_0 to temperature, including the uncertainty in $R_0(T)$.
247 Because the magnitude of realized R_0 depends on system-specific factors like breeding
248 habitat availability, reservoir and human host availability, vector control, species interactions,
249 and additional climate factors, we focused on the relative relationship between R_0 and
250 temperature [8]. We rescaled the R_0 model results to range from 0 to 1 (i.e., 'relative R_0'),
251 preserving the temperature-dependence (including the absolute thermal limits and thermal
252 optima) while making each model span the same scale. To compare trait responses and R_0
253 models, we quantify three key temperature values: the optimal temperature for transmission
254 (T_{opt}) and the lower and upper thermal limits (T_{min} and T_{max}, respectively) where temperature is
255 predicted to prohibit transmission ($R_0 = 0$).
256

257 **RESULTS**

258 *Trait thermal responses*

259 We fit thermal response functions from empirical data for most of the vector and virus
260 traits that affect transmission (Table S1 and Fig 1). All mosquito traits were temperature-
261 sensitive (three main *Culex* species: Fig 3, Fig 4; *Ae. taeniorhynchus*, *Ae. triseriatus*, *Ae. vexans*,
262 *Cx. theileri*, and *Culiseta melanura*: Fig S1). For most species, the extensive data for larval traits
263 (mosquito development rate [MDR] and survival [*pLA*]) produced clear unimodal thermal

264 responses with relatively low uncertainty (Fig 3A,B, Fig S1A,B). For biting rate (*a*) and
265 fecundity traits (*pO*, *EFGC, ER*, *EV*), trait data were often more limited and fits were more
266 uncertain, but still consistent with the expected unimodal thermal responses based on previous
267 studies [2,4–6] and theory [46] (Fig 3C, Fig 4, Fig S1C-F). However, adult lifespan (*lf*) data
268 clearly contrasted with expectations from previous studies of more tropical mosquitoes. Lifespan
269 decreased linearly over the entire temperature range of available data (coldest treatments: 14–
270 16ºC, Fig 3D; 22ºC, Fig S1D) instead of peaking at intermediate temperatures (e.g., previously
271 published optima for more tropical species: 22.2–23.4ºC) [2–4,6,7].

272 In general, the adult mosquito traits (biting rate, lifespan, and fecundity [*a*, *lf*, *pO*, *EFGC,*
273 *ER*, *EV*]) varied more among species than the larval traits (development rate and survival [*MDR*
274 and *pLA*]), although the high degree of uncertainty resulted in overlapping 95% credible intervals
275 (CIs) between species for most traits (Fig 3, Fig 4, Fig S1), with two exceptions. First, the
276 thermal response for lifespan (*lf*) for *Cx. tarsalis* was significantly less steep than the response
277 for *Cx. pipiens* (Fig 3D; 95% CIs for slope coefficients: *Cx. tarsalis* = 1.12–2.24, *Cx. pipiens* =
278 3.83–5.84). Second, the symmetry of the unimodal functional form was generally consistent for
279 each trait across species, with the exceptions that the thermal responses for the proportion
280 ovipositing (*pO*) and egg viability (*EV*) were symmetrical for *Cx. pipiens* and asymmetrical for
281 *Cx. quinquefasciatus* (Fig 4 A,C). The lifespan pattern (thermal response of *Cx. tarsalis* less
282 steep than *Cx. pipiens*) did not match any *a priori* prediction, but the differences for *pO* and EV
283 matched predictions based on the geographic ranges of the vectors: lower-latitude *Cx.*
284 *quinquefasciatus* performed better at warmer temperatures for *pO* (Fig 3A), and higher-latitude

285 *Cx. pipiens* performed better at cooler temperatures for *EV* (Fig 3C).

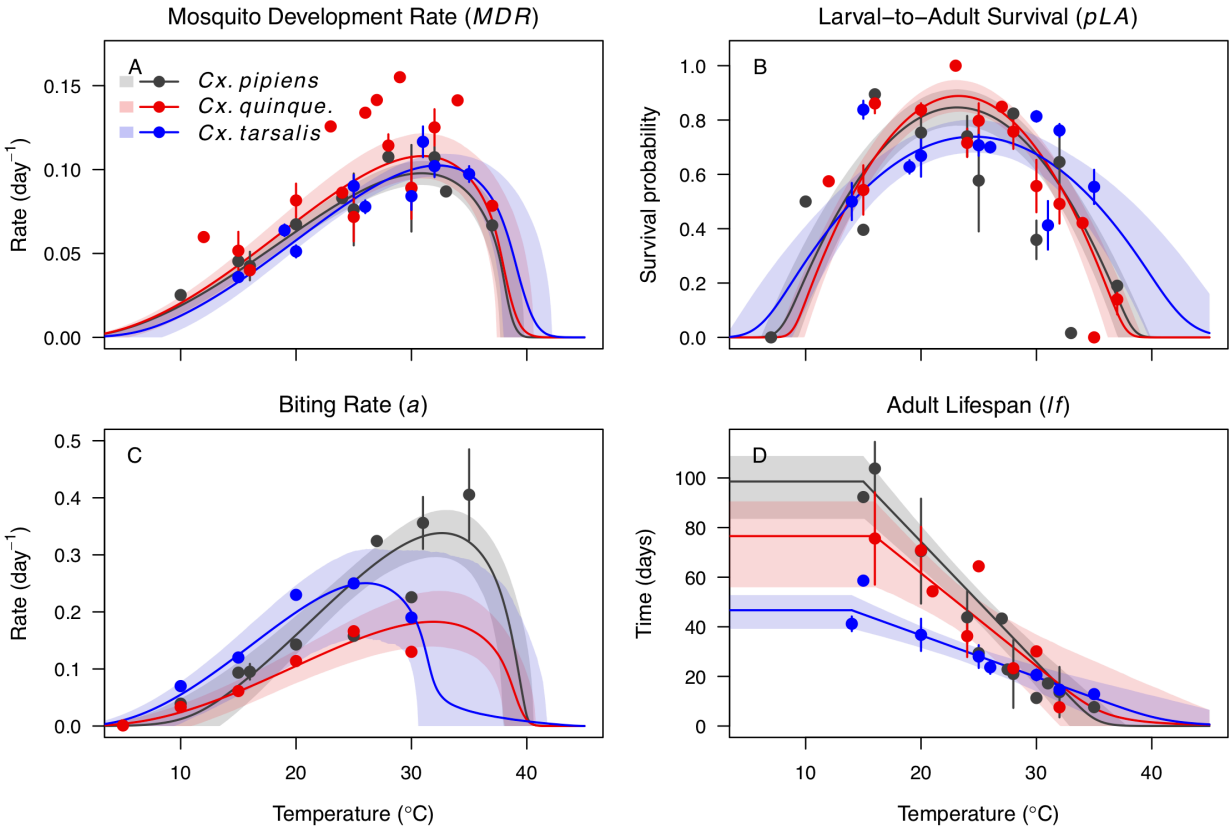

286

287 **Figure 3: *Culex* spp. mosquito traits respond strongly and consistently to temperature.** The
288 thermal responses of mosquito traits for the North American vectors of West Nile virus: *Culex*
289 *pipiens* (dark grey), *Cx. quinquefasciatus* (red), and *Cx. tarsalis* (blue). (A) Mosquito
290 development rate (*MDR*), (B) larval-to-adult survival (*pLA*), (C) biting rate (*a*), and (D) adult
291 lifespan (*lf*). Points without error bars are reported means from single studies; points with error
292 bars are averages of means from multiple studies (+/- standard error, for visual clarity only;
293 thermal responses were fit to reported means, see Figs S2–5). Solid lines are posterior means;
294 shaded areas are 95% credible intervals of the trait mean. See Fig S1 for thermal responses for
295 *Aedes taeniorhynchus*, *Aedes triseriatus*, *Ae. vexans*, *Culiseta melanura*.

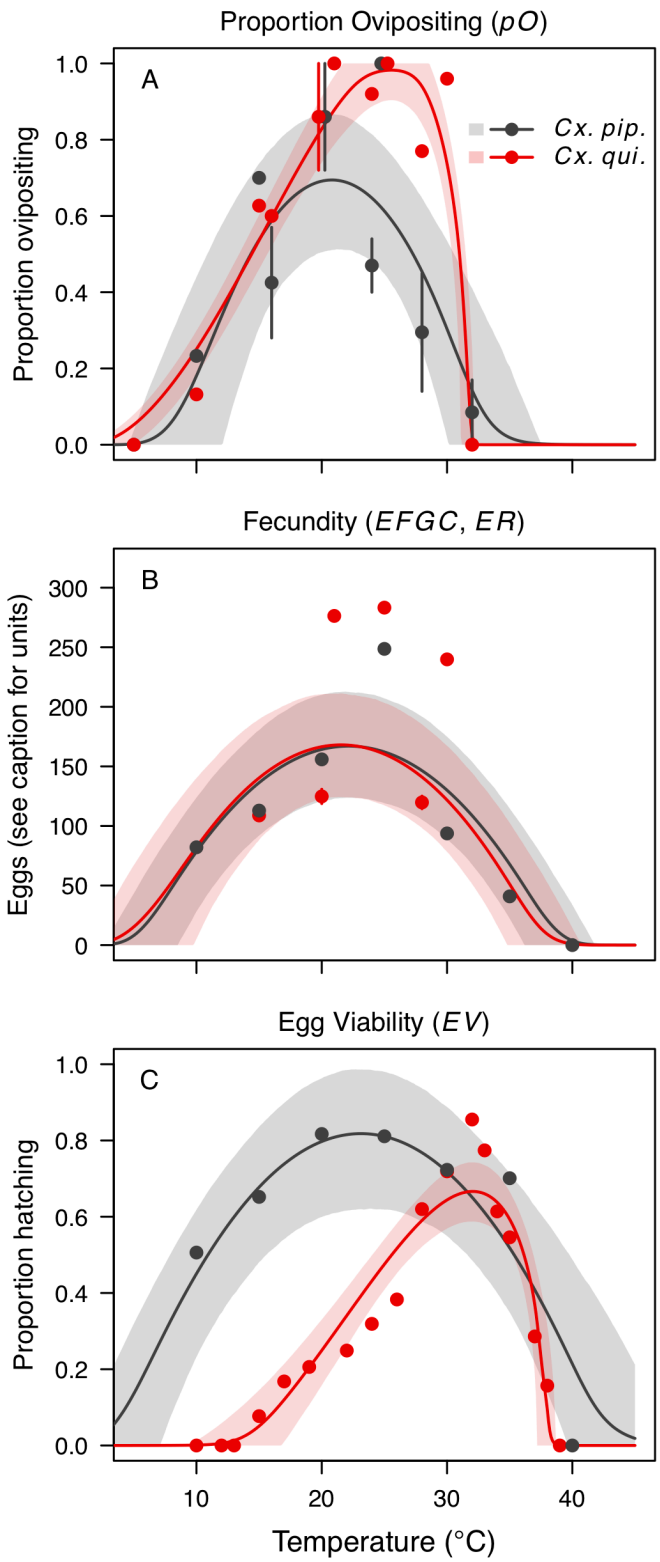

Figure 4: *Culex pipiens* and *Cx. quinquefasciatus* fecundity traits respond strongly to temperature but with different functional forms. The thermal responses of mosquito traits for the primary vectors of West Nile virus: *Culex pipiens* (dark grey) and *Cx. quinquefasciatus* (red). (A) Proportion ovipositing (*pO*), (B) fecundity (eggs per female per gonotrophic cycle, *EFGC,* or eggs per raft, *ER*), and (C) egg viability (*EV*). Points without error bars are reported means from single studies; points with error bars are averages of means from multiple studies (+/- standard error, for visual clarity only; thermal responses were fit to reported means, see Fig S6). Solid lines are posterior distribution means; shaded areas are 95% credible intervals of the trait mean. See Fig S1 for thermal responses for *Ae. vexans*, *Cx. theileri*, and *Culiseta melanura*.

The thermal responses for pathogen development rate were similar among most vector–virus pairs (Fig 5), with a few notable exceptions: WNV in *Cx. quinquefasciatus* had a warmer lower thermal limit (Fig 5A); WNV in *Cx. univittatus* had a cooler optimum and upper thermal limit (Fig 5A); and SINV in *Ae. taeniorhynchus* had limited data that indicated very little response to temperature (Fig 5C). By contrast, the thermal response of vector competence varied substantially across vectors and viruses (Fig 6). For example, infection efficiency (*c*) of *Cx. pipiens* peaked at warmer temperatures for WNV than for SINV (Fig 6A,G; 95% CIs: SINV = 14.1–30.5ºC, WNV = 31.9–36.1ºC), transmission efficiency (*b*) of *Cx. tarsalis* peaked at warmer temperatures for WNV and SLEV than for WEEV (Fig 6B,E,H; CIs: WEEV = 19.2–23.2ºC, SLEV = 23.5–29.7ºC, WNV = 23.9–29.3ºC), and the lower thermal limit for vector competence (*bc*) for WNV was much warmer in *Cx. pipiens* than in *Cx. univittatus* (Fig 6C; CIs: *Cx. univittatus* = 1.5–7.1ºC, *Cx. pipiens* = 15.0–17.9ºC). Infection data for RVFV were only available in *Ae. taeniorhynchus*, a New World species that is not a known vector for the virus in nature.

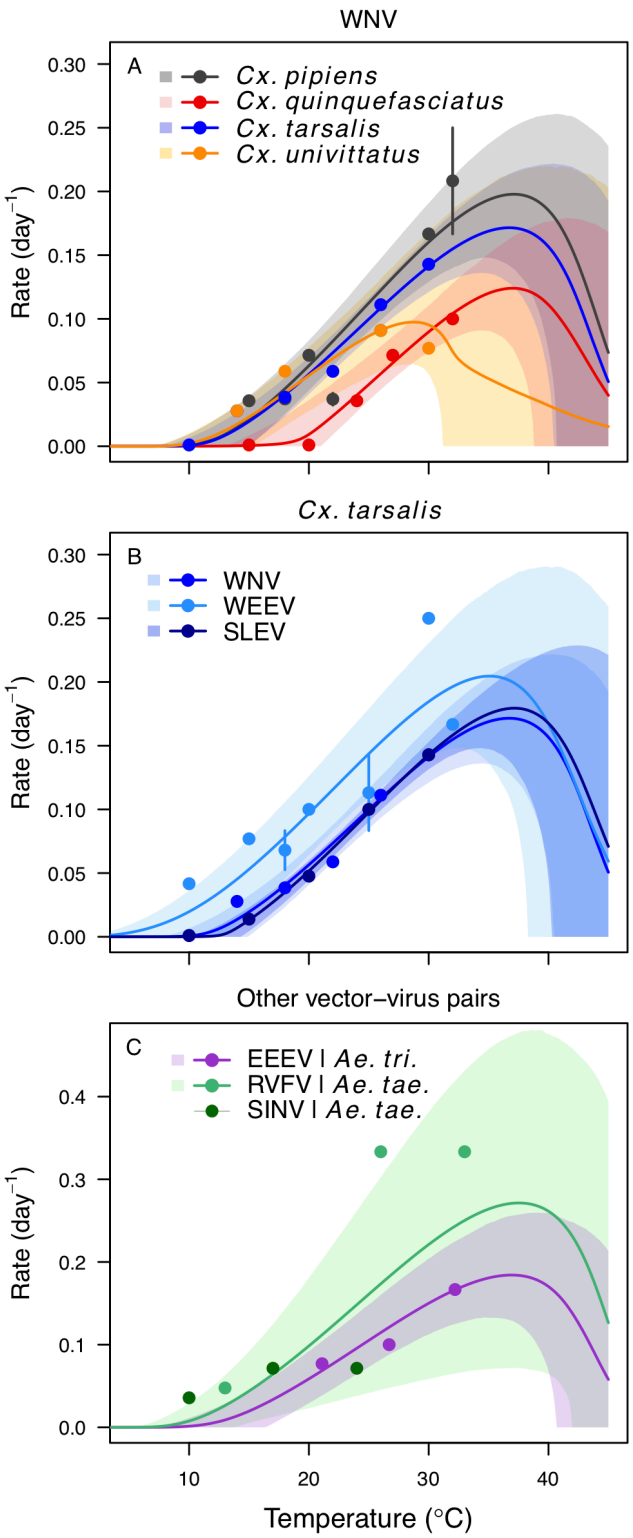

Figure 5: Pathogen development rates have high thermal optima. Thermal responses of pathogen development rate (*PDR*). (A) West Nile virus in *Culex pipiens* (dark grey), *Cx. quinquefasciatus* (red), *Cx. tarsalis* (blue), and *Cx. univitattus* (orange). (B) Three viruses in *Cx. tarsalis*: West Nile virus (same as in A, blue), Western Equine Encephalitis virus (light blue), and St. Louis Encephalitis virus (dark blue). (C) Eastern Equine Encephalitis virus in *Aedes triseriatus* (violet), Rift Valley Fever virus in *Ae. taeniorhynchus* (light green), Sindbis virus in *Ae. taeniorhynchus* (dark green). We did not fit a thermal response for Sindbis virus in *Ae. taeniorhynchus* because the limited data responded weakly to temperature and did not match our priors. We used informative priors based on thermal biology theory and data from other systems to fit the decrease at high temperatures (see *Model Overview*); other traits determined the upper limits of the R_0 models. Points without error bars are reported means from single studies; points with error bars are averages of means from multiple studies (+/- standard error, for visual clarity only; thermal responses were fit to reported means, see Fig S7). Solid lines are posterior distribution means; shaded areas are 95% credible intervals of the trait mean.

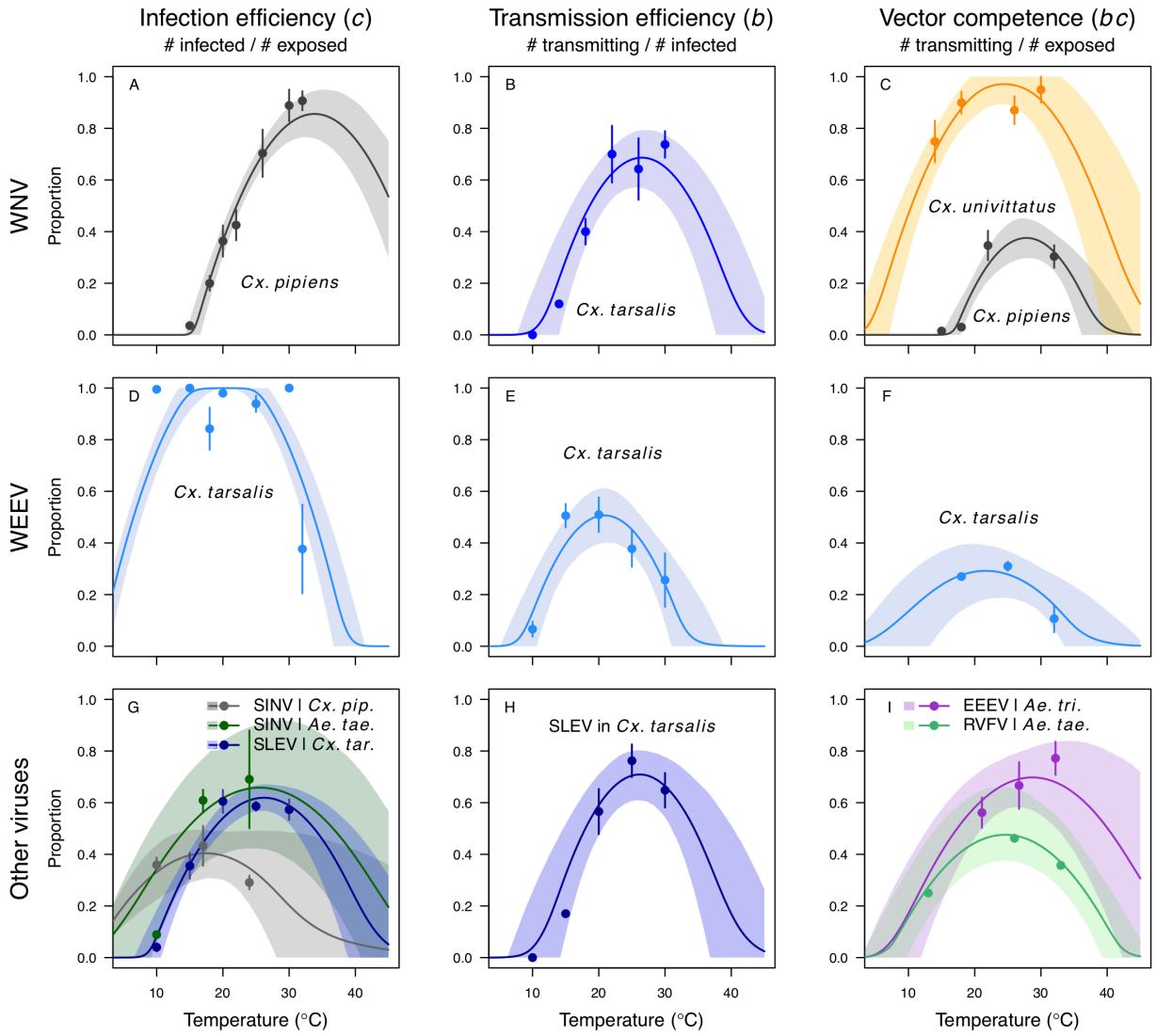

Figure 6: Vector competence responds strongly to temperature and varies across vector and virus species. Thermal responses of infection efficiency (*c*, # infected / # exposed; first column), transmission efficiency (*b*, # transmitting / # infected; second column) or vector competence (*bc*, # infected / # exposed; third column) for vector–virus pairs. First row (A,B,C): West Nile virus in *Culex pipiens* (dark grey), *Cx. tarsalis* (blue), and *Cx. univitattus* (yellow/orange). Second row: (D,E,F) Western Equine Encephalitis virus in *Cx. tarsalis* (light blue). Third row (G,H,I): Sindbis virus in *Aedes taeniorhynchus* (dark green), Sindbis virus in *Cx. pipiens* (light gray), St. Louis Encephalitis virus in *Cx. tarsalis* (dark blue), Eastern Equine Encephalitis virus in *Ae. triseriatus* (violet), and Rift Valley Fever virus in *Ae. taeniorhynchus* (light green). Points are means of replicates from single or multiple studies (+/- standard error, for visual clarity only; thermal responses were fit to replicate-level data, see Fig S8, Fig S9). Solid lines are posterior distribution means; shaded areas are 95% credible intervals of the trait mean.

382 *Temperature-dependent R_0 models*

383 Relative R_0 responded unimodally to temperature for all the vector–virus pairs, with
384 many peaking at fairly cool temperatures (medians: 22.7–26.0ºC, see Table 2 for CIs; Fig 7). The
385 lower thermal limits (medians: 8.7–19.0ºC, see Table 2 for CIs; Fig 7) were more variable than
386 the optima or the upper thermal limits (medians: 31.9–37.8ºC, see Table 2 for CIs; Fig 7),
387 although confidence intervals overlapped in most cases because lower thermal limits also had
388 higher uncertainty (Fig 7). The *Ae. taeniorhynchus* models were clear outliers, with much
389 warmer distributions for the upper thermal limits, and optima that trended warmer as well.

390 Differences in relative R_0 stemmed from variation both in vector traits (e.g., in Fig 7A,
391 with WNV in different vector species) and in virus infection traits (e.g., in Fig 7B, with different
392 viruses in *Cx. tarsalis*). The upper thermal limit was warmer for WNV transmitted by *Cx. pipiens*
393 (34.9ºC [CI: 32.9–37.5ºC] than by *Cx. quinquefasciatus* (31.8ºC [CI: 31.1–32.2ºC]), counter to
394 the *a priori* prediction based on vector geographic ranges. This result implies that warming from
395 climate change may differentially impact transmission by these two vectors. Additionally, the
396 lower thermal limit for WNV varied widely (but with slightly overlapping 95% CIs) across
397 different vector species (Fig 7D), from 19.0ºC (14.2–21.0ºC) in *Cx. quinquefasciatus* to 16.8ºC
398 (14.9–17.8ºC) in *Cx. pipiens* to 12.2ºC (9.7–15.3ºC) in *Cx. tarsalis* to 11.1ºC (8.1–15.4ºC) in *Cx.*
399 *univittatus* (an African and Eurasian vector; Table 2). Based on these trends in the thermal limits
400 of R_0, the seasonality of transmission and the upper latitudinal and elevational limits could vary
401 for WNV transmitted by these different species.

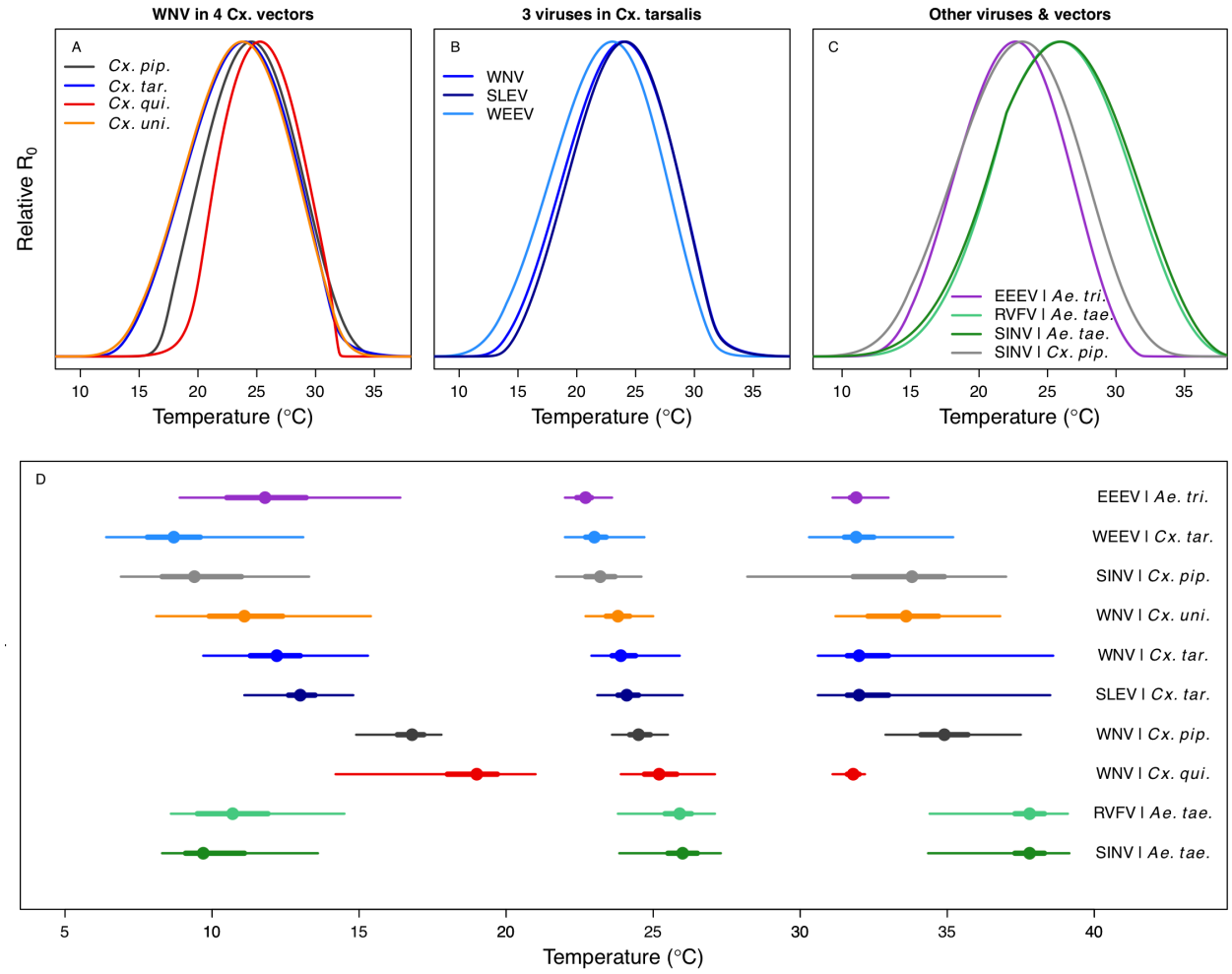

Figure 7: Unimodal thermal responses of transmission (relative R_0) for ten vector-virus pairs. Posterior mean relative R_0 for (A) West Nile virus (WNV) in *Culex pipiens* (dark grey), *Cx. tarsalis* (blue), *Cx. quinquefasciatus* (red), and *Cx. univitattus* (orange); (B) three viruses in *Cx. tarsalis*: WNV (same as in A, blue), Western Equine Encephalitis virus (WEEV, light blue), and St. Louis Encephalitis virus (SLEV, dark blue); (C) Sindbis virus (SINV) in *Aedes taeniorhynchus* (dark green) and *Cx. pipiens* (light grey), Rift Valley Fever virus (RVFV) in *Ae. taeniorhynchus* (light green), and Eastern Equine Encephalitis virus (EEEV) in *Ae. triseriatus* (violet). (D) Posterior median and uncertainty estimates for the lower thermal limit, optimum, and upper thermal limit. Points show medians, thick lines show middle 50% density, thin lines show 95% credible intervals. Models are ordered by increasing median optimal temperature.

TABLE 2:

R_0 Model	T_{min} (ºC)	Optimum (ºC)	T_{max} (ºC)	Thermal breadth (ºC)
From this study:				
EEEV in *Ae. triseriatus*	11.7 (8.8 – 16.3)	22.7 (22.0 – 23.6)	31.9 (31.1 – 33.0)	20.0 (15.4 – 23.0)
WEEV in *Cx. tarsalis*	8.6 (6.3 – 13.0)	23.0 (22.0 – 24.7)	31.9 (30.3 – 35.2)	23.3 (18.2 – 27.0)
SINV in *Cx. pipiens*	9.4 (6.9 – 13.3)	23.2 (21.7 – 24.6)	33.8 (28.2 – 37.0)	23.8 (17.3 – 28.6)
WNV in *Cx. univittatus*	11.0 (8.0 – 15.3)	23.8 (22.7 – 25.0)	33.6 (31.2 – 36.9)	22.5 (18.2 – 26.3)
WNV in *Cx. tarsalis*	12.1 (9.6 – 15.2)	23.9 (22.9 – 25.9)	32.0 (30.6 – 38.6)	20.1 (16.3 – 26.7)
SLEV in *Cx. tarsalis*	12.9 (11.0 – 14.8)	24.1 (23.1 – 26.0)	32.0 (30.6 – 38.5)	19.2 (16.5 – 25.6)
WNV in *Cx. pipiens*	16.8 (14.9 – 17.8)	24.5 (23.6 – 25.5)	34.9 (32.9 – 37.6)	18.2 (15.8 – 21.2)
WNV in *Cx. quinquefasciatus*	19.0 (14.1 – 20.9)	25.2 (23.9 – 27.1)	31.8 (31.1 – 32.2)	12.7 (10.6 – 17.6)
RVFV in *Ae. taeniorhynchus*	10.6 (8.6 – 14.4)	25.9 (23.8 – 27.1)	37.8 (34.4 – 39.1)	27.0 (21.8 – 29.7)
SINV in *Ae. taeniorhynchus*	9.7 (8.3 – 13.6)	26.0 (23.9 – 27.3)	37.8 (34.4 – 39.2)	27.7 (22.6 – 30.0)
From previous studies:				
Falciparum malaria [3]	19.1 (16.0 – 23.2)	25.4 (23.9 – 27.0)	32.6 (29.4 – 34.3)	13.2 (8.3 – 17.1)
DENV in *Ae. albopictus* [4]	16.2 (13.0 – 19.8)	26.4 (25.4 – 27.6)	31.4 (29.5 – 34.0)	15.2 (11.2 – 19.3)
Ross River virus [6]	17.0 (15.8 – 18.0)	26.4 (26.0 – 26.6)	31.4 (30.4 – 33.0)	14.2 (12.8 – 16.2)
ZIKV in *Ae. aegypti* [7]	22.8 (20.5 – 23.8)	28.9 (28.2 – 29.6)	34.5 (34.1 – 36.2)	11.7 (10.4 – 14.5)
DENV in *Ae. aegypti* [4]	17.8 (14.6 – 21.2)	29.1 (28.4 – 29.8)	34.5 (34.1 – 35.8)	16.7 (13.2 – 20.2)

Table 2: Thermal optima and limits for transmission of mosquito-borne pathogens. Median temperature of the lower thermal limit (T_{min}), optimum, and upper thermal limit (T_{max}), with 95% credible intervals in parentheses.

Different traits determined the lower and upper thermal limits and optimum for transmission across vector–virus pairs. The lower thermal limit for transmission was most often determined by parasite development rate (*PDR*; WNV and SLEV in *Cx. tarsalis*, WNV in *Cx. quinquefasciatus*) or biting rate (*a*; WNV in *Cx. univitattus*, WEEV in *Cx. tarsalis*, EEEV in *Ae. triseriatus,* RVFV and SINV in *Ae. taeniorhynchus*, SINV in *Cx. pipiens*; Figs S12–20), which tend to respond asymmetrically to temperature, with high optima. However, vector competence (*bc*) determined the lower limit for WNV in *Cx. pipiens* (Fig S11). The upper thermal limit was determined by biting rate (*a*) for the three *Cx. tarsalis* models and by adult lifespan (*lf*) for all others, although proportion ovipositing (*pO*) was also important for WNV in *Cx. quinquefasciatus* (Figs S11-S20). In all models, lifespan (*lf*) and biting rate (*a*) had the strongest impact on the optimal temperature for transmission, with biting rate increasing transmission at

429 low temperatures and lifespan decreasing transmission at high temperatures (Figs S11-S20). This
430 result is consistent with previous mechanistic models of tropical mosquito-borne diseases,
431 despite the qualitative difference in the shape of the lifespan thermal response between those
432 tropical mosquitoes and the more temperate mosquitoes investigated here [2–4,6,7].
433

434 *Model validation with human case data*

435 We validated the R_0 models for WNV with independent data on human cases because the
436 temperature-dependent trait data for those models were relatively high quality and because
437 human case data were available from the Centers for Disease Control and Prevention across a
438 wide climatic gradient in the contiguous United States. We averaged county-level incidence and
439 mean summer temperatures from 2001–2016 to estimate the impact of temperature over space,
440 while ignoring interannual variation in disease that is largely driven by changes in host immunity
441 and drought [5]. We used generalized additive models (GAMs, which produce flexible,
442 smoothed responses) to ask: does average incidence respond unimodally to mean summer
443 temperature? If so, what is the estimated optimal temperature for transmission? Can we detect
444 upper or lower thermal limits for transmission? Incidence of human neuroinvasive West Nile
445 disease responded unimodally to average summer temperature and peaked at 24ºC (23.5–24.2ºC
446 depending on the spline settings; Fig 8, Fig S24), closely matching the optima from the
447 mechanistic models for the three North American *Culex* species (23.9–25.2ºC; Table 2).
448 However, the human disease data did not show evidence for lower or upper thermal limits: mean
449 incidence remained positive and with relatively flat slopes below ~19ºC and above ~28ºC,
450 although sample size was very low above 28ºC and below 15ºC resulting in wide confidence
451 intervals (Fig 8, Fig S24).

452 We used national month-of-onset data for WNV, EEEV, and SLEV to ask: is the
453 seasonality of incidence consistent with our models for temperature-dependent transmission?
454 The month-of-onset for cases of WNV was consistent with predicted transmission, $R_0(T)$ (Fig 9).
455 As expected (based on previous studies and the time required for mosquito populations to
456 increase, become infectious, and bite humans, and for humans to present symptoms and seek
457 medical care [4,6]), there was a two-month lag between initial increases in $R_0(T)$ and incidence:
458 cases began rising in June to the peak in August. The dramatic decline in transmission between
459 September and October corresponds also closely to the predicted decline in relative R_0, but
460 without the expected lag. In general, the seasonal patterns of SLEV and EEEV incidence were
461 similar to WNV, but differed by three orders of magnitude from ~20,000 cases of WNV to ~40-
462 50 cases of EEEV and SLEV during the peak month (Fig 9). However, transmission of SLEV
463 and EEEV are predicted to begin increasing one month earlier than WNV (March versus April,
464 Fig 9), because the mechanistic models predict that the lower thermal limits for SLEV and EEEV
465 are cooler than those for WNV in two of the three North American vectors (*Cx. pipiens* and *Cx.*
466 *quinquefasciatus*, Fig 7). The month-of-onset data partially support this prediction, as cases of
467 SLEV (but not EEEV) disease begin to increase earlier in the year than WNV, relative to the
468 summer peak.

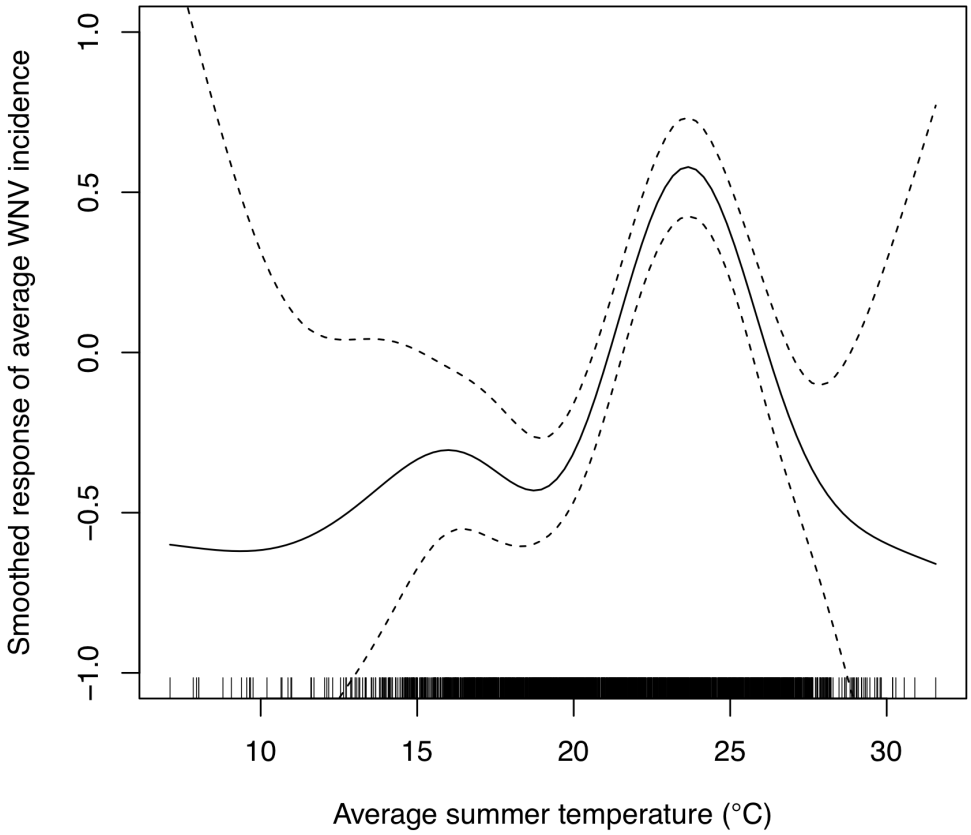

Figure 8: Incidence of human neuro-invasive West Nile disease across US counties responds unimodally to temperature, peaking at 24°C. A generalized additive model (GAM) was fit to county-level data (n = 3,109) of mean temperature from May-September and incidence of neuro-invasive West Nile disease, both averaged from 2001-2016. See Fig S24 for fits across a range of smoothing parameters.

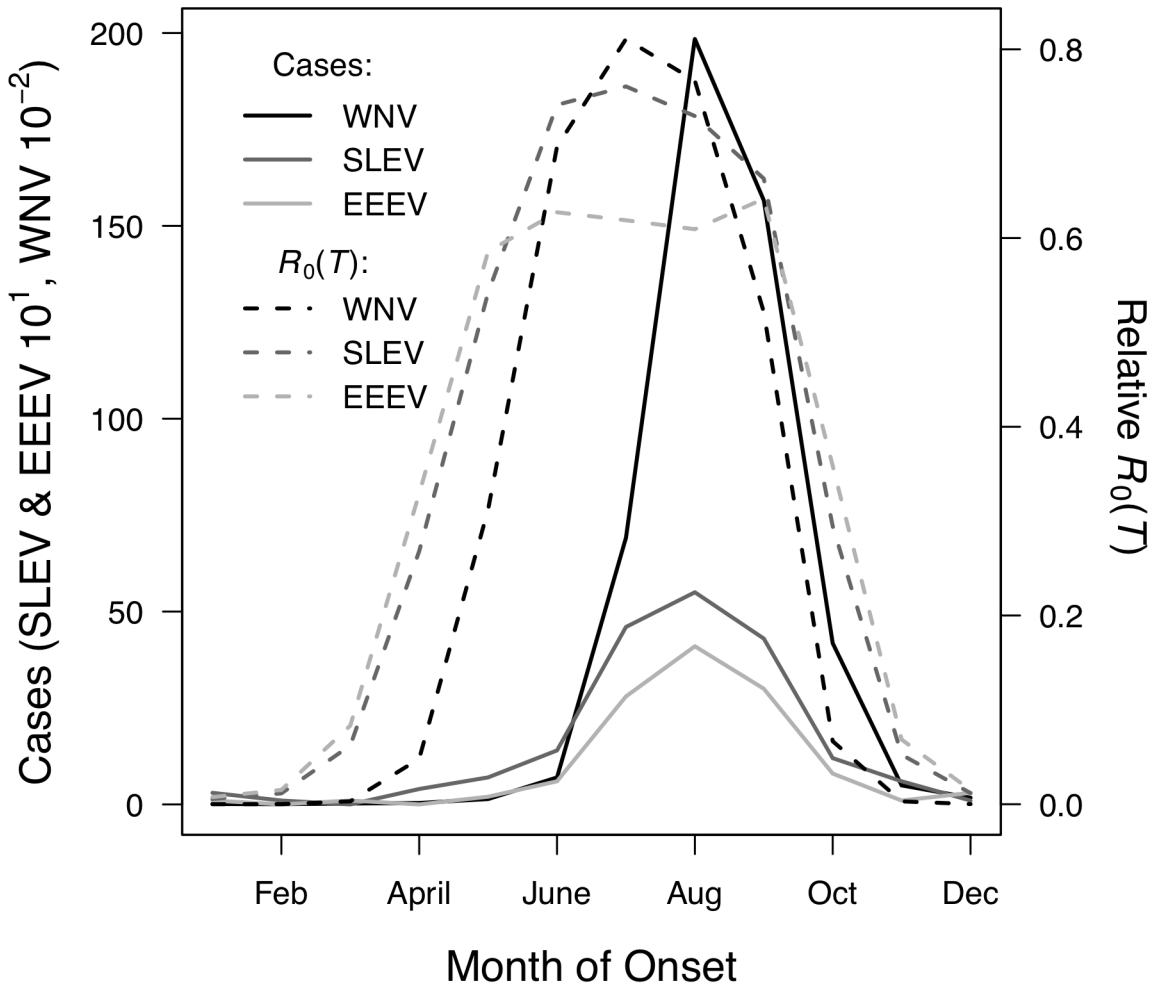

Figure 9: Temperature shapes the seasonal pattern of human cases of mosquito-borne viral diseases. Incidence (solid lines) lags behind predicted temperature-dependent R_0 (dashed lines) for human cases of neuro-invasive disease caused by West Nile virus (WNV, black), St. Louis encephalitis virus (SLEV, dark gray), and Eastern Equine Encephalitis virus (EEEV, light gray) by 2 months. This lag matches patterns in other mosquito-borne diseases, and is caused by the time required for mosquito populations to increase, become infectious, and bite humans, and for humans to present symptoms and seek medical care.

485 **DISCUSSION**

486 As climate changes, it is critical to understand how changes in temperature will affect the
487 transmission of mosquito-borne diseases. Toward this goal, we developed temperature-
488 dependent, mechanistic transmission models for 10 vector–virus pairs. The viruses—West Nile
489 virus (WNV), St. Louis Encephalitis virus (SLEV), Eastern and Western Equine Encephalitis
490 viruses (EEEV and WEEV), Sindbis virus (SINV), and Rift Valley fever virus (RVFV)—sustain
491 substantial transmission in temperate areas (except RVFV), and are transmitted by shared vector
492 species, including *Cx. pipiens*, *Cx. quinquefasciatus*, and *Cx. tarsalis* (except EEEV; Fig 1).
493 Although most traits responded unimodally to temperature, as expected [2–4,6–8], lifespan
494 decreased linearly with temperature over the entire temperature range of available data (> 14ºC)
495 for these *Culex* vectors (Fig 3). Transmission responded unimodally to temperature, with the
496 thermal limits and optima for transmission varying among some of the focal mosquito and virus
497 species (Fig 7, Table 2), largely due to differences in the thermal responses of mosquito biting
498 rate, lifespan, vector competence, and parasite development rate. Human case data for WNV
499 disease across the US exhibited a strong unimodal thermal response (Fig 8), and month-of-onset
500 data for three viruses was consistent with the predicted seasonality of transmission (Fig 9). Thus,
501 the mechanistic models captured geographical and seasonal patterns of human incidence, despite
502 the complexity of the enzootic cycles and spillover into humans. Our analysis was somewhat
503 limited by the lack of data for several trait-species combinations, or by data that were sparse,
504 particularly at high temperatures. However, our key results—maximal transmission at
505 intermediate temperatures—are unlikely to change, and underscore the importance of
506 considering unimodal thermal responses when predicting how climate change will impact
507 mosquito-borne disease transmission.

508 The monotonically decreasing thermal responses for lifespan in these more temperate
509 mosquitoes (Fig 3D) contrast with unimodal responses of more tropical species [2,4,6,8], and
510 may reflect differing thermal physiology between species that use diapause or quiescence, two
511 forms of dormancy, to persist over winter and those that do not (see *Model Overview*) [47–49].
512 *Ae. albopictus*, a species that occurs in both tropical and temperate zones, exhibits a latitudinal
513 gradient in the United States in which more temperate populations diapause while sub-tropical
514 populations do not [50]. Experiments could test this hypothesis by measuring whether the
515 functional form of the thermal response for lifespan differs between northern and southern US
516 *Ae. albopictus* populations. Despite the difference in the shape of the thermal response, lifespan
517 played a similarly important role here as in previous studies of mosquito-borne pathogens,
518 strongly limiting transmission at high temperatures (Figs S11–20). Nonetheless, the linear
519 thermal responses for lifespan ultimately promotes higher transmission at relatively cool
520 temperatures because unlike in more tropical species, lifespan did not decline at cool
521 temperatures within the range measured (> 14ºC). At more extreme temperatures expected to be
522 fatal even for diapausing mosquitoes (i.e., below 0ºC), we expect lifespan to eventually decline,
523 so that the response over broader temperature ranges is likely unimodal.
524 Predicted transmission for many of the diseases in this study peaked at and extended to
525 cooler temperatures than for previously studied diseases with more tropical distributions (see Fig
526 7 and Table 2 for 95% credible intervals)[8]. Here, the optimal temperatures for transmission
527 varied from 22.7–25.2ºC (excluding *Ae. taeniorhynchus* models, Fig 7). By contrast, models
528 predict that transmission peaks at 25.4ºC for malaria [2,3], 26.4ºC for Ross River virus [6] and
529 dengue in *Ae. albopictus* [4], 28.9ºC for Zika in *Ae. aegypti* [4], and 29.1ºC for dengue in *Ae.*
530 *aegypti* [4,7]. Many models also had cooler lower thermal limits (medians: 8.7–19.0ºC) than

531 those of diseases with more tropical distributions (medians: 16.0–17.8ºC)[8]. In combination
532 with similar upper thermal limits (see below), these patterns led to wider thermal breadths (18.2–
533 27.7ºC; Fig 7) for most of the viruses here compared to the more tropical pathogens (11.7–
534 16.7ºC), excepting WNV in *Cx. quinquefasciatus* (12.7ºC), the vector most restricted to lower
535 latitude, sub-tropical geographic areas (Fig 2). These results match a previous finding that
536 temperate insects had wider thermal breadths than tropical insects [51], and likely reflect thermal
537 adaptation to greater variation in temperature in temperate areas compared to tropical areas [52].
538 Additionally, SINV—a virus with substantial transmission at very high latitudes in Finland
539 [26]—had the second coolest lower thermal limit (Fig 7, Table 2). Further, lower-latitude *Cx.*
540 *quinquefasciatus* outperformed higher-latitude *Cx. pipiens* at warmer temperatures for proportion
541 ovipositing (*pO*; Fig 3A), while the reverse occurred at cooler temperatures for egg viability (*EV*;
542 Fig 3C). Collectively, these results imply that, to some extent, measurements of physiological
543 traits can predict geographic patterns of vectors or disease transmission at broad scales.
544 However, geographic range differences (Fig 2) did not consistently predict variation in thermal
545 responses among the *Culex* species in this study (e.g., biting rate [*a*, Fig 3C] and adult lifespan
546 [*lf*, Fig 3D]), indicating that life history and transmission trait responses at constant temperatures
547 do not always predict the geographic distributions of species. Instead, the ability to tolerate
548 temperature extremes may limit species distributions more than their performance at average or
549 constant temperatures [53]. Moreover, although diseases like malaria and dengue are generally
550 considered to be "tropical", historically their distributions extended further into temperate
551 regions [54,55]. Thus, current distributions of disease may reflect a realized niche restricted by
552 social factors more than a fundamental niche based on ecological factors like temperature.

553 In contrast to the optima, lower thermal limits, and thermal breadths, the upper thermal
554 limits for the vector–virus pairs in this study (31.9–34.9ºC, excluding *Ae. taeniorhynchus*
555 models; Fig 7D, Table 2) closely matched those of more tropical diseases (31.5–34.7ºC) [2–
556 4,6,7]. This similarity likely arises because maximum summer temperatures in temperate areas
557 can match or even exceed maximum temperatures in tropical areas [52]. Accordingly, there may
558 be a fundamental upper thermal constraint on transmission that applies similarly to all
559 mosquitoes-borne diseases, driven by short mosquito lifespans at high temperatures. The
560 relatively high upper thermal limits in both *Ae. taeniorynchus* transmission models were driven
561 by the thermal response of lifespan, which was fit to few data points; more data are needed to
562 determine if it reflects the true thermal response in that species [Fig S1]. These results indicate
563 that as temperatures rise due to climate change, temperate diseases are unlikely to be displaced
564 by warming alone, although they may also expand toward the poles, even as tropical diseases
565 may expand farther into temperate zones.
566 Independent human case data support unimodal thermal responses for transmission and
567 the importance of temperature in shaping geographic patterns of mosquito-borne disease. Human
568 cases of WNV [56–62] and SINV [63,64] are often positively associated with temperature. Here,
569 we found incidence of neuroinvasive WNV disease peaked at intermediate mean summer
570 temperatures across counties in the US (Fig 8) that matched the optima predicted by our models.
571 This result adds to prior evidence for reduced transmission of WNV [65] and other mosquito-
572 borne diseases [2,16–19] at high temperatures. Although we did not detect lower or upper
573 thermal limits (Fig 8), this result is unsurprising based on fundamental differences between the
574 types of temperature data used to parameterize and validate the models. The R_0 model prediction
575 is derived from data collected in a controlled laboratory environment at constant temperatures,

576 while average incidence in the field reflects temperatures that vary at a variety of temporal scales
577 (daily, seasonal, and interannual). Thus, we hypothesize that temperature variation over time
578 may sustain transmission in regions with otherwise unsuitable mean summer temperatures by
579 providing time windows that are suitable for transmission [38,39,41].

580 The temperature-dependent models also predict the seasonality of human cases of WNV,
581 EEEV, and SLEV (Fig 9). The 2-month lag between climate suitability and the onset of human
582 cases, which matches previous results from other mosquito-borne diseases [4,6], arises from the
583 time following the onset of suitable conditions required for mosquito populations to increase
584 [66], become infectious, and bite humans, and for humans to present symptoms and seek medical
585 care [67,68]. Transmission of the more temperate viruses here may incur additional lags because
586 human cases only result from enzootic transmission and multiple rounds of amplification within
587 reservoir hosts may be required before prevalence is sufficiently high to spill over into humans.
588 Additionally, as wild birds disperse in late summer, both *Cx. pipiens* and *Cx. tarsalis* shift their
589 feeding preferences from birds to humans, increasing transmission to people and influencing the
590 seasonal dynamics of WNV [69]. Drought, precipitation, and reservoir immunity also strongly
591 drive transmission of WNV [5,59,60,62] and may interact with temperature. SLEV, EEEV, and
592 WEEV are less common in nature, and thus less well-studied, but the lower thermal limits in our
593 study support previous findings that transmission WEEV is favored over SLEV in cooler
594 conditions [70]. Additionally, the seasonal patterns of incidence data (Fig 9) provide some
595 support for the model prediction that SLEV transmission is possible at cooler temperatures than
596 WNV by North American vectors (Table 2). By contrast, mean temperature is not associated
597 with outbreaks of RVFV, although they are highly predictable based on precipitation driven by
598 El Niño–Southern Oscillation cycles [71,72]. Thus, disease dynamics depend on the interaction

599 between temperature and other environmental factors, and the relative importance of temperature
600 versus other drivers varies across systems.

601 Most prior studies with mechanistic models for temperature-dependent transmission of
602 WNV do not capture the unimodal thermal response that our mechanistic models predict and that
603 we observe in the human case data (Table 3). Two previous models predicted that transmission
604 of WNV would increase up to the warmest temperatures they considered, 28ºC [73] and 35ºC
605 [74]. In both cases, the daily survival rates estimated from lab experiments were far less sensitive
606 to temperature than our measure of adult lifespan, and neither model was validated with field
607 data. A third study with models for *Cx. pipiens*, *Cx. quiquefasciatus*, and *Cx. tarsalis*, like our
608 study, predicted unimodal thermal responses for transmission, with very similar optima but with
609 lower thermal limits that were ~5ºC warmer, resulting in much narrower thermal breadths (Fig
610 S22) [5]. This previous model [5] was validated with annual, state-level WNV human case data
611 (in contrast to our county-level data averaged over multiple years), and detected a positive effect
612 of temperature, with no decline at high temperatures [5]. The best spatial and temporal scales for
613 validating temperature-dependent transmission models and detecting the impacts of temperature
614 remain an open question. For instance, different approaches may be necessary to detect thermal
615 optima and thermal limits. Critically, differences in modeling and validation approaches can lead
616 to strongly divergent conclusions and predictions for the impact of climate change.

TABLE 3:

R_0 Model	Optimum (ºC)
From this study:	
WNV in *Cx. pipiens*	24.5
WNV in *Cx. quinquefasciatus*	25.2
WNV in *Cx. tarsalis*	23.9
WNV in *Cx. univittatus*	23.8
From previous studies:	
WNV in *Cx. pipiens* [5]	24.9
WNV in *Cx. quinquefasciatus* [5]	24.3
WNV in *Cx. tarsalis* [5]	24.9
WNV in *Cx. pipiens* [70]	28
WNV in *Cx. pipiens molestus* [70]	28
WNV in *Cx.* and *Ae. spp.* [71]	35

Table 3: Predicted optima for transmission of West Nile virus. Predicted optima for transmission from this study and previous models.

Given the unimodal relationship between temperature and transmission of these temperate mosquito-borne pathogens, we expect climate warming to lead to predictable shifts in disease transmission [20,22,23]. Warming should extend the transmission season earlier into the spring and later into the fall and increase transmission potential in higher latitudes and altitudes, although this prediction may be impacted by changes in bird migrations. However, the thermal optima for these temperate vector–virus pairs are relatively cool, so in many locations, warming could result in summer temperatures that exceed the thermal optima for transmission more frequently, reducing overall transmission or creating a bimodal transmission season [75]. Based on the average summer temperature data (2001–2016) in our analysis (Fig 8), currently the majority of people (70%) and counties (68%) are below the optimal temperature for transmission (23.9 ºC, fit by the GAM), while 30-32% are above the optimum. The numbers are similar when restricted to counties with observed West Nile virus cases: 69% and 70%, respectively. Thus, all else being equal, we might expect a net increase in transmission of West Nile virus in response to

634 the warming climate, even as hot temperatures suppress transmission in some places. Still,
635 warming is unlikely to eliminate any of these more temperate pathogens since the upper thermal
636 limits for transmission are well above temperatures pathogens regularly experience in their
637 current geographic ranges. More generally, our results raise concerns about the common practice
638 of extrapolating monotonic relationships between temperature and disease incidence fit from
639 observational data into warmer climate regimes to predict future cases [59,61].

640 While the data-driven models presented here represent the most comprehensive synthesis
641 to date of trait thermal response data and their impact on transmission for these mosquito–
642 pathogen systems with substantial transmission in temperate regions, additional temperature-
643 dependent trait data would increase the accuracy and decrease the uncertainty in these models
644 where data were sparse or missing. Our data synthesis and uncertainty analysis suggest
645 prioritizing parasite development rate (*PDR*) and vector competence (*bc*) data and biting rate (*a*)
646 data because those thermal responses varied widely among vector–virus pairs and determined the
647 lower thermal limits and optima for transmission in many models. Additionally, vector
648 competence and/or parasite development rate data were missing in many cases (WNV in *Cx.*
649 *quinquefasciatus*, EEEV in *Cs. melanura*, RVFV in vectors from endemic areas, transmission
650 efficiency [*b*] for SINV) or sparse (EEEV and WNV in *Cx. univittatus*), as were biting rate data
651 (*Cx. univittatus*, RVFV vectors). Lifespan data—key for determining transmission optima and
652 upper thermal limits—were the missing for *Ae. triseriatus*, *Cs. melanura*, *Cx. univittatus*, and
653 RVFV vectors, and at temperatures below 14 ºC for all vector species, so it was unclear which
654 functional form these thermal responses should take (linear or quadratic). While the other
655 mosquito demographic traits did not determine thermal limits for transmission in models here,
656 fecundity (typically as *EFD*), larval-to-adult survival (*pLA*), and egg viability (*EV*) determined

657 thermal limits for malaria [2] and Ross River virus [6]. Thus, more fecundity data (missing for
658 *Cx. tarsalis*, *Cx. univittatus*, and *Ae. triseriatus*; sparse for *Cx. pipiens* and *Cx. quinquefasciatus*)
659 would also reduce model uncertainty. New data are particularly important for RVFV, which has
660 a tropical distribution but for which the model depends on traits measured in *Cx. pipiens*
661 collected from temperate regions and infection traits measured in *Ae. taeniorhynchus*, a North
662 American species. RVFV is transmitted by a diverse community of vectors across the African
663 continent, but experiments should prioritize hypothesized primary vectors (e.g., *Ae.*
664 *circumluteolus* or *Ae. mcintoshi*) or secondary vectors that already have partial trait data (e.g.,
665 *Ae. vexans* or *Cx. theileri*) [27,76]. Although temperature itself does not predict the occurrence of
666 RVFV outbreaks, it may affect the size of epidemics once they are triggered by precipitation.
667 Additionally, the thermal response of vector competence may vary across vector populations
668 [77] and/or virus isolates even within the same species, so more data may also improve the
669 accuracy of models without missing data.

670 As carbon emissions continue to increase and severe climate change becomes
671 increasingly inevitable [78], it is critical that we understand how temperature will shape
672 transmission of mosquito-borne diseases in a warmer future world. While data gaps are still
673 limiting, the comparative approach is powerful for predicting similarities and differences across
674 vectors and viruses, including differences between primarily tropical and temperate diseases [8].
675 Accounting for the effects of temperature variation [38,41,79] is an important next step for using
676 these models to accurately predict transmission. Additionally, the potential for evolution to
677 warmer climates is uncertain because of limited knowledge on the level of genetic variation in
678 thermal responses for most vectors or mosquito-borne pathogens within or between populations
679 (but see [80,81]). Further, vectors and pathogens may experience different selective pressures, as

680 mosquito populations may depend on either increased fecundity or longevity at high
681 temperatures, while pathogens require longer vector lifespans [8]. Thus, future trajectories of
682 these diseases will depend not just on suitability of mean temperatures but also on temperature
683 variation, thermal adaptation of vectors and viruses, land use (which governs mosquito–wildlife–
684 human interactions), vector control activities, human and wildlife immune dynamics, and
685 potential future emergence and spread of new vectors and viruses.
686

687 **MATERIALS AND METHODS**

688 All analyses were conducted using R 3.1.3 [82].
689

690 *Vector species range maps*

691 The distributions of *Cx. pipiens* and *Cx. quinquefasciatus* are georectified maps adapted
692 from [35,83]. The northern boundary of *Cx. tarsalis* was taken from [84]. For the southern
693 boundary, we drew a convex polygon using five datasets [85–89] in the Global Biodiversity
694 Information Facility (https://www.gbif.org/).
695

696 *Temperature-dependent Trait Data*

697 We found 38 studies with appropriate temperature-dependent trait data from controlled
698 laboratory experiments [5,56,80,81,90–124]. When necessary, we digitized the data using Web
699 Plot Digitizer [125], a free online tool. When lifespan data were reported by sex, only female
700 data were used. Vector competence trait data (*b*, *c*, or *bc*) were only included if time at sampling
701 surpassed the estimated extrinsic incubation period (*EIP*, the inverse of *PDR*) at that
702 temperature, which resulted in the exclusion of some studies [126,127].

Fitting Thermal Responses

We fit trait thermal responses with a Bayesian approach using the 'r2jags' package [128], an R interface for the popular JAGS program [129] for the analysis of Bayesian graphical models using Gibbs sampling. It is a (near) clone of BUGS (Bayesian inference Using Gibbs Sampling) [130]. In JAGS, samples from a target distribution are obtained via Markov Chain Monte Carlo (MCMC). More specifically, JAGS uses a Metropolis-within-Gibbs approach, with an Adaptive Rejection Metropolis sampler used at each Gibbs step (for more information on MCMC algorithms see [131]).

For each thermal response being fit to trait data, we identified the most appropriate functional form (quadratic, Briére, or linear; eqs. 3–5) for that specific trait–species combination [8]. For traits with ambiguous functional responses, we fit the quadratic and Briere and used the deviance information criterion (DIC) [132] to pick the best fit. We assumed normal likelihood distributions with temperature-dependent mean values described by the appropriate function (eqs. 3–5) and a constant standard deviation described by an additional fitted parameter ($\tau = 1/\sigma^2$). The 95% credible intervals in Figs. 3-6 estimate the uncertainty in the mean thermal response; 95% prediction intervals that incorporate the estimated standard deviation in the data are shown in Figs S2-9.

We set all thermal response functions to zero when $T < T_{min}$ and $T > T_{max}$ (for eq. 3 and 4) or when $T > -z/m$ (eq. 5) to prevent trait values from becoming negative. For traits that were proportions or probabilities, we also limited the thermal response functions at 1. For the linear thermal responses, we calculated the predicted thermal response in a similarly piecewise manner in order to be conservative: for temperatures at or above the coldest observed data point, we used

726 the trait values predicted by the fitted thermal response (i.e., the typical method); for
727 temperatures below the coldest observed data point, we substituted the trait estimate at the
728 coldest observed data point (i.e., forcing the thermal response to plateau, rather than continue
729 increasing beyond the range of observed data).

730 For the fitting process, we ran three concurrent MCMC chains for 25000 iterations each,
731 discarding the first 5000 iterations for burn-in (convergence was checked visually). We thinned
732 the resultant chains, saving every eighth step. These settings resulted in 7500 samples in the full
733 posterior distribution that we kept for further analysis.

734

735 *Generation of Priors*

736 We used data-informed priors to decrease the uncertainty in our estimated thermal
737 responses and constrain the fitted thermal responses to be biologically plausible, particularly
738 when data were sparse. These priors used our total dataset, which contained temperature-
739 dependent trait data for all of the main species in the analysis (but with the focal species
740 removed, see below), as well as from additional temperate *Aedes* and *Culex* species
741 [92,94,102,106,111,112,133–138].

742 We fit each thermal response with a sequential two-step process, where both steps
743 employed the same general fitting method (described above in *Fitting Thermal Responses*) but
744 used different priors and data. In step 1, we generated high-information priors by fitting a
745 thermal response to data from all species except the focal species of interest (i.e., a 'leave-one-
746 out' approach). For example, for the prior for biting rate for *Cx. pipiens*, we used the biting rate
747 data for all species except *Cx. pipiens*. For this step, we set general, low-information priors that
748 represented minimal biological constrains on these functions (e.g., typically mosquitoes die if

749 temperatures exceed 45ºC, so all biological processes are expected to cease; T_{min} must be less
750 than T_{max}). The bounds of these uniformly distributed priors were: $0 < T_{min} < 24$, $26 < T_{max} < 45$
751 (quadratic) or $28 < T_{max} < 45$ (Briére), $0 < q < 1$, $-10 < m < 10$, and $0 < b < 250$. Then in step 2,
752 we fit a thermal response to data from the focal species using the high-information priors from
753 step 1.

754 Because we cannot directly pass posterior samples from JAGS as a prior, we modified
755 the results from step 1 to use them in step 2. We used the 'MASS' package [139] to fit a gamma
756 probability distribution to the posterior distributions for each thermal response parameter (T_{min},
757 T_{max}, and q [eq. 3 and 4]; or m and z [eq. 5]) obtained in step 1. The resulting gamma distribution
758 parameters can be used directly to specify the priors in the JAGS model. Because the prior
759 datasets were often very large, in many cases the priors were too strong and overdetermined the
760 fit to the focal data. In a few other cases, we had philosophical reasons to strongly constrain the
761 fit to the focal data even when they were sparse (e.g., to constrain T_{max} to very high temperatures
762 so that other traits with more information determine the upper thermal limit for R_0). Thus, we
763 deflated or inflated the variance as needed (i.e., we fixed the gamma distribution mean but
764 altered the variance by adjusting the parameters that describe the distribution accordingly). See
765 S1 Text for more details and specific variance modifications for each thermal response.

766

767 *Constructing R_0 Models*

768 When data were missing for a vector–virus pair, we used two criteria to decide which
769 thermal response to use as a substitute: 1) the ecological similarly (i.e., geographic range
770 overlap) of species with available thermal responses, and 2) how restrictive the upper and lower
771 bounds of the available thermal responses were. All else being equal, we chose the more

conservative (i.e., least restrictive) option so that R_0 would be less likely to be determined by trait thermal responses that did not originate from the focal species. See S1 Text for more information about specific models.

When there was more than one option for how to parameterize a model (e.g., vector competence data for WEEV in *Cx. tarsalis* were available in two forms: separately as *b* and *c,* and combined as *bc*), we calculated R_0 both ways. The results were very similar, except for the model for RVFV with lifespan data from *Cx. pipiens* lifespan in place of *Ae. taeniorhynchus* (Fig S21). See S1 Text for sensitivity and uncertainty methods and S1 Fig S11-20 for results.

Model validation: spatial analysis

We obtained county-level neuroinvasive WNV disease data from 2001-2016 for the contiguous US (n = 3,109) through the CDC's county-level disease monitoring program [140]. Data were available as total human cases per year, which we adjusted to average cases per 1,000 people (using 2010 US county-level census data) to account for population differences. We averaged cases across years beginning with the first year that had reported cases in a given county to account for the initial spread of WNV and the strong impact of immunity on interannual variation [5]. Ninety-eight percent of human cases of WNV in the US occur between June and October (data described below), and cases of mosquito-borne disease often lag behind temperature by 1–2 months [6,66]. Thus, we extracted monthly mean temperature data between the months of May–September for all years between 2001-2016 and averaged the data to estimate typical summer conditions for each county. Specifically, we took the centroid geographic coordinate for every county in the contiguous US with the 'rgeos' package [141] and

794 extracted corresponding historic climate data (Climate Research Unit 3.1 rasters) [142] from
795 $0.5°^2$ cells (approx. 2,500-3,000 km^2) using the 'raster' package [143].
796 We fit a generalized additive model (GAM) for average incidence as a function of
797 average summer temperature using the 'mgcv' package [144]. We used a gamma distribution
798 with a log-link function to restrict incidence to positive values and capture heteroskedasticity in
799 the data (i.e., higher variance with higher predicted means), adding a small, near-zero constant
800 (0.0001) to all incidence values to allow the log-transformation for counties with zero incidence.
801 GAMs use additive functions of smooth predictor effects to fit responses that are extremely
802 flexible in the shape of the response. We restricted the number of knots to minimize overfitting
803 ($k = 5$; see Fig S24 for results across varying values of k). For comparison, we also used the
804 'loess' function in base R 'stats' package [82] to fit locally estimated scatterplot smoothing
805 (LOESS) regressions of the same data. LOESS regression is a simpler but similarly flexible
806 method for estimating the central tendency of data. See Fig S25 for LOESS model results.
807
808 *Model validation: seasonality analysis*
809 We calculated monthly temperature-dependent relative R_0 to compare with month-of-
810 onset data for neuro-invasive WNV, EEEV, and SLEV disease aggregated nationwide from
811 2001-2016 [140,145,146], using the same monthly, county-level temperature data as above. For
812 WNV, we used the subset of counties with reported cases (68% of counties). For SLEV and
813 EEEV we used all counties from states with reported cases (16 and 20 states, respectively). We
814 weighted each county $R_0(T)$ by its population size to calculate a national estimate of $R_0(T)$. For
815 WNV, the county-level estimates of $R_0(T)$ used models for three *Culex* species (*Cx. pipiens*, *Cx.*
816 *quinquefasciatus*, and *Cx. tarsalis*) weighted according to the proportion of WNV-positive

817 mosquitoes reported at the state level, reported in [5]. SLEV and EEEV both only had one R_0
818 model. The estimated monthly temperature-dependent relative R_0 values and month-of-onset data
819 were compared visually.
820
821 *Funding*
822 EAM, MSS, JC, LRJ, and MN were supported by the National Science Foundation (NSF,
823 DEB-1518681; https://nsf.gov/). LRJ was supported by the NSF (DMS-1750113). AV and MN
824 were supported by the Stanford Vice Provost for Undergraduate Education Summer Research
825 Program in the Biology Department; MN was supported by the Introductory Seminars Program
826 at Stanford University. HS was supported by a Luther and Alice Hamlett Undergraduate
827 Research Scholarship at Virginia Tech. EAM was also supported by the National Institutes of
828 Health (NIGMS R35 MIRA: 1R35GM133439-01), Stanford Woods Institute for the
829 Environment (https://woods.stanford.edu/research/environmental-venture-projects), the Hellman
830 Fellowship (http://www.hellmanfellows.org/), and the Terman Fellowship.
831
832 *Acknowledgements*
833 We gratefully acknowledge the students of the Spring 2017 Stanford University
834 Introductory Seminar course BIO 2N: Global Change and the Ecology and Evolution of
835 Infectious Diseases, who helped with preliminary literature searches, data collection, and model
836 fitting: Uche Amakiri, Michelle Bach, Isabelle Carpenter, Phillip Cathers, Audriana Fitzmorris,
837 Alex Fuentes, Margaux Giles, Gillian Gittler, Emma Leads Armstrong, Erika Malaspina, Elise
838 Most, Stephen Moye, Jackson Rudolph, Simone Speizer, William Wang, and Ethan Wentworth.
839 We thank the Stanford University Introductory Seminars program for support. We thank

840 Michelle Evans for creating Figure 2. We thank Marc Fischer, Nicole Lindsey, and Lyle
841 Peterson at the CDC for providing the month-of-onset case data, and Sara Paull for providing
842 state-level data for proportion of WNV vectors. We thank Nicholas Skaff for guidance with
843 EEEV vector ecology.
844
845 *Competing interests*: The authors declare that they have no competing interests.

846 **REFERENCES**

847

848 1. Rogers DJ, Randolph SE. Climate Change and Vector-Borne Diseases. Advances in
849 Parasitology. 2006;62: 345–381. doi:10.1016/S0065-308X(05)62010-6

850 2. Mordecai EA, Paaijmans KP, Johnson LR, Balzer C, Ben-Horin T, de Moor E, et al. Optimal
851 temperature for malaria transmission is dramatically lower than previously predicted.
852 Ecology letters. 2013;16: 22–30. doi:10.1111/ele.12015

853 3. Johnson LR, Ben-Horin T, Lafferty KD, McNally A, Mordecai E, Paaijmans KP, et al.
854 Understanding uncertainty in temperature effects on vector-borne disease: A Bayesian
855 approach. Ecology. 2015;96: 203–213. doi:10.1890/13-1964.1

856 4. Mordecai EA, Cohen JM, Evans MV, Gudapati P, Johnson LR, Lippi CA, et al. Detecting
857 the impact of temperature on transmission of Zika, dengue, and chikungunya using
858 mechanistic models. PLoS Neglected Tropical Diseases. 2017;11: e0005568.
859 doi:10.1371/journal.pntd.0005568

860 5. Paull SH, Horton DE, Ashfaq M, Rastogi D, Kramer LD, Diffenbaugh NS, et al. Drought
861 and immunity determine the intensity of West Nile virus epidemics and climate change
862 impacts. Proceedings of the Royal Society B: Biological Sciences. 2017;284: 20162078.
863 doi:10.1098/rspb.2016.2078

864 6. Shocket MS, Ryan SJ, Mordecai EA. Temperature explains broad patterns of Ross River
865 virus transmission. eLife. 2018;7: e37762. doi:10.7554/eLife.37762

866 7. Tesla B, Demakovsky LR, Mordecai EA, Ryan SJ, Bonds MH, Ngonghala CN, et al.
867 Temperature drives Zika virus transmission: evidence from empirical and mathematical
868 models. Proceedings of the Royal Society B: Biological Sciences. 2018;285: 20180795.
869 doi:10.1098/rspb.2018.0795

870 8. Mordecai EA, Caldwell JM, Grossman MK, Lippi CA, Johnson LR, Neira M, et al. Thermal
871 biology of mosquito-borne disease. Ecology Letters. 2019;22: 1690–1708.
872 doi:10.1111/ele.13335

873 9. Martens WJM, Jetten TH, Focks DA. Sensitivity of malaria, schistosomiasis and dengue to
874 global warming. Climatic Change. 1997;35: 145–156. doi:10.1023/A:1005365413932

875 10. Parham PE, Michael E. Modeling the effects of weather and climate change on malaria
876 transmission. Environmental Health Perspectives. 2010;118: 620–626.
877 doi:10.1289/ehp.0901256

878 11. Liu-Helmersson J, Stenlund H, Wilder-Smith A, Rocklöv J. Vectorial capacity of *Aedes*
879 *aegypti*: Effects of temperature and implications for global dengue epidemic potential. PLoS
880 ONE. 2014;9. doi:10.1371/journal.pone.0089783

12. Wesolowski A, Qureshi T, Boni MF, Sundsøy PR, Johansson MA, Rasheed SB, et al. Impact of human mobility on the emergence of dengue epidemics in Pakistan. Proceedings of the National Academy of Sciences. 2015;112: 11887–11892. doi:10.1073/pnas.1504964112

13. Siraj AS, Bouma MJ, Santos-Vega M, Yeshiwondim AK, Rothman DS, Yadeta D, et al. Temperature and population density determine reservoir regions of seasonal persistence in highland malaria. Proceedings of the Royal Society B: Biological Sciences. 2015;282: 20151383. doi:10.1098/rspb.2015.1383

14. Werner AK, Goater S, Carver S, Robertson G, Allen GR, Weinstein P. Environmental drivers of Ross River virus in southeastern Tasmania, Australia: towards strengthening public health interventions. Epidemiology and Infection. 2012;140: 359–371. doi:10.1017/S0950268811000446

15. Lowe R, Stewart-Ibarra AM. Climate and Non-Climate Drivers of Dengue Epidemics in Southern Coastal Ecuador. The American Journal of Tropical Medicine and Hygiene. 2013;88: 971–981. doi:10.4269/ajtmh.12-0478

16. Peña-García VH, Triana-Chávez O, Arboleda-Sánchez S. Estimating Effects of Temperature on Dengue Transmission in Colombian Cities. Annals of Global Health. 2017;83: 509. doi:10.1016/j.aogh.2017.10.011

17. Perkins TA, Metcalf CJE, Grenfell BT, Tatem AJ. Estimating Drivers of Autochthonous Transmission of Chikungunya Virus in its Invasion of the Americas. PLoS Currents. 2015;7. doi:10.1371/currents.outbreaks.a4c7b6ac10e0420b1788c9767946d1fc

18. Gatton ML, Kay BH, Ryan PA. Environmental predictors of Ross River virus disease outbreaks in Queensland, Australia. Am J Trop Med Hyg. 2005;72: 792–799. doi:72/6/792 [pii]

19. Shah MM, Krystosik AR, Ndenga BA, Mutuku FM, Caldwell JM, Otuka V, et al. Malaria smear positivity among Kenyan children peaks at intermediate temperatures as predicted by ecological models. Parasites & Vectors. 2019;12: 288. doi:10.1186/s13071-019-3547-z

20. Lafferty KD. The ecology of climate change and infectious diseases. Ecology. 2009;90: 888–900. doi:10.1890/09-1656.1

21. Rohr JR, Dobson AP, Johnson PTJ, Kilpatrick AM, Paull SH, Raffel TR, et al. Frontiers in climate change-disease research. Trends in Ecology & Evolution. 2011;26: 270–277. doi:10.1016/j.tree.2011.03.002

22. Lafferty KD, Mordecai EA. The rise and fall of infectious disease in a warmer world. F1000Research. 2016;5: 2040. doi:10.12688/f1000research.8766.1

23. Ryan SJ, McNally A, Johnson LR, Mordecai EA, Ben-Horin T, Paaijmans KP, et al. Mapping physiological suitability limits for malaria in Africa under climate change. Vector borne and zoonotic diseases. 2015;15: 718–25. doi:10.1089/vbz.2015.1822

24. Kilpatrick AM. Globalization, Land Use, and the Invasion of West Nile Virus. Science. 2011;334: 323–327. doi:10.1126/science.1201010

25. Weaver SC, Barrett ADT. Transmission cycles, host range, evolution and emergence of arboviral disease. Nature Reviews Microbiology. 2004;2: 789–801. doi:10.1038/nrmicro1006

26. Adouchief S, Smura T, Sane J, Vapalahti O, Kurkela S. Sindbis virus as a human pathogen-epidemiology, clinical picture and pathogenesis: Sindbis virus as a human pathogen. Reviews in Medical Virology. 2016;26: 221–241. doi:10.1002/rmv.1876

27. Linthicum KJ, Britch SC, Anyamba A. Rift Valley Fever: An Emerging Mosquito-Borne Disease. Annual Review of Entomology. 2016;61: 395–415. doi:10.1146/annurev-ento-010715-023819

28. Go YY, Balasuriya UBR, Lee C. Zoonotic encephalitides caused by arboviruses: transmission and epidemiology of alphaviruses and flaviviruses. Clinical and Experimental Vaccine Research. 2014;3: 58. doi:10.7774/cevr.2014.3.1.58

29. Centers for Disease Control and Prevention. St. Louis Encephalitis: Statistics and Maps. 2018 Dec. Available: https://www.cdc.gov/sle/technical/epi.html

30. Centers for Disease Control and Prevention. Eastern Equine Encephalitis: Epidemiology & Geographic Distribution. 2018 Sep. Available: https://www.cdc.gov/easternequineencephalitis/tech/epi.html

31. Bates S. Rare eastern equine encephalitis has killed 9 people in the U.S. in 2019. Science News. 1 Oct 2019. Available: https://www.sciencenews.org/article/rare-disease-eastern-equine-encephalitis-killed-nine-people-2019

32. Sang R, Arum S, Chepkorir E, Mosomtai G, Tigoi C, Sigei F, et al. Distribution and abundance of key vectors of Rift Valley fever and other arboviruses in two ecologically distinct counties in Kenya. Bird B, editor. PLoS Neglected Tropical Diseases. 2017;11: e0005341. doi:10.1371/journal.pntd.0005341

33. Harley D, Sleigh A, Ritchie S. Ross River Virus Transmission, Infection, and Disease: a Cross-Disciplinary Review. Clinical Microbiology Reviews. 2001;14: 909–932. doi:10.1128/CMR.14.4.909

34. Gonçalves BP, Kapulu MC, Sawa P, Guelbéogo WM, Tiono AB, Grignard L, et al. Examining the human infectious reservoir for Plasmodium falciparum malaria in areas of differing transmission intensity. Nature Communications. 2017;8. doi:10.1038/s41467-017-01270-4

35. Farajollahi A, Fonseca DM, Kramer LD, Marm Kilpatrick A. “Bird biting” mosquitoes and human disease: A review of the role of Culex pipiens complex mosquitoes in epidemiology. Infection, Genetics and Evolution. 2011;11: 1577–1585. doi:10.1016/j.meegid.2011.08.013

36. Diekmann O, Heesterbeek JAP, Roberts MG. The construction of next-generation matrices for compartmental epidemic models. Journal of the Royal Society Interface. 2010;7: 873–885. doi:10.1098/rsif.2009.0386

37. Dietz K. The estimation of the basic reproduction number for infectious diseases. Statistical Methods in Medical Research. 1993;2: 23–41. doi:10.1177/096228029300200103

38. Paaijmans KP, Blanford S, Bell AS, Blanford JI, Read AF, Thomas MB. Influence of climate on malaria transmission depends on daily temperature variation. Proceedings of the National Academy of Sciences of the United States of America. 2010;107: 15135–9. doi:10.1073/pnas.1006422107

39. Murdock C, Evans M, McClanahan T, Miazgowicz K, Tesla B. Fine-scale variation in microclimate across and urban landscape changes the capacity of *Aedes albopictus* to vector arboviruses. PLoS Neglected Tropical Diseases. 2017;11: e0005640. doi:10.5061/dryad.s3953

40. Huber JH, Childs ML, Caldwell JM, Mordecai EA. Seasonal temperature variation influences climate suitability for dengue, chikungunya, and Zika transmission. Althouse B, editor. PLoS Neglected Tropical Diseases. 2018;12: e0006451. doi:10.1371/journal.pntd.0006451

41. Lambrechts L, Paaijmans KP, Fansiri T, Carrington LB, Kramer LD, Thomas MB, et al. Impact of daily temperature fluctuations on dengue virus transmission by *Aedes aegypti*. Proceedings of the National Academy of Sciences. 2011;108: 7460–7465. doi:10.1073/pnas.1101377108

42. Bacaër N. Approximation of the Basic Reproduction Number R 0 for Vector-Borne Diseases with a Periodic Vector Population. Bulletin of Mathematical Biology. 2007;69: 1067–1091. doi:10.1007/s11538-006-9166-9

43. Bacaër N, Ait Dads EH. On the biological interpretation of a definition for the parameter R 0 in periodic population models. Journal of Mathematical Biology. 2012;65: 601–621. doi:10.1007/s00285-011-0479-4

44. Bacaër N, Guernaoui S. The epidemic threshold of vector-borne diseases with seasonality: The case of cutaneous leishmaniasis in Chichaoua, Morocco. Journal of Mathematical Biology. 2006;53: 421–436. doi:10.1007/s00285-006-0015-0

45. Briere J-F, Pracros P, Le Roux A-Y, Pierre J-S. A Novel Rate Model of Temperature-Dependent Development for Arthropods. Environmental Entomology. 1999;28: 22–29. doi:10.1093/ee/28.1.22

46. Amarasekare P, Savage V. A Framework for Elucidating the Temperature Dependence of Fitness. The American Naturalist. 2012;179: 178–191. doi:10.1086/663677

47. Vinogradova EB. *Culex pipiens pipiens* mosquitoes taxonomy, distribution, ecology, physiology, genetics, applied importance and control. Sofia: Pensoft; 2000.

990 48. Nelms BM, Macedo PA, Kothera L, Savage HM, Reisen WK. Overwintering biology of
991 Culex (Diptera: Culicidae) mosquitoes in the Sacramento Valley of California. J Med
992 Entomol. 2013;50: 773–790.

993 49. Diniz DFA, de Albuquerque CMR, Oliva LO, de Melo-Santos MAV, Ayres CFJ. Diapause
994 and quiescence: dormancy mechanisms that contribute to the geographical expansion of
995 mosquitoes and their evolutionary success. Parasites & Vectors. 2017;10.
996 doi:10.1186/s13071-017-2235-0

997 50. Urbanski JM, Benoit JB, Michaud MR, Denlinger DL, Armbruster P. The molecular
998 physiology of increased egg desiccation resistance during diapause in the invasive mosquito,
999 Aedes albopictus. Proceedings of the Royal Society B: Biological Sciences. 2010;277: 2683–
1000 2692. doi:10.1098/rspb.2010.0362

1001 51. Deutsch CA, Tewksbury JJ, Huey RB, Sheldon KS, Ghalambor CK, Haak DC, et al. Impacts
1002 of climate warming on terrestrial ectotherms across latitude. Proceedings of the National
1003 Academy of Sciences. 2008;105: 6668–6672. doi:10.1073/pnas.0709472105

1004 52. Sunday JM, Bates AE, Dulvy NK. Global analysis of thermal tolerance and latitude in
1005 ectotherms. Proceedings of the Royal Society B: Biological Sciences. 2011;278: 1823–1830.
1006 doi:10.1098/rspb.2010.1295

1007 53. Overgaard J, Kearney MR, Hoffmann AA. Sensitivity to thermal extremes in Australian
1008 *Drosophila* implies similar impacts of climate change on the distribution of widespread and
1009 tropical species. Global Change Biology. 2014;20: 1738–1750. doi:10.1111/gcb.12521

1010 54. Hay SI, Guerra CA, Tatem AJ, Noor AM, Snow RW. The global distribution and population
1011 at risk of malaria: past, present, and future. The Lancet Infectious Diseases. 2004;4: 327–
1012 336. doi:10.1016/S1473-3099(04)01043-6

1013 55. Brathwaite Dick O, San Martín JL, Montoya RH, del Diego J, Zambrano B, Dayan GH. The
1014 History of Dengue Outbreaks in the Americas. The American Journal of Tropical Medicine
1015 and Hygiene. 2012;87: 584–593. doi:10.4269/ajtmh.2012.11-0770

1016 56. Reisen WK, Fang Y, Martinez VM. Effects of Temperature on the Transmission of West
1017 Nile Virus by *Culex tarsalis* (Diptera: Culicidae). Journal of Medical Entomology. 2006;43:
1018 309–317. doi:10.1603/0022-2585(2006)043[0309:EOTOTT]2.0.CO;2

1019 57. Platonov AE, Fedorova MV, Karan LS, Shopenskaya TA, Platonova OV, Zhuravlev VI.
1020 Epidemiology of West Nile infection in Volgograd, Russia, in relation to climate change and
1021 mosquito (Diptera: Culicidae) bionomics. Parasitology Research. 2008;103: 45–53.
1022 doi:10.1007/s00436-008-1050-0

1023 58. Hahn MB, Monaghan AJ, Hayden MH, Eisen RJ, Delorey MJ, Lindsey NP, et al.
1024 Meteorological Conditions Associated with Increased Incidence of West Nile Virus Disease
1025 in the United States, 2004–2012. The American Journal of Tropical Medicine and Hygiene.
1026 2015;92: 1013–1022. doi:10.4269/ajtmh.14-0737

1027 59. Marcantonio M, Rizzoli A, Metz M, Rosà R, Marini G, Chadwick E, et al. Identifying the
1028 Environmental Conditions Favouring West Nile Virus Outbreaks in Europe. Gourbiere S,
1029 editor. PLoS ONE. 2015;10: e0121158. doi:10.1371/journal.pone.0121158

1030 60. Ahmadnejad F, Otarod V, Fathnia A, Ahmadabadi A, Fallah MH, Zavareh A, et al. Impact of
1031 Climate and Environmental Factors on West Nile Virus Circulation in Iran. J Arthropod
1032 Borne Dis. 2016;10: 315–327.

1033 61. Semenza JC, Tran A, Espinosa L, Sudre B, Domanovic D, Paz S. Climate change projections
1034 of West Nile virus infections in Europe: implications for blood safety practices.
1035 Environmental Health. 2016;15. doi:10.1186/s12940-016-0105-4

1036 62. Shand L, Brown WM, Chaves LF, Goldberg TL, Hamer GL, Haramis L, et al. Predicting
1037 West Nile Virus Infection Risk From the Synergistic Effects of Rainfall and Temperature.
1038 Journal of Medical Entomology. 2016;53: 935–944. doi:10.1093/jme/tjw042

1039 63. Brummer-Korvenkontio M, Vapalahti O, Kuusisto P, Saikku P, Manni T, Koskela P, et al.
1040 Epidemiology of Sindbis virus infections in Finland 1981–96: possible factors explaining a
1041 peculiar disease pattern. Epidemiology and Infection. 2002;129.
1042 doi:10.1017/S0950268802007409

1043 64. Jalava K, Sane J, Ollgren J, Ruuhela R, Rätti O, Kurkela S, et al. Climatic, ecological and
1044 socioeconomic factors as predictors of Sindbis virus infections in Finland. Epidemiology and
1045 Infection. 2013;141: 1857–1866. doi:10.1017/S095026881200249X

1046 65. Mallya S, Sander B, Roy-Gagnon M-H, Taljaard M, Jolly A, Kulkarni MA. Factors
1047 associated with human West Nile virus infection in Ontario: a generalized linear mixed
1048 modelling approach. BMC Infectious Diseases. 2018;18. doi:10.1186/s12879-018-3052-6

1049 66. Stewart Ibarra AM, Ryan SJ, Beltrán E, Mejía R, Silva M, Muñoz Á. Dengue Vector
1050 Dynamics (*Aedes aegypti*) Influenced by Climate and Social Factors in Ecuador:
1051 Implications for Targeted Control. Mores CN, editor. PLoS ONE. 2013;8: e78263.
1052 doi:10.1371/journal.pone.0078263

1053 67. Jacups SP, Whelan PI, Markey PG, Cleland SJ, Williamson GJ, Currie BJ. Predictive
1054 indicators for Ross River virus infection in the Darwin area of tropical northern Australia,
1055 using long-term mosquito trapping data. Tropical Medicine and International Health.
1056 2008;13: 943–952. doi:10.1111/j.1365-3156.2008.02095.x

1057 68. Hu W, Tong S, Mengersen K, Oldenburg B. Rainfall, mosquito density and the transmission
1058 of Ross River virus: A time-series forecasting model. Ecological Modelling. 2006;196: 505–
1059 514. doi:10.1016/j.ecolmodel.2006.02.028

1060 69. Kilpatrick AM, Kramer LD, Jones MJ, Marra PP, Daszak P. West Nile Virus Epidemics in
1061 North America Are Driven by Shifts in Mosquito Feeding Behavior. Ostfeld R, editor. PLoS
1062 Biology. 2006;4: e82. doi:10.1371/journal.pbio.0040082

1063 70. Hess AD, Cherubin CE, Lamotte LC. Relation of Temperature to Activity of Western and St.
1064 Louis Encephalitis Viruses *. The American Journal of Tropical Medicine and Hygiene.
1065 1963;12: 657–667. doi:10.4269/ajtmh.1963.12.657

1066 71. Anyamba A, Chretien J-P, Small J, Tucker CJ, Formenty PB, Richardson JH, et al.
1067 Prediction of a Rift Valley fever outbreak. Proceedings of the National Academy of
1068 Sciences. 2009;106: 955–959. doi:10.1073/pnas.0806490106

1069 72. Linthicum KJ, Anyamba A, Tucker CJ, Kelley PW, Myers MF, Peters CJ. Climate and
1070 satellite indicators to forecast Rift Valley fever epidemics in Kenya. Science. 1999;285: 397–
1071 400.

1072 73. Vogels CBF, Hartemink N, Koenraadt CJM. Modelling West Nile virus transmission risk in
1073 Europe: effect of temperature and mosquito biotypes on the basic reproduction number.
1074 Scientific Reports. 2017;7. doi:10.1038/s41598-017-05185-4

1075 74. Kushmaro A, Friedlander TA, Levins R. Temperature Effects on the Basic Reproductive
1076 Number (R0) Of West Nile Virus, Based On Ecological Parameters: Endemic Vs. New
1077 Emergence Regions. Journal of Tropical Diseases. 2015;s1. doi:10.4172/2329-891X.1000S1-
1078 001

1079 75. Molnár PK, Kutz SJ, Hoar BM, Dobson AP. Metabolic approaches to understanding climate
1080 change impacts on seasonal host-macroparasite dynamics. Ecology letters. 2013;16: 9–21.
1081 doi:10.1111/ele.12022

1082 76. Braack L, Gouveia de Almeida AP, Cornel AJ, Swanepoel R, de Jager C. Mosquito-borne
1083 arboviruses of African origin: review of key viruses and vectors. Parasites & Vectors.
1084 2018;11. doi:10.1186/s13071-017-2559-9

1085 77. Kilpatrick AM, Ebel GD, Reddy MR, Fonseca DM, Kramer LD. Spatial and Temporal
1086 Variation in Vector Competence of Culex pipiens and Cx. restuans Mosquitoes for West Nile
1087 Virus. The American Journal of Tropical Medicine and Hygiene. 2010;83: 607–613.
1088 doi:10.4269/ajtmh.2010.10-0005

1089 78. Intergovernmental Panel on Climate Change. Climate Change 2014: Synthesis Report.
1090 Contribution of Working Groups I, II and III to the Fifth Assessment. Geneva, Switzerland:
1091 IPCC; 2014 pp. 1–151.

1092 79. Bernhardt JR, Sunday JM, Thompson PL, O'Connor MI. Nonlinear averaging of thermal
1093 experience predicts population growth rates in a thermally variable environment.
1094 Proceedings of the Royal Society B: Biological Sciences. 2018;285: 20181076.
1095 doi:10.1098/rspb.2018.1076

1096 80. Kilpatrick AM, Meola MA, Moudy RM, Kramer LD. Temperature, viral genetics, and the
1097 transmission of West Nile virus by *Culex pipiens* mosquitoes. PLoS Pathogens. 2008;4.
1098 doi:10.1371/journal.ppat.1000092

81. Ruybal JE, Kramer LD, Kilpatrick AM. Geographic variation in the response of *Culex pipiens* life history traits to temperature. Parasites & Vectors. 2016;9. doi:10.1186/s13071-016-1402-z

82. R Core Team. R: A language and for statistical computing. Vienna, Austria: R Foundation for Statistical Computing; 2016.

83. Smith JL, Fonseca DM. Rapid assays for identification of members of the Culex (Culex) pipiens complex, their hybrids, and other sibling species (Diptera: culicidae). Am J Trop Med Hyg. 2004;70: 339–345.

84. Darsie Jr, Richard F, Ward, Ronald A. Identification and Geographical Distribution of the Mosquitoes of North America, North of Mexico. University Press of Florida; 2016.

85. Huerta Jiménez H. Actualización de la Colección de Artrópodos con importancia médica (CAIM), Laboratorio de Entomología, InDRE. Comisión nacional para el conocimiento y uso de la biodiversidad; 2018. doi:10.15468/y2rff2

86. López Cárdenas J. Apoyo para la infraestructura de la colección de artrópodos con y sin importancia médica del Laboratorio estatal de Salud Pública del estado de Guanajuato. Comisión nacional para el conocimiento y uso de la biodiversidad; 2018. doi:10.15468/5mjcse

87. Ortega Morales AI. Catálogo digital y clave ilustrada de los mosquitos (Diptera: Culicidae) de las zonas áridas de los estados de Nuevo León y Tamaulipas, México. Comisión nacional para el conocimiento y uso de la biodiversidad; 2018. doi:10.15468/otexwf

88. Ponce García G. Computarización de la Colección de insectos y ácaros de importancia médica de la Facultad de Ciencias Biológicas, Universidad Autónoma de Nuevo León. Comisión nacional para el conocimiento y uso de la biodiversidad; 2018. doi:10.15468/sma9a5

89. Walter Reed Biosystematics Unit. Mosquito Occurrence Dataset. Smithsonian Institution; 2018. doi:10.15468/tw2y9b

90. Andreadis SS, Dimotsiou OC, Savopoulou-Soultani M. Variation in adult longevity of *Culex pipiens f. pipiens*, vector of the West Nile Virus. Parasitology Research. 2014;113: 4315–4319. doi:10.1007/s00436-014-4152-x

91. Brust RA. WEIGHT AND DEVELOPMENT TIME OF DIFFERENT STADIA OF MOSQUITOES REARED AT VARIOUS CONSTANT TEMPERATURES. The Canadian Entomologist. 1967;99: 986–993. doi:10.4039/Ent99986-9

92. Buth JL, Brust RA, Ellis RA. Development time, oviposition activity and onset of diapause in *Culex tarsalis*, *Culex restuans* and *Culiseta inornata* in southern Manitoba. J Am Mosq Control Assoc. 1990;6: 55–63.

1134 93. Chamberlain RW, Sudia WD. The effects of temperature upon the extrinsic incubation of
1135 eastern equine encephalitis in mosquitoes. Am J Hyg. 1955;62: 295–305.

1136 94. Ciota AT, Matacchiero AC, Kilpatrick AM, Kramer LD. The Effect of Temperature on Life
1137 History Traits of *Culex* Mosquitoes. Journal of Medical Entomology. 2014;51: 55–62.
1138 doi:10.1603/ME13003

1139 95. Cornel AJ, Jupp PG, Blackburn NK. Environmental Temperature on the Vector Competence
1140 of *Culex univittatus* (Diptera: Culicidae) for West Nile Virus. Journal of Medical
1141 Entomology. 1993;30: 449–456. doi:10.1093/jmedent/30.2.449

1142 96. Dodson BL, Kramer LD, Rasgon JL. Effects of larval rearing temperature on immature
1143 development and West Nile virus vector competence of *Culex tarsalis*. Parasites & Vectors.
1144 2012;5: 199. doi:10.1186/1756-3305-5-199

1145 97. Dohm DJ, O'Guinn ML, Turell MJ. Effect of environmental temperature on the ability of
1146 *Culex pipiens* (Diptera: Culicidae) to transmit West Nile virus. Journal of Medical
1147 Entomology. 2002;39: 221–225. doi:10.1603/0022-2585-39.1.221

1148 98. Kramer LD, Hardy JL, Presser SB. Effect of temperature of extrinsic incubation on the
1149 vector competence of *Culex tarsalis* for western equine encephalomyelitis virus. Am J Trop
1150 Med Hyg. 1983;32: 1130–1139.

1151 99. Li J, Zhu G, Zhou H, Tang J, Cao J. Effect of temperature on the development of *Culex*
1152 *pipiens pallens*. Chin J Vector Biol & Control. 2017;28: 35–37.

1153 100. Loetti V, Schweigmann N, Burroni N. Development rates, larval survivorship and wing
1154 length of *Culex pipiens* (Diptera: Culicidae) at constant temperatures. Journal of Natural
1155 History. 2011;45: 2203–2213. doi:10.1080/00222933.2011.590946

1156 101. Lundström JO, Turell MJ, Niklasson B. Effect of environmental temperature on the
1157 vector competence of *Culex pipiens and Cx. torrentium* for Ockelbo virus. Am J Trop Med
1158 Hyg. 1990;43: 534–542.

1159 102. Madder DJ, Surgeoner GA, Helson BV. Number of generations, egg production, and
1160 developmental time of Culex pipiens and Culex restauns (Diptera: Culicidae) in southern
1161 Ontario. J Med Entomol. 1983;20: 275–287.

1162 103. Mahmood F, Crans WJ. A thermal heat summation model to predict the duration of the
1163 gonotrophic cycle of Culiseta melanura in nature. J Am Mosq Control Assoc. 1997;13: 92–
1164 94.

1165 104. Mahmood F, Crans WJ. Effect of temperature on the development of Culiseta melanura
1166 (Diptera: Culicidae) and its impact on the amplification of eastern equine encephalomyelitis
1167 virus in birds. J Med Entomol. 1998;35: 1007–1012.

1168 105. McHaffey DG. Photoperiod and temperature influences on diapause in eggs of the
1169 floodwater mosquito *Aedes vexans* (Meigen) (Diptera: Culicidae). J Med Entomol. 1972;9:
1170 564–571.

1171 106. Mogi M. Temperature and Photoperiod Effects on Larval and Ovarian Development of
1172 New Zealand Strains of *Culex quinquefasciatus* (Diptera: Culicidae). Annals of the
1173 Entomological Society of America. 1992;85: 58–66. doi:10.1093/aesa/85.1.58

1174 107. Mpho M, Holloway GJ, Callaghan A. A comparison of the effects of organophosphate
1175 insecticide exposure and temperature stress on fluctuating asymmetry and life history traits
1176 in *Culex quinquefasciatus*. Chemosphere. 2001;45: 713–720.

1177 108. Mpho M, Callaghan A, Holloway GJ. Temperature and genotypic effects on life history
1178 and fluctuating asymmetry in a field strain of *Culex pipiens*. Heredity. 2002;88: 307–312.
1179 doi:10.1038/sj.hdy.6800045

1180 109. Mpho M, Callaghan A, Holloway GJ. Effects of temperature and genetic stress on life
1181 history and fluctuating wing asymmetry in *Culex pipiens* mosquitoes. European Journal of
1182 Entomology. 2002;99: 405–412. doi:10.14411/eje.2002.050

1183 110. Nayar JK. Effects of constant and fluctuating temperatures on life span of *Aedes*
1184 *taeniorhynchus* adults. Journal of Insect Physiology. 1972;18: 1303–1313.
1185 doi:10.1016/0022-1910(72)90259-4

1186 111. Oda T, Mori A, Ueda M, Kurokawa K, others. Effects of temperatures on the oviposition
1187 and hatching of eggs in *Culex pipiens molestus* and *Culex pipiens quinquefasciatus*. Tropical
1188 Medicine. 1980;22: 167–180.

1189 112. Oda T, Uchida K, Mori A, Mine M, Eshita Y, Kurokawa K, et al. Effects of high
1190 temperature on the emergence and survival of adult *Culex pipiens molestus* and *Culex*
1191 *quinquefasciatus* in Japan. J Am Mosq Control Assoc. 1999;15: 153–156.

1192 113. Rayah EAE, Groun NAA. Effect of temperature on hatching eggs and embryonic survival
1193 in the mosquito Culex quinquefasciatus. Entomologia Experimentalis et Applicata. 1983;33:
1194 349–351. doi:10.1111/j.1570-7458.1983.tb03281.x

1195 114. Reisen WK, Milby MM, Presser SB, Hardy JL. Ecology of Mosquitoes and St. Louis
1196 Encephalitis Virus in the Los Angeles Basin of California, 1987–1990. Journal of Medical
1197 Entomology. 1992;29: 582–598. doi:10.1093/jmedent/29.4.582

1198 115. Reisen WK, Meyer RP, Presser SB, Hardy JL. Effect of temperature on the transmission
1199 of western equine encephalomyelitis and St. Louis encephalitis viruses by *Culex tarsalis*
1200 (Diptera: Culicidae). J Med Entomol. 1993;30: 151–160.

1201 116. Reisen WK. Effect of temperature on *Culex tarsalis* (Diptera: Culicidae) from the
1202 Coachella and San Joaquin Valleys of California. J Med Entomol. 1995;32: 636–645.

1203 117. Rueda LM, Patel KJ, Axtell RC, Stinner RE. Temperature-dependent development and
1204 survival rates of *Culex quinquefasciatus* and *Aedes aegypti* (Diptera: Culicidae). J Med
1205 Entomol. 1990;27: 892–898.

1206 118. Shelton RM. The effect of temperatures on development of eight mosquito species.
1207 Mosquito News. 1973;33: 1–12.

1208 119. Tekle A. The Physiology of Hibernation and Its Role in the Geographical Distribution of
1209 Populations of the *Culex Pipiens* Complex. The American Journal of Tropical Medicine and
1210 Hygiene. 1960;9: 321–330. doi:10.4269/ajtmh.1960.9.321

1211 120. Teng H-J, Apperson CS. Development and Survival of Immature *Aedes albopictus* and
1212 *Aedes triseriatus* (Diptera: Culicidae) in the Laboratory: Effects of Density, Food, and
1213 Competition on Response to Temperature. Journal of Medical Entomology. 2000;37: 40–52.
1214 doi:10.1603/0022-2585-37.1.40

1215 121. Trpiš M, Shemanchuk JA. EFFECT OF CONSTANT TEMPERATURE ON THE
1216 LARVAL DEVELOPMENT OF *AEDES VEXANS* (DIPTERA: CULICIDAE). The
1217 Canadian Entomologist. 1970;102: 1048–1051. doi:10.4039/Ent1021048-8

1218 122. Turell MJ, Rossi CA, Bailey CL. Effect of Extrinsic Incubation Temperature on the
1219 Ability of *Aedes Taeniorhynchus* and *Culex Pipiens* to Transmit Rift Valley Fever Virus.
1220 The American Journal of Tropical Medicine and Hygiene. 1985;34: 1211–1218.
1221 doi:10.4269/ajtmh.1985.34.1211

1222 123. Turell MJ, Lundström JO. Effect of environmental temperature on the vector competence
1223 of *Aedes aegypti* and *Ae. taeniorhynchus* for Ockelbo virus. Am J Trop Med Hyg. 1990;43:
1224 543–550.

1225 124. van der Linde TC de K, Hewitt PH, Nel A, van der Westhuizen MC. Development rates
1226 and percentage hatching of Culex (Culex) theileri; Theobald (Diptera: Culicidae) eggs at
1227 various constant temperatures. Journal of the Entomological Society of Southern Africa,.
1228 1990;53: 17–26.

1229 125. Rohatgi A. WebPlotDigitizer. 2018. Available: https://automeris.io/WebPlotDigitizer

1230 126. Vogels CBF, Fros JJ, Göertz GP, Pijlman GP, Koenraadt CJM. Vector competence of
1231 northern European Culex pipiens biotypes and hybrids for West Nile virus is differentially
1232 affected by temperature. Parasites & Vectors. 2016;9. doi:10.1186/s13071-016-1677-0

1233 127. Fros JJ, Geertsema C, Vogels CB, Roosjen PP, Failloux A-B, Vlak JM, et al. West Nile
1234 Virus: High Transmission Rate in North-Western European Mosquitoes Indicates Its
1235 Epidemic Potential and Warrants Increased Surveillance. Liang S, editor. PLoS Neglected
1236 Tropical Diseases. 2015;9: e0003956. doi:10.1371/journal.pntd.0003956

1237 128. Su Y-S, Yajima M. R2jags: A Package for Running jags from R. 2009.

129. Plummer M. JAGS: A program for analysis of Bayesian graphical models using Gibbs sampling. Proceedings of the 3rd International Workshop on Distributed Statistical Computing. 2003; 1–10. doi:ISSN 1609-395X

130. Spiegelhalter D, Thomas A, Best N, Lunn D. WinBUGS user manual. 2003.

131. Gilks WR, Richardson S, Spiegelhalter DJ, editors. Markov chain Monte Carlo in practice. Boca Raton, Fla: Chapman & Hall; 1998.

132. Spiegelhalter DJ, Best NG, Carlin BP, van der Linde A. Bayesian measures of model complexity and fit. Journal of the Royal Statistical Society: Series B (Statistical Methodology). 2002;64: 583–639. doi:10.1111/1467-9868.00353

133. Kiarie-Makara MW, Ngumbi PM, Lee D-K. Effects of Temperature on the Growth and Development of *Culex pipiens* Complex Mosquitoes (Diptera: Culicidae). Journal of Pharmacy and Biological Sciences. 2015;10: 1–10.

134. McHaffey DG, Harwood RF. Photoperiod and Temperature Influences on Diapause in Eggs of the Floodwater Mosquito, *Aedes Dorsalis* (Meigen) (Diptera: Culicidae)1. Journal of Medical Entomology. 1970;7: 631–644. doi:10.1093/jmedent/7.6.631

135. McHaffey DG. Photoperiod and temperature influences on diapause in eggs of the floodwater mosquito *Aedes nigromaculis* (Ludlow) (Diptera : Culicidae). Mosquito News. 1972;32: 51–61.

136. Muturi EJ, Lampman R, Costanzo K, Alto BW. Effect of Temperature and Insecticide Stress on Life-History Traits of Culex restuans and Aedes albopictus (Diptera: Culicidae). Journal of Medical Entomology. 2011;48: 243–250. doi:10.1603/ME10017

137. Olejnícek J, Gelbic I. Differences in response to temperature and density between two strains of the mosquito, *Culex pipiens molestus* forskal. J Vector Ecol. 2000;25: 136–145.

138. Parker BM. Temperature and Salinity as Factors Influencing the Size and Reproductive Potentials of *Aedes dorsalis* (Diptera: Culicidae). Annals of the Entomological Society of America. 1982;75: 99–102. doi:10.1093/aesa/75.1.99

139. Venables WN, Ripley BD. Modern applied statistics with S. 4th ed. New York: Springer; 2002.

140. Centers for Disease Control and Prevention. West Nile Virus: Final Cumulative Maps & Data for 1999-2017. 2018 Dec. Available: https://www.cdc.gov/westnile/statsmaps/cumMapsData.html

141. Bivand R, Rundel C. rgeos: Interface to Geometry Engine - Open Source (GEOS) R Package version 0.4-1.

142. Harris I, Jones PD, Osborn TJ, Lister DH. Updated high-resolution grids of monthly climatic observations - the CRU TS3.10 Dataset: UPDATED HIGH-RESOLUTION GRIDS

1273 OF MONTHLY CLIMATIC OBSERVATIONS. International Journal of Climatology.
1274 2014;34: 623–642. doi:10.1002/joc.3711

1275 143. Hijmans RJ. raster: Geographic data analysis and modeling, R package version 2.2.31.

1276 144. Wood SN. Generalized additive models: an introduction with R. Boca Raton, FL:
1277 Chapman & Hall/CRC; 2006.

1278 145. Curren EJ, Lindsey NP, Fischer M, Hills SL. St. Louis Encephalitis Virus Disease in the
1279 United States, 2003–2017. The American Journal of Tropical Medicine and Hygiene.
1280 2018;99: 1074–1079. doi:10.4269/ajtmh.18-0420

1281 146. Lindsey NP, Staples JE, Fischer M. Eastern Equine Encephalitis Virus in the United
1282 States, 2003–2016. The American Journal of Tropical Medicine and Hygiene. 2018;98:
1283 1472–1477. doi:10.4269/ajtmh.17-0927

1284 147. Petersen LR, Brault AC, Nasci RS. West Nile Virus: Review of the Literature. JAMA.
1285 2013;310: 308. doi:10.1001/jama.2013.8042

1286 148. Ronca SE, Murray KO, Nolan MS. Cumulative Incidence of West Nile Virus Infection,
1287 Continental United States, 1999–2016. Emerging Infectious Diseases. 2019;25: 325–327.
1288 doi:10.3201/eid2502.180765

1289 149. Government of Canada. Surveillance of West Nile virus. Government of Canada; 2018
1290 Dec. Available: https://www.canada.ca/en/public-health/services/diseases/west-nile-
1291 virus/surveillance-west-nile-virus.html

1292 150. European Centre for Disease Prevention and Control. Surveillance and disease data for
1293 West Nile fever. European Centre for Disease Prevention and Control; 2018 Dec. Available:
1294 https://ecdc.europa.eu/en/west-nile-fever/surveillance-and-disease-data

1295 151. World Health Organization. Rift Valley Fever Fact Sheet. World Health Organization;
1296 2018 Feb. Available: https://www.who.int/en/news-room/fact-sheets/detail/rift-valley-fever

1297

SUPPLEMENTAL MATERIAL for

Shocket et al. 'Transmission of West Nile virus and other temperate mosquito-borne viruses peaks at intermediate environmental temperatures'

List of Contents

1. Model, thermal response, and trait data information:
    a. R_0 model specifications 2
    b. Table S1: Trait thermal responses used in transmission (R_0) models 5
    c. Table S2-S6: Trait thermal response functions, data sources, and posterior estimates 6
    d. Table S7-S9: Priors for trait thermal response functions 10
2. Supplemental methods:
    a. Priors for trait thermal responses 13
    b. Sensitivity and uncertainty analyses 14
3. Supplemental figures and validation table:
    a. Fig S1: Mosquito trait thermal responses for additional vector species: *Aedes taeniorhynchus*, *Ae. triseriatus*, *Aedes vexans*, *Culex theileri* and *Culiseta melanura* 15
    b. Fig S2-9: Thermal responses for traits with individual data points 16
    c. Fig S10: Medians & 95% credible intervals for thermal limits and optima of R_0 models 24
    d. Fig S11-20: Sensitivity and uncertainty analyses for R_0 models 25
    e. Fig S21: Histograms of T_{min}, optimum, and T_{max} for R_0 models 35
    f. Fig S22: Comparisons of alternative model parameterizations 36
    g. Fig S23: Comparison with previous transmission models for WNV 37
    h. Fig S24: GAM models fit with varying knot parameters 38
    i. Table S10: GAM models fit with varying knot parameters 39
    j. Fig S25: LOESS models plotted with binned WNV incidence 40
    k. Fig S26: Raw county-level WNV incidence data 41
4. References 42

R_0 Model Specifications

The equation for R_0 (eq. 2 in main text) as a function of temperature (T) that was used in previous analyses [1–6] has fecundity measured as eggs per female per day (EFD):

$$\text{Full } R_0\text{: } R_0(T) = \left(\frac{a(T)^2 bc(T) e^{-\frac{\mu(T)}{PDR(T)}} EFD(T) EV(T) pLA(T) MDR(T)}{N\, r\, \mu(T)^3}\right)^{1/2} \qquad \text{eq. 2}$$

Fecundity data were not available directly as eggs per female per day, so we had to transform the available data to obtain the quantities needed for these models. The data for *Cx. pipiens* were reported as eggs per female per gonotrophic cycle ($EFGC$). To obtain EFD, we needed to divide $EFGC$ by the length of the gonotrophic cycle. In general, the gonotrophic cycle is assumed to be approximately the inverse of the biting rate. In fact, our 'biting rate' (a) data were observations of gonotrophic cycle duration. Accordingly, $EFD = EFGC * a$, resulting in the following equation for R_0:

$$R_0(T) = \left(\frac{a(T)^3 bc(T) e^{-\frac{\mu(T)}{PDR(T)}} EFGC(T) EV(T) pLA(T) MDR(T)}{N\, r\, \mu(T)^3}\right)^{1/2} \qquad \text{eq. S1}$$

All but two of the vector–virus parameterizations used this form (eq. S1) of the R_0 model (see Table S1, exceptions described below).

The fecundity data for *Cx. quinquefasciatus* were reported as eggs per raft (ER). Females lay rafts once per gonotrophic cycle. Thus, in order to obtain an approximation to EFD (eggs per female per day), we again divide by the number of days per gonotrophic cycle and, further, we multiply by the proportion of females ovipositing (pO), since not every female lays an egg raft. These changes result in the following equation for R_0:

$$R_0(T) = \left(\frac{a(T)^3 bc(T) e^{-\frac{\mu(T)}{PDR(T)}} ER(T) pO(T) EV(T) pLA(T) MDR(T)}{N\, r\, \mu(T)^3}\right)^{1/2} \qquad \text{eq. S2}$$

The *Cx. quinquefasciatus*–WNV model used eq. S2.

The *Ae. triseriatus*–EEEV also used eq. S2 (i.e., included *pO*) but substituted the *Cx. pipiens* thermal response for *EFGC* in place of the *Cx. quinquefasciatus* thermal response for *ER* for the following reasons. There were no fecundity trait data available for *Ae.* triseriatus. (*Ae. triseratus* was chosen as the focal species for the EEEV model because it is the only species with temperature-dependent vector competence data available, and it is a possible bridge vector for EEEV transmission to humans). *Cs. melanura* is the primary vector for maintaining enzootic cycles of EEEV in birds [7], more often cited in the literature in association with EEEV (e.g., [8]), and had data for *pO* (proportion ovipositing) available. Thus, we chose to include this thermal response in model because it contained information that could affect the upper and lower bounds of transmission (even though most models did not include *pO* [proportion ovipositing], because they use the *Cx. pipiens* EFGC [eggs per female per gonotrophic cycle] thermal response that includes *pO* implicitly). Then we needed to choose which egg production metric to include. We chose the *Cx. pipiens* EFGC thermal response over the *Cx. quinquefasciatus* ER thermal response because the former was the better choice according to both criteria: *Cx. pipiens* has a more similar species range to *Ae. triseriatus* and *Cs. melanura* and its thermal response was slightly more conservative (less restrictive = cooler lower thermal limit and warmer upper thermal limit). Although technically the units are not correct (see above), the thermal responses for *Cx. pipiens* EFGC and *Cx. quinquefasciatus* ER are so similar despite having different units (Fig 4B), we decided that the other two criteria were more important than being strict with regard to the units, as it is feasible to have an ER thermal response that is quite similar to the EFGC thermal response. Ultimately, because the thermal responses for EFGC and ER are so similar,

this decision only has a small impact on the R_0 results (see Fig S21A comparing four alternative model specifications / parameterizations for the *Ae. triseriatus*-EEEV model).

In eqs. 2, S1, and S2, the remaining parameters that depend on temperature (T) are: adult mosquito mortality (μ, the inverse of lifespan [lf]), pathogen development rate (PDR, the inverse of the extrinsic incubation period: the time required for exposed mosquitoes to become infectious), egg viability (proportion of eggs hatching into larvae, EV), proportion of larvae surviving to adulthood (pLA), and mosquito development rate (MDR, the inverse of the development period), and vector competence (bc, the proportion of exposed mosquitoes that become infectious). Vector competence is the product of infection efficiency (c, the proportion of exposed mosquitoes that develop a disseminated infection) and transmission efficiency (b, the proportion of infected mosquitoes that become infectious, with virus present in saliva). The form of vector competence varied between models based on the availability of data: $bc(T)$ [reported a single parameter], $c(T)*b(T)$ [both parameters reported separately], $c(T)$ only, or $b(T)$ only (see Table S1). The two remaining parameters do not depend on temperature: human density (N) and the rate at which infected hosts recover and become immune (r).

Table S1: Trait thermal responses used in transmission (R_0) models. Viruses: West Nile (WNV), Eastern and Western Equine Encephalitis (EEEV and WEEV), St. Louis Encephalitis (SLEV), Sindbis (SINV), and Rift Valley Fever (RVFV). *Ae. vex.* = *Ae. vexans, Cs. mel.* = *Culiseta melanura*; all other vectors (*Cx.* = *Culex*) listed under model names. Traits are: fecundity (as eggs/female/gonotrophic cycle [*EFGC*] or eggs per raft*proportion ovipositing [*ER*pO*]), egg viability (*EV*), larval-to-adult survival (*pLA*), mosquito development rate (*MDR*), lifespan (*lf*), biting rate (*a*), vector competence (*bc*, *b*c*, *b*, or *c*, as available), and parasite development rate (*PDR*). The WNV–*Cx. quinquefasciatus* model uses eq. S2 (*ER*pO*); the EEEV–*Ae. triseriatus* model uses *EFGC* from *Cx. pipiens* and *pO* from *Cs. melanura*; all other models use eq. S1 (*EFGC*). When data were missing for a vector–virus pair, we substituted the most conservative (i.e., least restrictive of transmission) trait thermal response from a vector that occurs within the geographic range of disease transmission. Several models had multiple potentially valid choices for traits; we explain and show compare these alternative models with the main text versions in Fig S21. Checkmarks indicate a thermal response from the vector in the model name. The parasite development rate data for SINV was insensitive to temperature (Fig 4), so the trait thermal response was omitted from the SINV models ('NA').

Model: virus–vector	***EFGC* or *ER*pO***	***EV***	***pLA***	***MDR***	***lf***	***a***	***bc, c*b c, or b***	***PDR***
WNV–*Cx. pipiens*	✓	✓	✓	✓	✓	✓	✓ (bc)	✓
WNV–*Cx. quinquefasciatus*	✓	✓	✓	✓	✓	✓	*Cx. uni.* (c*b)	✓
WNV–*Cx. tarsalis*	*Cx. pip.*	*Cx. pip*	✓	✓	✓	✓	✓ (b)	✓
WNV–*Cx. univittatus*	*Cx. pip.*	*Cx. pip.*	*Cx. pip.*	*Cx. pip.*	*Cx. pip.*	*Cx. pip.*	✓ (bc)	✓
WEEV–*Cx. tarsalis*	*Cx. pip.*	*Cx. pip.*	✓	✓	✓	✓	✓ (c*b)	✓
SLEV–*Cx. tarsalis*	*Cx. pip.*	*Cx. pip.*	✓	✓	✓	✓	✓ (c*b)	✓
EEEV–*Ae. triseriatus*	*Cx. pip.*, *Cs. mel.*	*Cx. pip.*	✓	✓	*Cx. pip.*	*Cs. mel.*	✓ (bc)	✓
SINV–*Cx. pipiens*	✓	✓	✓	✓	✓	✓	✓ (c)	NA
SINV–*Ae. taeniorhynchus*	*Cx. pip.*	*Ae. vex.*	*Ae. vex.*	*Ae. vex.*	✓	*Cx. pip.*	✓ (c)	NA
RVFV–*Ae. taeniorhynchus*	*Cx. pip.*	*Cx. the.*	*Ae. vex.*	*Ae. vex.*	✓	*Cx. pip.*	✓ (bc)	✓

Table S2: Trait thermal response functions, data sources, and posterior estimates: biting rate and fecundity traits. Asymmetrical responses fit with Brière function (**B**): $B(T) = qT(T - T_{min})(T_{max} - T)^{1/2}$; symmetrical responses fit with quadratic function (**Q**): $Q(T) = -q(T - T_{min})(T - T_{max})$. Median function coefficients and optima (with 95% credible intervals).

Trait / Species **[data source]**	***F(x)***	***q*** **(CIs)**	T_{min} **(CIs)**	T_{max} **(CIs)**	T_{opt} **(CIs)**
Biting rate (*a*)					
Cx. pipiens	B	$1.70 \cdot 10^{-4}$	9.4	39.6	32.7
[9–12]		($1.18–2.29 \cdot 10^{-4}$)	(2.8–13.4)	(37.9–40.6)	(31.3–33.6)
Cx. quinquefasciatus	B	$7.28 \cdot 10^{-5}$	3.1	39.3	31.9
[9,13]		($5.31–11.8 \cdot 10^{-5}$)	(0.1–10.9)	(38.0–40.8)	(30.6–33.3)
Cx. tarsalis	B	$1.67 \cdot 10^{-4}$	2.3	32.0	25.9
[13]		($0.87–2.56 \cdot 10^{-4}$)	(0.1–9.4)	(30.6–41.7)	(24.8–33.9)
Cs. melanura	B	$1.87 \cdot 10^{-4}$	7.8	31.8	26.4
[14]		($1.49–2.31 \cdot 10^{-4}$)	(5.5–11.4)	(31.0–33.4)	(25.7–27.9)
Fecundity					
Cx. pipiens (*EFGC*)	Q	$5.98 \cdot 10^{-1}$	5.3	38.9	22.1
[12]		($4.31–7.91 \cdot 10^{-1}$)	(2.6–8.5)	(36.2–41.8)	(20.1–24.4)
Cx. quinquefasciatus (*ER*)	Q	$6.36 \cdot 10^{-1}$	5.0	37.7	21.4
[15,16]		($4.50–9.05 \cdot 10^{-1}$)	(1.3–9.8)	(34.8–40.7)	(18.9–24.4)
Proportion ovipositing (*pO*)					
Cx. pipiens	Q	$4.45 \cdot 10^{-3}$	8.2	33.2	20.8
[9,17]		($2.54–7.77 \cdot 10^{-3}$)	(4.6–12.1)	(30.1–37.5)	(18.6–23.4)
Cx. quinquefasciatus	B	$6.67 \cdot 10^{-4}$	1.7	31.8	24.9
[9,15,17]		($5.80–7.91 \cdot 10^{-4}$)	(0.2–4.8)	(31.1–32.2)	(21.8–26.0)
Cs. melanura	Q	$6.31 \cdot 10^{-3}$	8.7	33.6	20.7
[14]		($4.52–7.89 \cdot 10^{-3}$)	(6.9–10.4)	(32.5–35.4)	(16.9–22.3)
Egg viability (*EV*)					
Ae. vexans		$1.24 \cdot 10^{-3}$	0	55.5	27.6
[18]		($0.73–1.95 \cdot 10^{-3}$)	(0–1.6)	(45.9–74.1)	(20.4–34.0)
Cx. pipiens	Q	$2.11 \cdot 10^{-3}$	3.2	42.6	23.0
[12]		($1.36–3.05 \cdot 10^{-3}$)	(0.5–7.1)	(39.7–48.3)	(20.7–26.3)
Cx. quinquefasciatus	B	$0.47 \cdot 10^{-3}$	13.6	38.0	32.1
[15,19]		($0.34–0.62 \cdot 10^{-3}$)	(9.3–16.8)	(37.2–38.7)	(31.3–32.7)
Cx. theileri	Q	$2.54 \cdot 10^{-3}$	5.5	45.4	23.6
[20]		($1.86–3.41 \cdot 10^{-3}$)	(2.6–8)	(42.4–49.0)	(18.2–27.0)

Additional data sources for other species used for fitting priors only (priors were fit using all data except that of the focal species). Fecundity (*ER*): *Cx. pipiens molestus* [15], *Cx. pipiens pallens* [16], and *Ae. dorsalis* [21]. Proportion ovipositing (*pO*): *Cx. pipiens molestus* [15] and *Ae. dorsalis* [21]. Egg viability (*EV*): *Cx. pipiens molestus* [15], *Aedes dorsalis* [22], and *Ae. nigromaculis* [23]. See *Supplemental Methods: Priors for trait thermal responses*.

Table S3: Trait thermal response functions, data sources, and posterior estimates: larval traits. Asymmetrical responses fit with Brière function (**B**): $B(T) = qT(T - T_{min})(T_{max} - T)^{1/2}$; symmetrical responses fit with quadratic function (**Q**): $Q(T) = -q(T - T_{min})(T - T_{max})$. Median function coefficients and optima (with 95% credible intervals).

Trait / Species **[data source]**	***F(x)***	***q*** **(CIs)**	T_{min} **(CIs)**	T_{max} **(CIs)**	T_{opt} **(CIs)**
Mosquito Dev. Rate (*MDR*)					
Ae. triseriatus	B	$4.30 \cdot 10^{-5}$	0.8	36.5	29.3
[24]		($3.01–5.83 \cdot 10^{-5}$)	(0–7.5)	(34.6–39.5)	(27.8–31.9)
Ae. vexans	B	$4.33 \cdot 10^{-5}$	1.9	38.2	30.9
[25,26]		($3.34–5.50 \cdot 10^{-5}$)	(0.1–10.5)	(37.0–39.5)	(29.8–32.2)
Cx. pipiens	B	$3.76 \cdot 10^{-5}$	0.1	38.5	30.9
[9–11,17,27–29]		($3.36–4.47 \cdot 10^{-5}$)	(0–4.0)	(37.6–39.8)	(30.2–31.9)
Cx. quinquefasciatus	B	$4.14 \cdot 10^{-5}$	0.1	38.6	31.0
[9,17,24,30,31]		($3.46–5.26 \cdot 10^{-5}$)	(0–5.5)	(37.4–40.6)	(30.0–32.6)
Cx. tarsalis	B	$4.12 \cdot 10^{-5}$	4.3	39.9	32.3
[32–34]		($3.15–5.47 \cdot 10^{-5}$)	(0–8.4)	(37.9–42.2)	(31.0–34.0)
Cs. melanura	B	$2.74 \cdot 10^{-5}$	8.6	37.6	31.1
[7]		($1.64–4.72 \cdot 10^{-5}$)	(0–16.8)	(35.1–40.4)	(28.7–33.7)
Larval survival (p_{LA})					
Ae. triseriatus	Q	$3.26 \cdot 10^{-3}$	8.3	35.7	22.0
[24,35]		($1.95–5.18 \cdot 10^{-3}$)	(4.9–11.4)	(32.9–39.7)	(19.9–24.6)
Ae. vexans	Q	$3.29 \cdot 10^{-3}$	9.1	40.8	25.0
[25,26]		($2.65–4.24 \cdot 10^{-3}$)	(8.1–10.6)	(38.4–43.6)	(23.9–26.2)
Cx. pipiens	Q	$3.60 \cdot 10^{-3}$	7.8	38.4	23.1
[9–11,17,27–29]		($2.96–4.42 \cdot 10^{-3}$)	(6.1–9.3)	(37.1–39.9)	(22.2–24.0)
Cx. quinquefasciatus	Q	$4.26 \cdot 10^{-3}$	8.9	37.7	23.3
[9,16,17,24,30,31,36]		($3.51–5.17 \cdot 10^{-3}$)	(7.6–9.9)	(36.2–39.2)	(22.5–24.0)
Cx. tarsalis	Q	$2.12 \cdot 10^{-3}$	5.9	43.1	24.6
[32–34]		($1.52–3.08 \cdot 10^{-3}$)	(3.0–8.8)	(39.8–47.5)	(22.9–26.4)
Cs. melanura	Q	$3.03 \cdot 10^{-3}$	10.1	36.2	23.2
[7]		($1.55–5.68 \cdot 10^{-3}$)	(5.7–15.1)	(32.8–40.7)	(20.4–26.5)

Additional data sources for other species used for fitting priors only (priors were fit using all data except that of the focal species). Mosquito Development Rate (*MDR*): *Cx. pipiens molestus* [37,38], *Cx. pipiens pallens* [37], *Cx. restuans* [10,24,33,39], *Cx. salinarius* [24], *Ae. solicitans* [24], and *Ae. nigromaculis* [25]. Larval survival (p_{LA}): *Cx. pipiens molestus* [36,38], *Cx. pipiens pallens* [16], *Cx. restuans* [10,17,24,33,39], *Cx. salinarius* [24], *Ae. sollicitans* [24], *Ae. nigromaculis* [25]. See *Supplemental Methods: Priors for trait thermal responses*.

Table S4: Trait thermal response functions, data sources, and posterior estimates: vector competence traits. Asymmetrical responses fit with Brière function (**B**): $B(T) = qT(T - T_{min})(T_{max} - T)^{1/2}$; symmetrical responses fit with quadratic function (**Q**): $Q(T) = -q(T - T_{min})(T - T_{max})$. Median function coefficients and optima (with 95% credible intervals).

Trait / Species **[data source]**	***F(x)***	***q*** **(CIs)**	T_{min} **(CIs)**	T_{max} **(CIs)**	T_{opt} **(CIs)**
Transmission efficiency (*b*)					
SLEV | *Cx. tarsalis* [40]	Q	$2.98 \cdot 10^{-3}$ ($1.63–5.31 \cdot 10^{-3}$)	10.8 (6.2–14.2)	41.6 (36.8–49.1)	26.2 (23.5–29.7)
WEEV | *Cx. tarsalis* [40]	Q	$3.17 \cdot 10^{-3}$ ($1.65–5.06 \cdot 10^{-3}$)	8.2 (5.1–10.7)	33.5 (31.0–38.9)	20.9 (19.2–23.2)
WNV | *Cx. tarsalis* [41]	Q	$2.94 \cdot 10^{-3}$ ($1.91–4.48 \cdot 10^{-3}$)	11.3 (7.6–14.0)	41.9 (37.7–47.0)	26.6 (23.9–29.3)
Infection efficiency (*c*)					
SINV | *Ae. taeniorhynchus* [42]	Q	$1.24 \cdot 10^{-3}$ ($0.75–2.17 \cdot 10^{-3}$)	1.4 (0–9.1)	48.4 (40.8–57.1)	25.4 (21.0–31.1)
SINV | *Cx. pipiens* [43]	Q	$1.33 \cdot 10^{-3}$ ($0.47–2.30 \cdot 10^{-3}$)	0 (0–0)	35.0 (28.1–61.1)	17.5 (14.1–30.5)
WNV | *Cx. pipiens* [44,45]	Q	$2.56 \cdot 10^{-3}$ ($2.05–3.19 \cdot 10^{-3}$)	15.6 (14.3–16.6)	52.2 (48.4–56.6)	33.9 (31.9–36.1)
SLEV | *Cx. tarsalis* [40]	Q	$2.03 \cdot 10^{-3}$ ($1.28–3.07 \cdot 10^{-3}$)	8.8 (6.6–10.6)	43.7 (38.9–51.4)	26.2 (24.2–29.7)
WEEV | *Cx. tarsalis* [40,46]	Q	$3.04 \cdot 10^{-3}$ ($2.52–3.68 \cdot 10^{-3}$)	1.3 (0.4–2.9)	38.8 (36.7–41.5)	15.5 (13.4–19.7)
Vector competence (*bc*)					
RVFV | *Ae. taeniorhynchus* [47]	Q	$1.51 \cdot 10^{-3}$ ($1.03–2.05 \cdot 10^{-3}$)	7.1 (2.8–9.8)	42.3 (39.3–46.5)	24.7 (22.0–27.0)
EEEV | *Ae. triseriatus* [48]	Q	$1.51 \cdot 10^{-3}$ ($0.96–2.24 \cdot 10^{-3}$)	7.0 (2.9–11.9)	50.3 (42.3–63.1)	28.8 (23.6–35.8)
WNV | *Cx. pipiens* [44]	Q	$3.05 \cdot 10^{-3}$ ($1.68–4.87 \cdot 10^{-3}$)	16.8 (15–17.9)	38.9 (36.1–44.1)	27.8 (26.6–30.1)
WEEV | *Cx. tarsalis* [46]	Q	$1.17 \cdot 10^{-3}$ ($0.55–2.36 \cdot 10^{-3}$)	5.1 (0.6–13.3)	37.0 (33.5–46.0)	21.4 (18.1–27.3)
WNV | *Cx. univittatus* [49]	Q	$2.32 \cdot 10^{-3}$ ($1.58–3.68 \cdot 10^{-3}$)	4.2 (1.5–7.1)	45.2 (39.6–53.0)	23.7 (19.4–27.3)

Table S5: Trait thermal response functions, data sources, and posterior estimates: parasite development rate. Asymmetrical responses fit with Brière function (**B**): $B(T) = qT(T - T_{min})(T_{max} - T)^{1/2}$; symmetrical responses fit with quadratic function (**Q**): $Q(T) = -q(T - T_{min})(T - T_{max})$. Median function coefficients and optima (with 95% credible intervals).

***Trait / Species* [data source]**	***F(x)***	***q* (CIs)**	***T_{min}* (CIs)**	***T_{max}* (CIs)**	***T_{opt}* (CIs)**
Parasite Dev. Rate (*PDR*)					
RVFV | *Ae. taeniorhynchus* [47]	B	$8.84 \cdot 10^{-5}$ ($2.51–15.5 \cdot 10^{-5}$)	9.0 (5.4–13.8)	45.9 (41.9–50.3)	37.8 (34.5–41.3)
EEEV | *Ae. triseriatus* [48]	B	$7.05 \cdot 10^{-5}$ ($5.21–9.68 \cdot 10^{-5}$)	11.6 (7.0–16.4)	44.8 (40.6–49.4)	37.2 (33.8–41.1)
WNV | *Cx. pipiens* [44,45]	B	$7.38 \cdot 10^{-5}$ ($5.38–9.94 \cdot 10^{-5}$)	11.4 (7.3–15.0)	45.2 (40.7–50.3)	37.5 (33.8–41.6)
WNV | *Cx. quinquefasciatus* [50]	B	$7.12 \cdot 10^{-5}$ ($4.58–10.2 \cdot 10^{-5}$)	19.0 (12.9–21.0)	44.1 (38.8–50.4)	37.7 (33.6–42.7)
SLEV | *Cx. tarsalis* [40]	B	$7.11 \cdot 10^{-5}$ ($5.60–8.95 \cdot 10^{-5}$)	12.8 (10.3–14.3)	45.2 (40.2–51.5)	37.7 (33.8–42.6)
WEEV | *Cx. tarsalis* [40,46]	B	$6.43 \cdot 10^{-5}$ ($4.44–10.4 \cdot 10^{-5}$)	4.0 (0–12.6)	44 .0 (38.3–50.9)	35.7 (31.0–41.4)
WNV | *Cx. tarsalis* [41]	B	$6.57 \cdot 10^{-5}$ ($5.11–8.85 \cdot 10^{-5}$)	11.2 (7.9–14.9)	44.7 (40.4–49.4)	37.0 (33.6–40.9)
WNV | *Cx. univittatus* [49]	B	$7.54 \cdot 10^{-5}$ ($4.13–11.1 \cdot 10^{-5}$)	10.2 (7.1–15.3)	34.4 (31.2–51.1)	28.8 (26.1–42.5)
SINV | *Ae. taeniorhynchus* [42]	NA	Not fitted because lack of temperature sensitivity			

Table S6: Trait thermal response functions, data sources, and posterior estimates: lifespan. Responses fit with a linear function (**L**): $L(T) = -mT + z$. Median function coefficients and T_{max} (with 95% credible intervals).

***Trait / Species* [data source]**	***F(x)***	***m***	***z***	***Tmax = z/m***
Lifespan (*lf*)				
Ae. taeniorhynchus [51]	L	2.02 (1.59–3.19)	85.9 (73.8–117.6)	42.7 (34.5–48.5)
Cx. pipiens [11,17,52]	L	4.86 (3.83–5.84)	169.8 (142.1–195.6)	34.9 (32.9–37.9)
Cx. quinquefasciatus [17,36]	L	3.80 (1.85–5.29)	136.3 (86.8–174.0)	35.9 (32.1–48.5)
Cx. tarsalis [32]	L	1.69 (1.12–2.24)	69.6 (55.8–83.5)	41.3 (36.6–50.8)

Additional data sources for other species used for fitting priors only (priors were fit using all data except that of the focal species). Lifespan (*lf*): *Cx. pipiens molestus* [36,37], *Cx. pipiens pallens* [37], and *Cx. restuans* [17]. See *Supplemental Methods: Priors for trait thermal responses*.

Table S7: Priors for trait thermal response functions: mosquito traits with unimodal responses. Gamma distribution parameters (α [shape] and β [rate]) for priors for fitting thermal response parameters (T_{min}, T_{max}, and q). Scaled variances are noted in parentheses, either by the system name (applied to all parameters) or by individual parameters. See *Supplemental Methods: Priors for trait thermal responses*.

Trait / System	***q*: *α***	***q*: *β***	***T_{min}*: *α***	***T_{min}*: *β***	***T_{max}*: *α***	***T_{max}*: *β***
Biting rate (*a*)						
Cx. pipiens (0.5)	8.84	64200	1.91	0.367	103	3.00
Cx. quinquefasciatus	39.1 (0.1)	234133 (0.1)	8.82 (0.1)	0.997 (0.1)	2992	75.8
Cx. tarsalis	40.1 (0.05)	227752 (0.05)	18.7 (0.05)	1.745 (0.05)	unif.	unif.
Cs. melanura	35.4 (0.75)	229694 (0.75)	7.77 (0.75)	0.895 (0.75)	2714 (0.1)	68.5 (0.1)
Fecundity						
Cx. pipiens (*EFGC*) (3)	9.23	15.6	2.38	0.419	139	3.52
Cx. quinquefasciatus (*ER*)	19.1	30.44	2.87	0.600	486	13.2
Prop. ovipositing (*pO*)						
Cx. pipiens (0.5)	9.50	1823	14.8	1.495	263	7.14
Cx. quinquefasciatus	32.9	55242	1.41	0.397	3346	106
Cs. melanura	14.4	2635	22.0	2.254	588	16.8
Egg viability (*EV*)						
Ae. vexans (0.01)	26.6	12259	11.6	1.916	486	10.8
Cx. pipiens (0.2)	29.4	14525	8.83	1.579	514	11.1
Cx. quinquefasciatus (0.1)	101	262268	1.08	1.032	1361	34.9
Cx. theileri	5.86	2266	4.46	0.591	266	6.06
Mos. dev. rate (*MDR*)						
Ae. triseriatus (0.2)	118	2697528	1.93	0.703	5542	145
Ae. vexans (0.5)	119	2739401	1.89	0.689	6661	174
Cx. pipiens (0.1)	71.9	1545915	2.03	0.596	2912	76.5
Cx. quinquefasciatus (0.1)	113	2569782	1.81	0.651	5900	155
Cx. tarsalis (0.1)	129	2940582	1.49	0.660	6431	169
Cs. melanura (0.1)	129	2941063	1.78	0.685	6915	181
Larval survival (p_{LA})						
Ae. triseriatus (0.05)	163	46723	231	27.3	4667	122
Ae. vexans (0.05)	135	37701	210	24.6	4040	107
Cx. pipiens (0.1)	102	27382	217	24.2	2872	76.7
Cx. quinquefasciatus (0.1)	88.8	26461	123	14.8	2608	68.4
Cx. tarsalis (0.025)	94.6	23240	237	26.2	2564	69.5
Cs. melanura (0.05)	148.9	41533	239	27.8	4391	116

Table S8: Priors for trait thermal response functions: infection traits. Gamma distribution parameters (α [shape] and β [rate]) for priors for fitting thermal response parameters (T_{min}, T_{max}, and q). Scaled variances are noted in parentheses, either by the system name (applied to all parameters) or by individual parameters. See *Supplemental Methods: Priors for trait thermal responses*.

Trait / System	***q*: *α***	***q*: *β***	***T_{min}*: *α***	***T_{min}*: *β***	***T_{max}*: *α***	***T_{max}*: *β***
Transmission efficiency (*b*)	7.72	3202	9.97	1.268	114	2.9
SLEV | *Cx. tarsalis* (0.5)	9.49	2373	79.6	6.181	153	3.74
WEEV | *Cx. tarsalis* (0.1)	8.46	3056	12.1	1.455	134	3.5
WNV | *Cx. tarsalis*	7.72	3202	9.97	1.268	114	2.9
Infection efficiency (*c*)						
SINV | *Ae. taeniorhynchus* (0.1)	61.7	45102	2.49	0.815	1214	25.1
SINV | *Cx. pipiens* (0.01)	57.3	40236	2.64	0.799	1124	23.28
WNV | *Cx. pipiens*	28.5	15944	1.44	0.852	237	5.393
SLEV | *Cx. tarsalis*	65.2 (0.01)	46656 (0.01)	1.67 (0.01)	0.692 (0.01)	1071 (0.1)	22.2 (0.1)
WEEV | *Cx. tarsalis* (0.01)	82.2	35791	392	30.502	1264	26.1
Vector competence (*bc*)						
RVFV | *Ae. taeniorhynchus* (2)	8.4	4775	2.316	0.421	147	3.39
EEEV | *Ae. triseriatus*	6.68 (3)	3612 (3)	2.027 (3)	0.383 (3)	119 (0.01)	2.86 (0.01)
WNV | *Cx. pipiens* (0.5)	17.6	7857	1.403	0.534	219	5.42
WEEV | *Cx. tarsalis* (0.5)	9.56	5344	3.021	0.498	180	4.05
WNV | *Cx. univittatus*	13.7 (0.01)	2327 (0.01)	380 (0.01)	22.434 (0.01)	527 (0.1)	14.4 (0.1)
Parasite dev. rate (*PDR*)						
RVFV | *Ae. taeniorhynchus*	20.2 (0.2)	331065 (0.2)	8.69 (2)	0.893 (2)	227 (2)	4.96 (2)
EEEV | *Ae. triseriatus* (2)	13.2	167635	6.76	0.609	183	4.05
WNV | *Cx. pipiens*	8.71 (2)	113904 (2)	3.51 (5)	0.356 (5)	140 (2)	3.17 (2)
WNV | *Cx. quinquefasciatus*	15.8	201154	8.09	0.772	202	4.44
SLEV | *Cx. tarsalis*	11.8	151149	6.31	0.584	179	3.97
WEEV | *Cx. tarsalis*	10.3	117795	9.97 (0.05)	0.768 (0.05)	162	3.62
WNV | *Cx. tarsalis* (2)	11.7	148079	5.92	0.541	169	3.77
WNV | *Cx. univittatus*	12.3	146439	9.02 (3)	0.773 (3)	174 (0.2)	3.87 (0.2)

Table S9: Priors for trait thermal response functions: lifespan. Gamma distribution parameters (α [shape] and β [rate]) for priors for fitting thermal response parameters (*m* and *z*). Scaled variances are noted in parentheses, either by the system name (applied to all parameters) or by individual parameters. See *Supplemental Methods: Priors for trait thermal responses*.

Trait / System **(var.)**	***m*: *α***	***m*: *β***	**z: *α***	**z: *β***
Lifespan (*lf*)				
Ae. taeniorhynchus (0.01)	119	52.9	268	3.19
Cx. pipiens (0.01)	117	42.4	238	2.39
Cx. quinquefasciatus (0.01)	110	32.9	207	1.78
Cx. tarsalis (0.1)	124	43.0	249	2.42

Supplemental Methods: Priors for trait thermal responses

We used gamma distribution parameters (α [shape] and β [rate]) for informative priors for each thermal response parameter (Brière and quadratic functions: T_{min}, T_{max}, and q); linear functions: m and z). First, we fit a thermal response function (with uniform priors) to all the *Aedes* and *Culex* data for a given trait except that of the focal vector species or vector–virus pair (i.e., the parameters for the priors for a for *Culex pipiens* were fit to the a data for all species except *Cx. pipiens*). Then we used the 'MASS' package in R to fit a gamma distribution hyperparameters to the distribution from each thermal response parameters.

The mean of the gamma distribution is equal to α/β, while the variance is determined by the magnitude of the parameters (smaller values = higher variance). When fitting thermal responses, the appropriate strength for the priors depends on the amount of data used to fit the priors and the amount of the data for the focal trait. Prior strengths can be modified by scaling the variance (i.e., multiplying the gamma parameters by <1 to increase the variance or >1 to decrease the variance) without impacting the mean. In many cases we had to increase the variance because of the large number of data points used to fit priors. In a few cases, we had to decrease the variation (e.g., to constrain T_{max} for Briere functions for *PDR* where we had no observations at high temperatures, in order to make it so *PDR* would not constrain R_0 where there was no data). For biting rate (a) for *Culex tarsalis*, we used a likelihood function where T_{min} and q had data informed priors and T_{max} had uniform priors (as used to fit the priors) in order to best capture the thermal response of the data.

Supplemental Methods: Sensitivity and uncertainty analyses

We performed two sensitivity analyses and one uncertainty analysis to understand what traits were most important for determining and contributing to uncertainty in the thermal limits and optima. For the first sensitivity analysis, we calculated the partial derivatives of R_0 with respect to each trait across temperature (T) and multiplied it by the derivative of the trait with temperature (i.e., the slope of the thermal response). Equations S3-S6 (below) apply to both versions of the R_0 model (eqs. S1 and S2). Equation S3 is for to all traits (x) that appear once in the numerator. Equation S4, for biting rate (a), differs from previous analyses [2–6] because biting rate was cubed to account for fecundity measured per gonotrophic cycle rather than per day. Equation S5 is for parasite development rate (PDR), and equation S6 is for lifespan (lf).

$$\frac{\partial R_0}{\partial x} \cdot \frac{\partial x}{\partial T} = \frac{R_0}{2x} \cdot \frac{\partial x}{\partial T} \qquad \text{eq. S3}$$

$$\frac{\partial R_0}{\partial a} \cdot \frac{\partial a}{\partial T} = \frac{3R_0}{2a} \cdot \frac{\partial a}{\partial T} \qquad \text{eq. S4}$$

$$\frac{\partial R_0}{\partial PDR} \cdot \frac{\partial PDR}{\partial T} = \frac{R_0}{2\, lf\, PDR^2} \cdot \frac{\partial PDR}{\partial T} \qquad \text{eq. S5}$$

$$\frac{\partial R_0}{\partial lf} \cdot \frac{\partial lf}{\partial T} = \frac{R_0(1+3PDR)}{2\, PDR\, lf^2} \cdot \frac{\partial lf}{\partial T} \qquad \text{eq. S6}$$

For the second sensitivity analysis, we held single traits constant while allowing all other traits to vary with temperature. For the uncertainty analysis, we calculated the 'total uncertainty' across temperature as the width of the 95% highest posterior density (HPD) interval across temperature for the full model. Then, we calculated the HPD for 'uncertainty for each trait' by fixing all traits except the focal trait at their posterior median value across temperature, while keeping the full posterior sample of the focal trait. Then, we divided the uncertainty for each trait by the total uncertainty, calculated across temperature, to estimate the proportion of uncertainty in R_0 that was due to the uncertainty in the focal trait.

Figure S1: Thermal responses for mosquito traits in additional vector species: *Ae. taeniorhynchus* (green), *Ae. triseriatus* (violet), *Aedes vexans* (teal), *Cx. theileri* (pink), and *Culiseta melanura* (brown). (A) Mosquito development rate (*MDR*), (B) larval-to-adult survival (*pLA*), and (C) biting rate (*a*), (D) lifespan (*lf*), (E) proportion ovipositing (*pO*) and (F) egg viability (*EV*). Points without error bars are reported means from single studies; points with error bars are averages of means from multiple studies (+/- standard error, for visual clarity only; thermal responses were fit to reported means). Solid lines are posterior distribution means; shaded areas are 95% credible intervals.

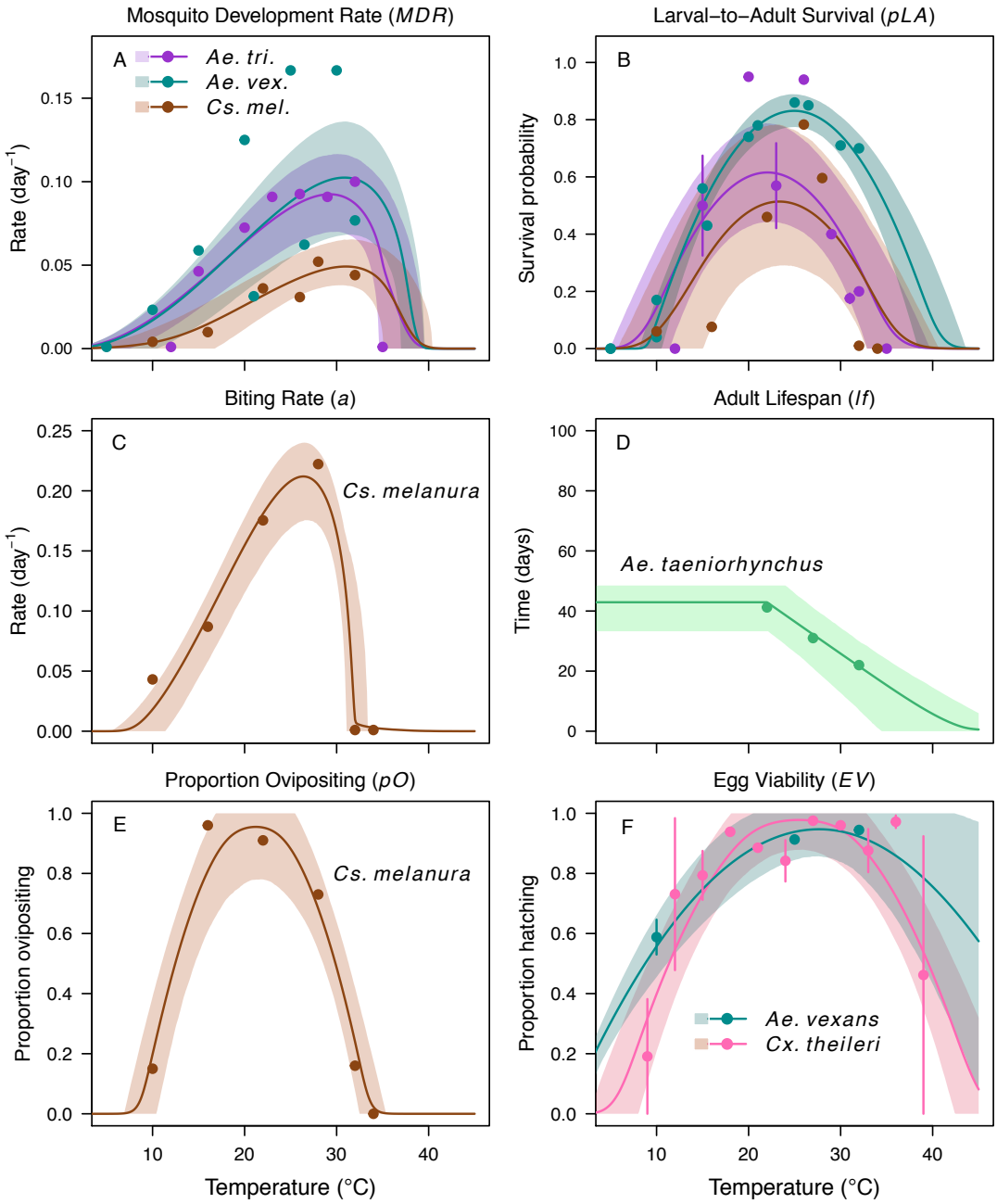

Figure S2: Thermal responses for biting rate (*a*) showing individual data points. (A) C*ulex pipiens*, (B), *Cx. quinquefasciatus*, (C) *Cx. tarsalis*, and (D) *Culiseta melanura*. Solid lines are posterior distribution means for the mean thermal response; black dashed lines are 95% credible intervals for the mean thermal response; red dashed lines are 95% prediction intervals for observed data (incorporating the fitted variance).

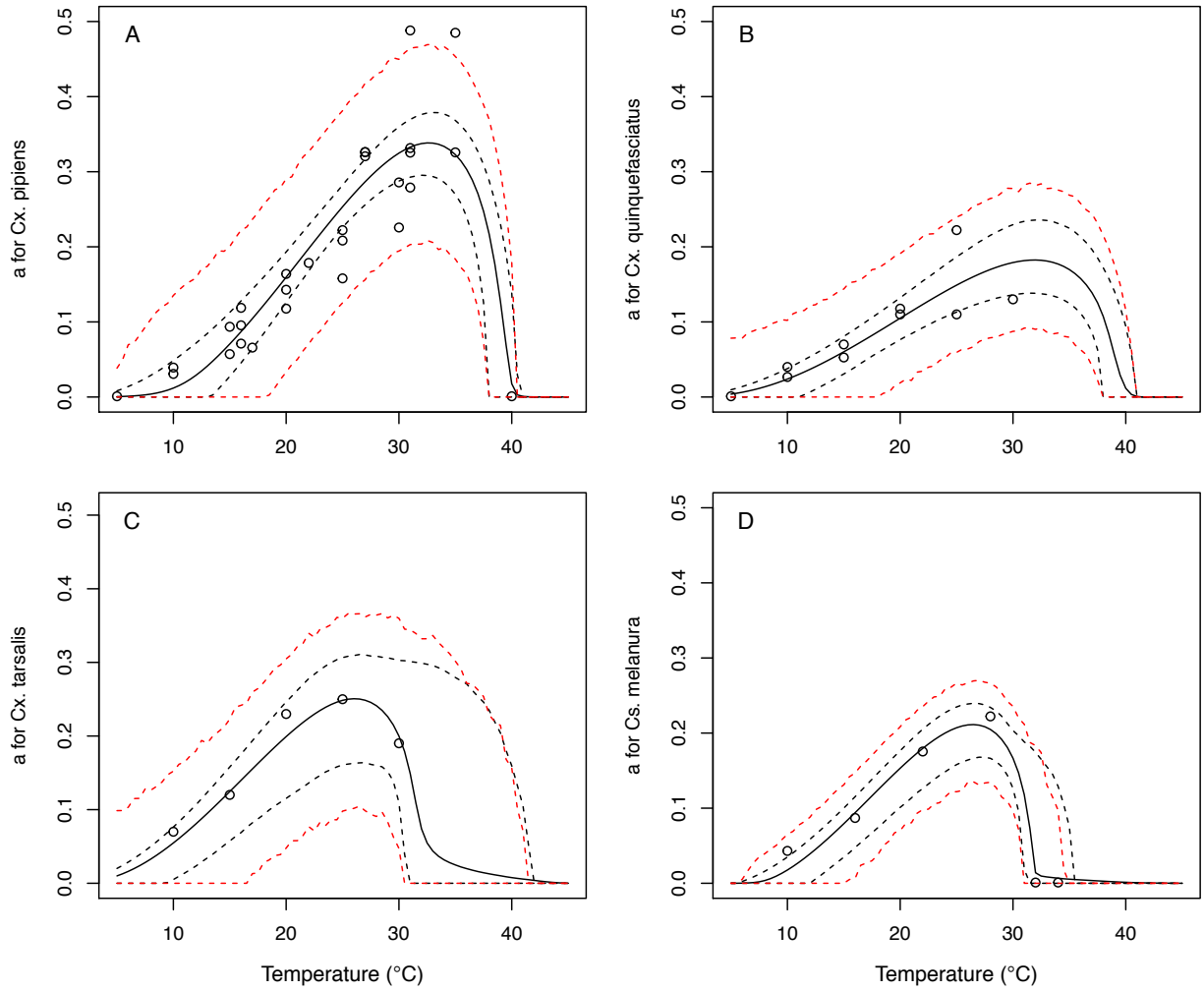

Figure S3: Thermal responses for larval-to-adult survival (*pLA*) showing individual data points. (A) *Culex pipiens*, (B), *Cx. quinquefasciatus*, (C) *Cx. tarsalis*, (D) *Aedes vexans*, (E) *Ae. triseriatus*, and (F) *Culiseta melanura*. Solid lines are posterior distribution means for the mean thermal response; black dashed lines are 95% credible intervals for the mean thermal response; red dashed lines are 95% prediction intervals for observed data (incorporating the fitted variance).

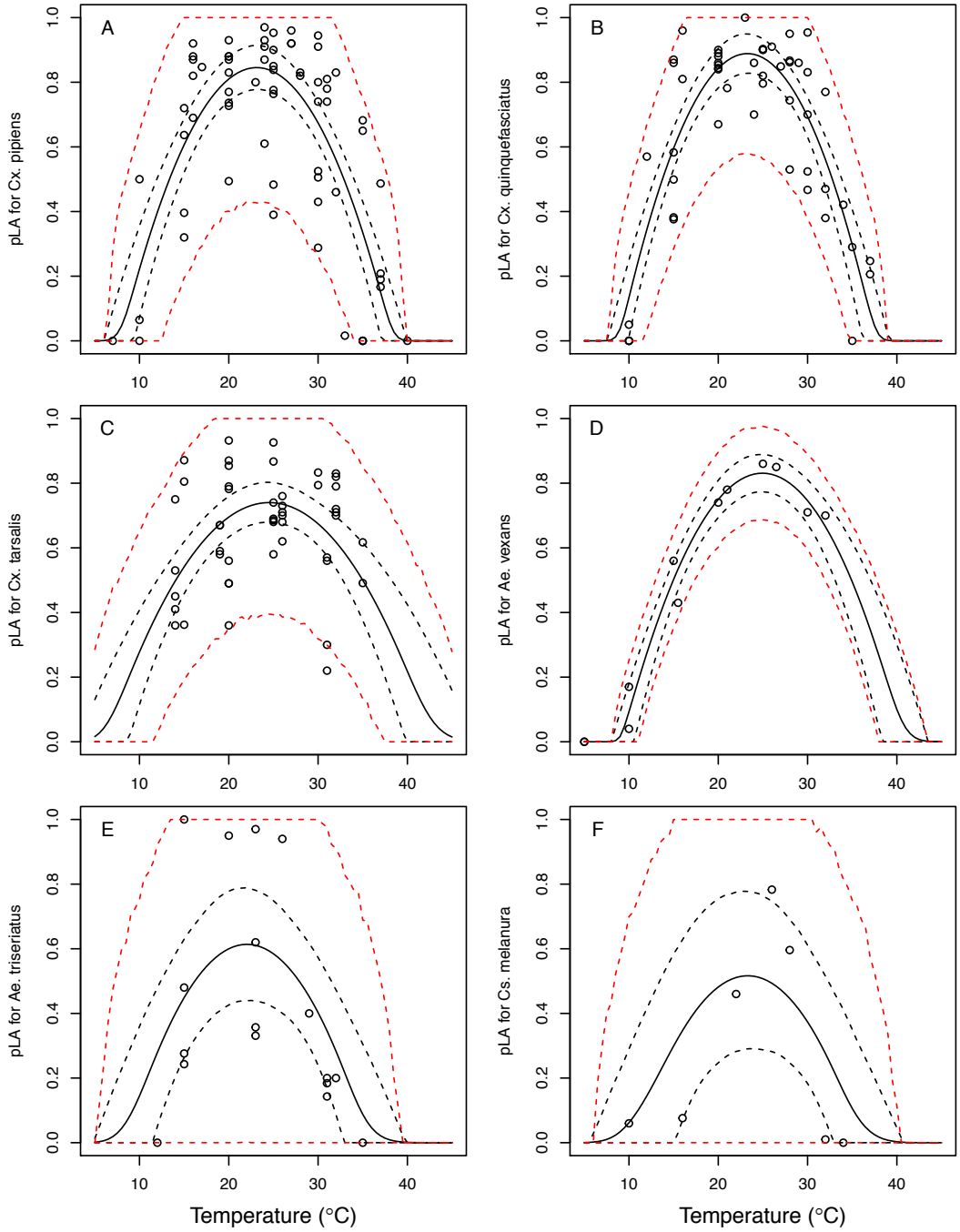

Figure S4: Thermal responses for mosquito development rate (*MDR*) showing individual data points. (A) *Culex pipiens*, (B), *Cx. quinquefasciatus*, (C) *Cx. tarsalis*, (D) *Aedes vexans*, (E) *Ae. triseriatus*, and (F) *Culiseta melanura*. Solid lines are posterior distribution means for the mean thermal response; black dashed lines are 95% credible intervals for the mean thermal response; red dashed lines are 95% prediction intervals for observed data (incorporating the fitted variance).

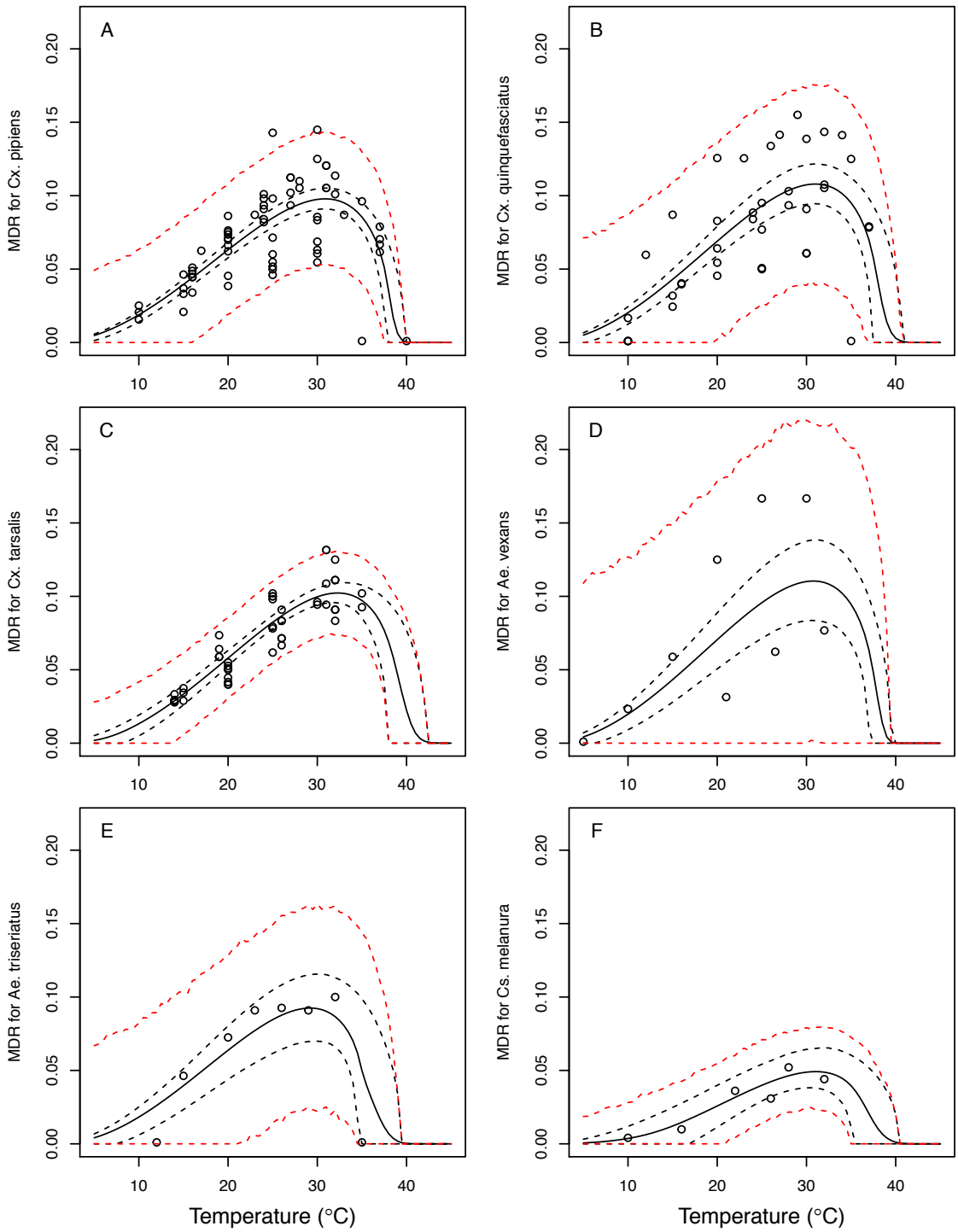

Figure S5: Thermal responses for adult mosquito lifespan (*lf*) showing individual data points. (A) *Culex pipiens*, (B), *Cx. quinquefasciatus*, (C) *Cx. tarsalis*, and (D) *Aedes taeniorhynchus*. When data were reported by sex, only female data were used. Solid lines are posterior distribution means for the mean thermal response; black dashed lines are 95% credible intervals for the mean thermal response; red dashed lines are 95% prediction intervals for observed data (incorporating the fitted variance).

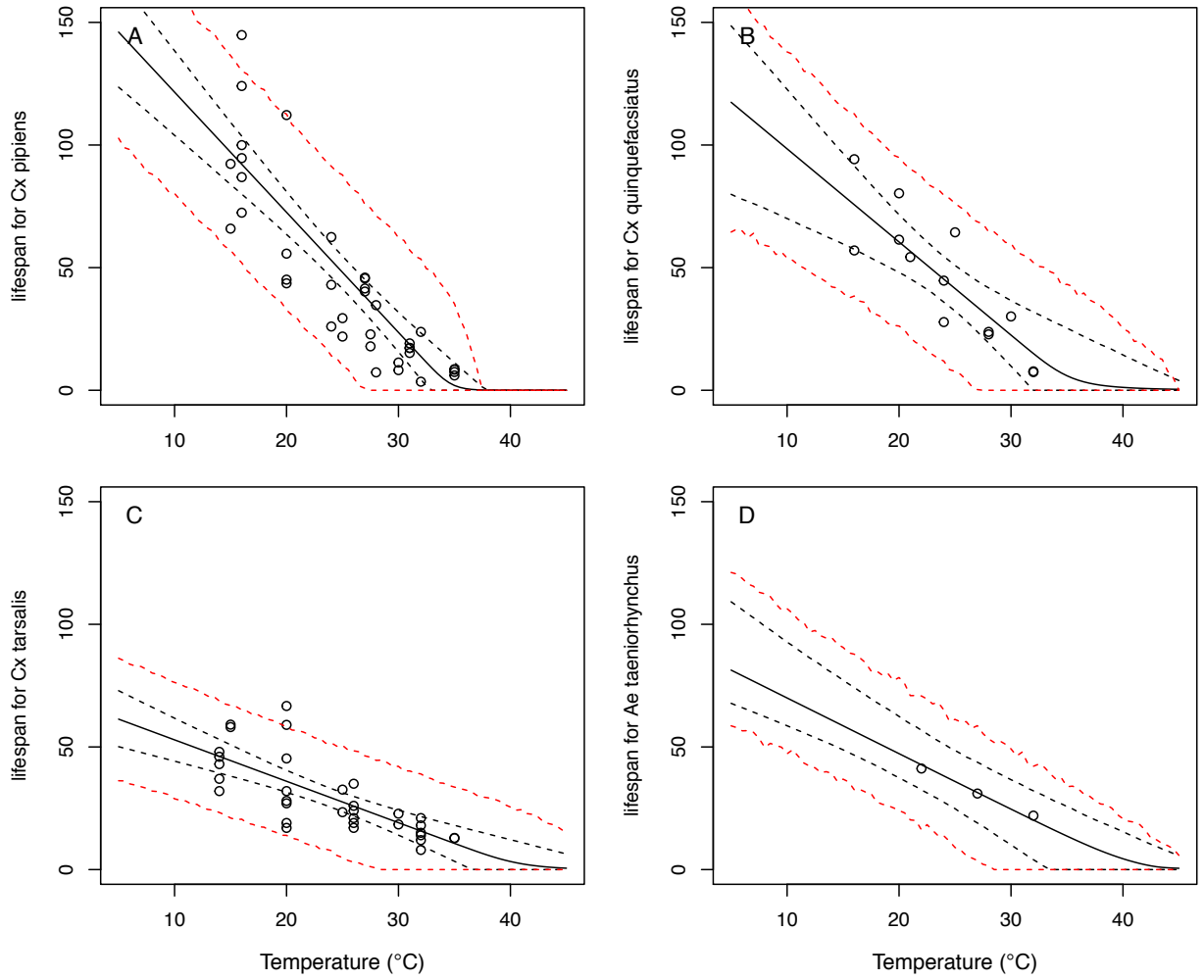

Figure S6: Thermal responses for fecundity traits showing individual data points. Traits: (A) Reproduction measured as eggs per female per gonotrophic cycle (*EFGC*), (B) reproduction measured as eggs per raft (*ER*) (C–E) proportion ovipositing (*pO*), and (F–I) egg viability (*EV*). Vector species: (A,C,F) *Culex pipiens*, (B,D,G), *Cx. quinquefasciatus*, (E) *Culiseta melanura*, (H) *Cx. theileri*, and (I) *Aedes vexans*. Solid lines are posterior distribution means for the mean thermal response; black dashed lines are 95% credible intervals for the mean thermal response; red dashed lines are 95% prediction intervals for observed data (incorporating the fitted variance).

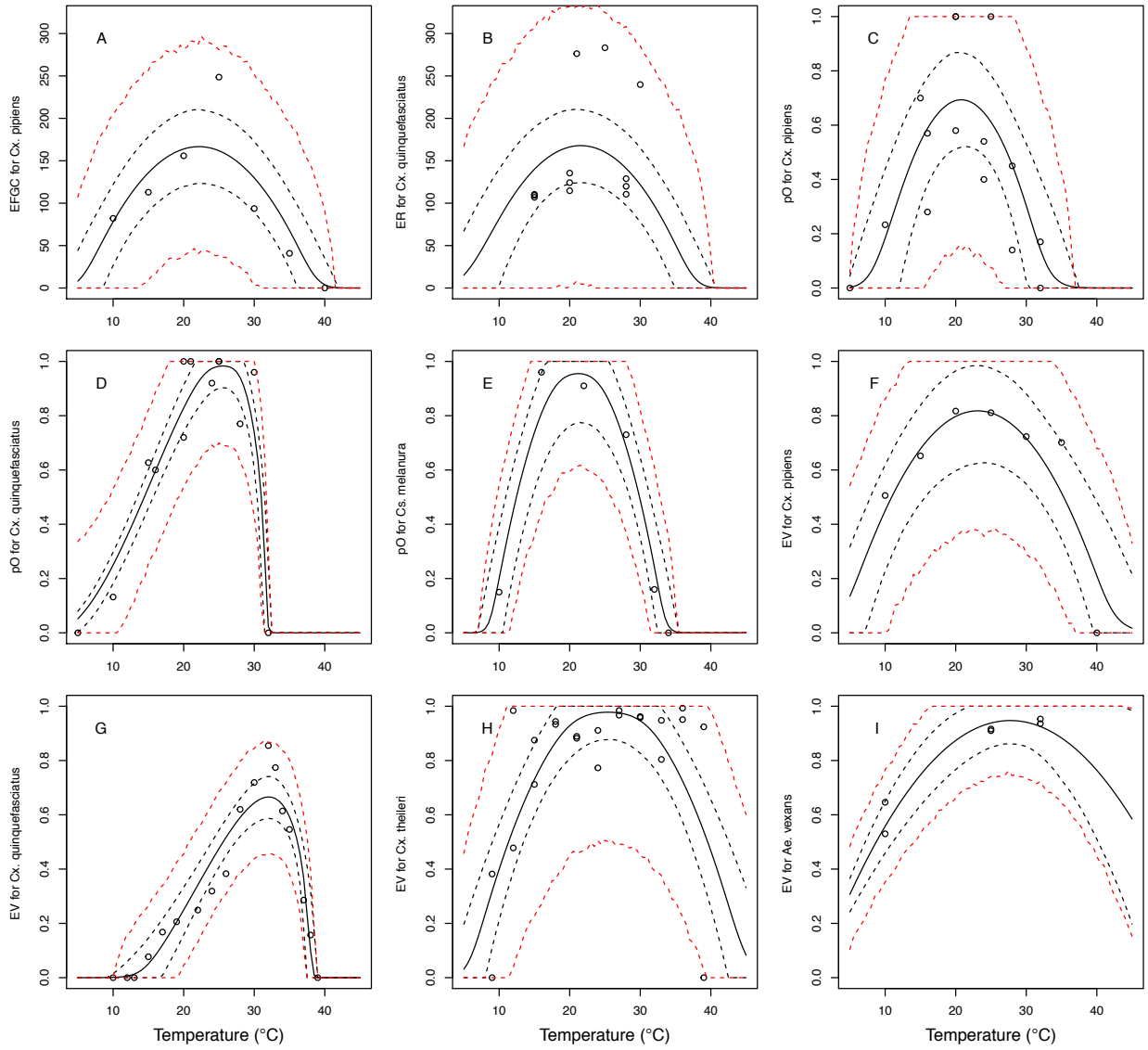

Figure S7: Thermal responses for pathogen development rate (*PDR*) showing individual data points. (A) West Nile virus (WNV) in *Culex pipiens*, (B), WNV in *Cx. quinquefasciatus*, (C) WNV in *Cx. tarsalis*, (D) WNV in *Cx. univittatus*, (E) St. Louis Encephalitis virus (SLEV) in *Cx. tarsalis*, (F) Western Equine Encephalitis virus (WEEV) in *Cx. tarsalis*, and (G) Eastern Equine Encephalitis virus (EEEV) in *Aedes triseriatus*. Solid lines are posterior distribution means for the mean thermal response; black dashed lines are 95% credible intervals for the mean thermal response; red dashed lines are 95% prediction intervals for observed data (incorporating the fitted variance).

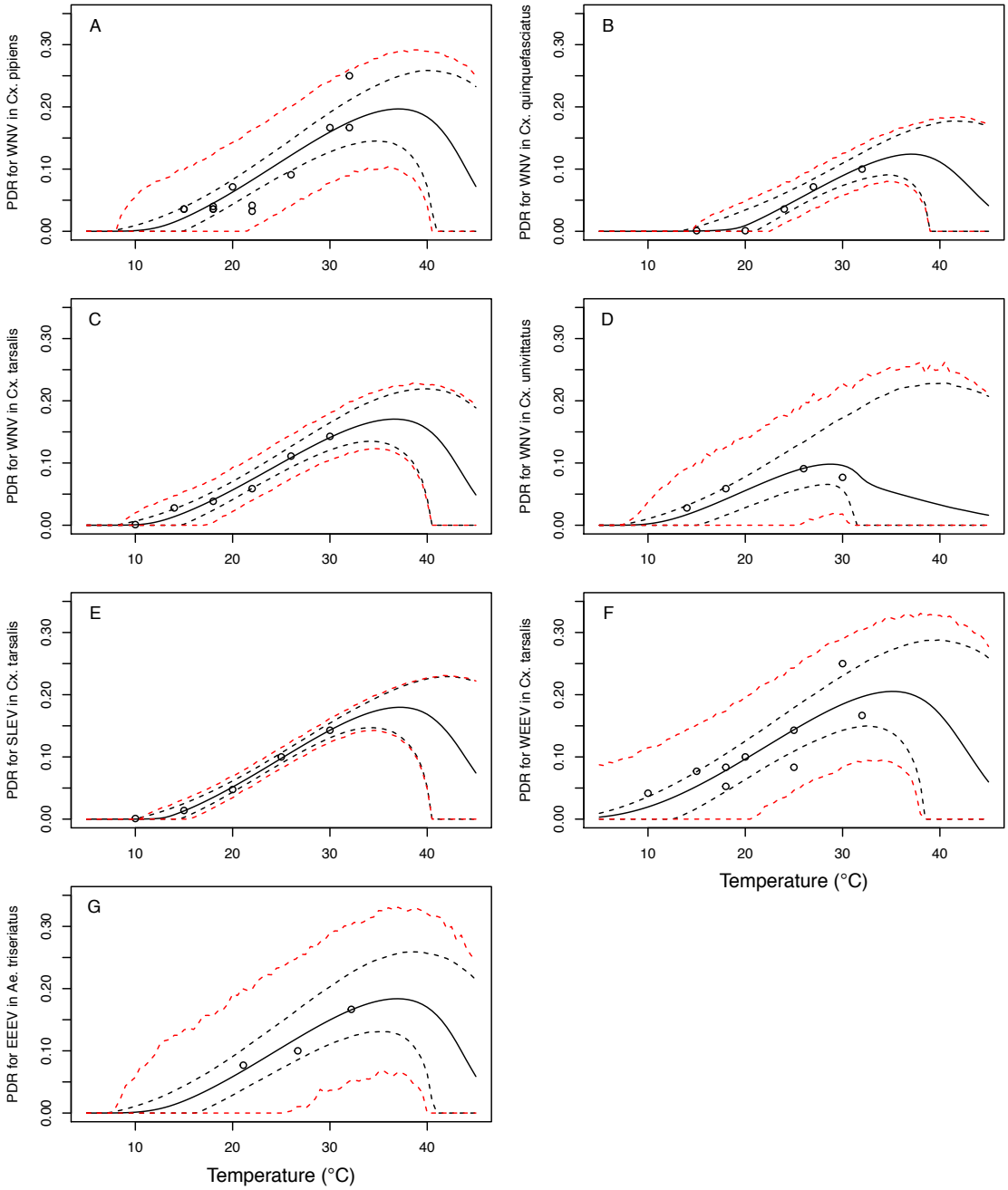

Figure S8: Thermal responses for vector competence traits in *Culex tarsalis*, showing individual data points. Traits: (A,B,F) transmission efficiency (*b*, # transmitting / # infected), (C,E) infection efficiency (*c*, # infected / # exposed), and (D) vector competence (*bc*, # infected / # exposed). Viruses: (A) West Nile virus (WNV), (B–D) Western Equine Encephalitis virus (WEEV), (E,F) St. Louis Encephalitis virus (SLEV). Solid lines are posterior distribution means for the mean thermal response; black dashed lines are 95% credible intervals for the mean thermal response; red dashed lines are 95% prediction intervals for observed data (incorporating the fitted variance).

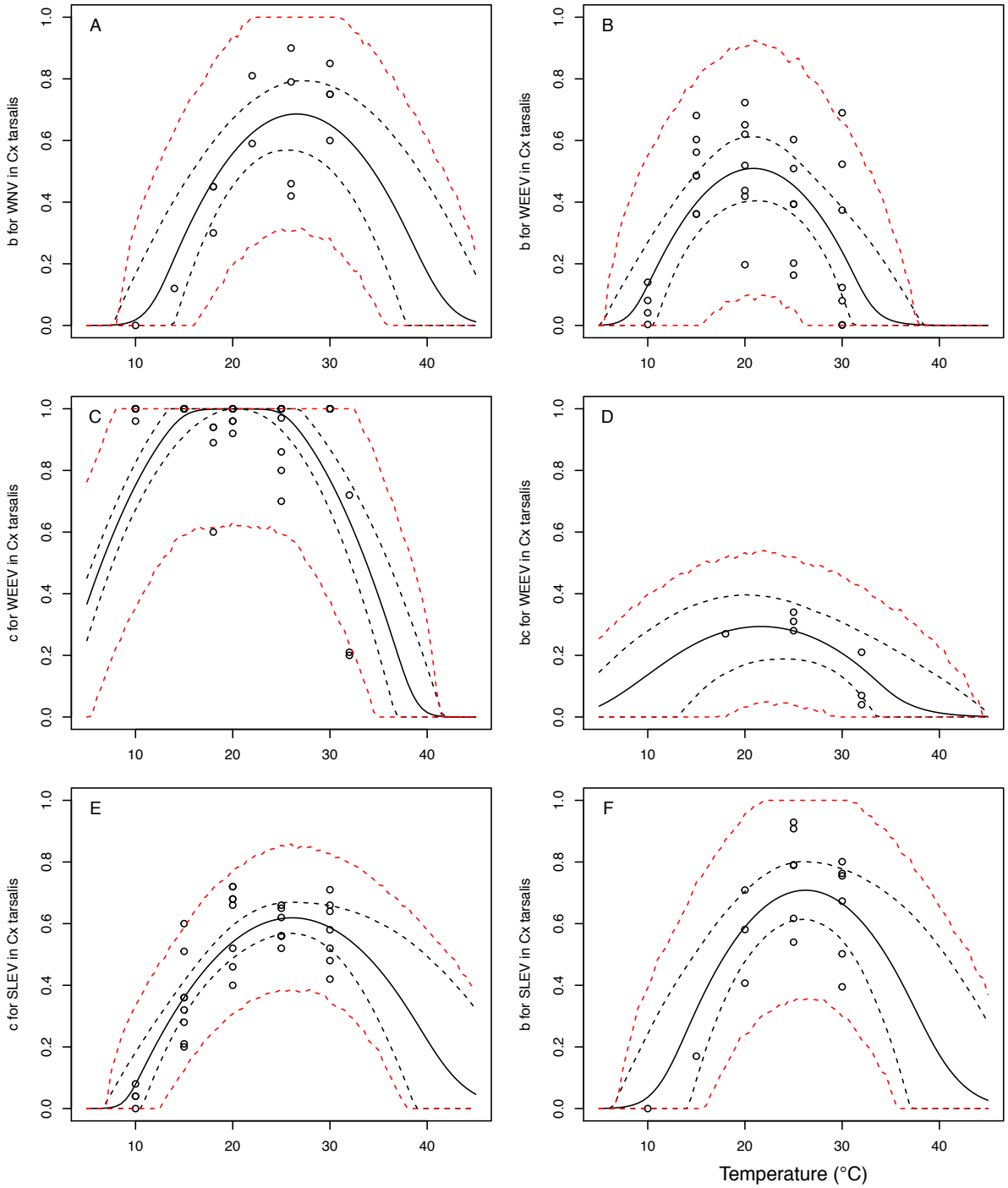

Figure S9: Thermal responses for vector competence traits showing individual data points. Traits: (A,E,F) infection efficiency (*c*, # infected / # exposed) and (B,C,D,G) vector competence (*bc*, # infected / # exposed). Viruses and vectors: (A,B) West Nile virus (WNV) in *Culex pipiens*, (C) WNV in *Cx. univittatus*, (D) Eastern Equine Encephalitis virus (EEEV) in *Ae. triseriatus*, (E) Sindbis virus (SINV) in *Culex pipiens*, (F) SINV in *Aedes taeniorhynchus*, and (G) Rift Valley Fever virus (RVFV) in *Ae. taeniorhynchus*. Solid lines are posterior distribution means for the mean thermal response; black dashed lines are 95% credible intervals for the mean thermal response; red dashed lines are 95% prediction intervals for observed data (incorporating the fitted variance).

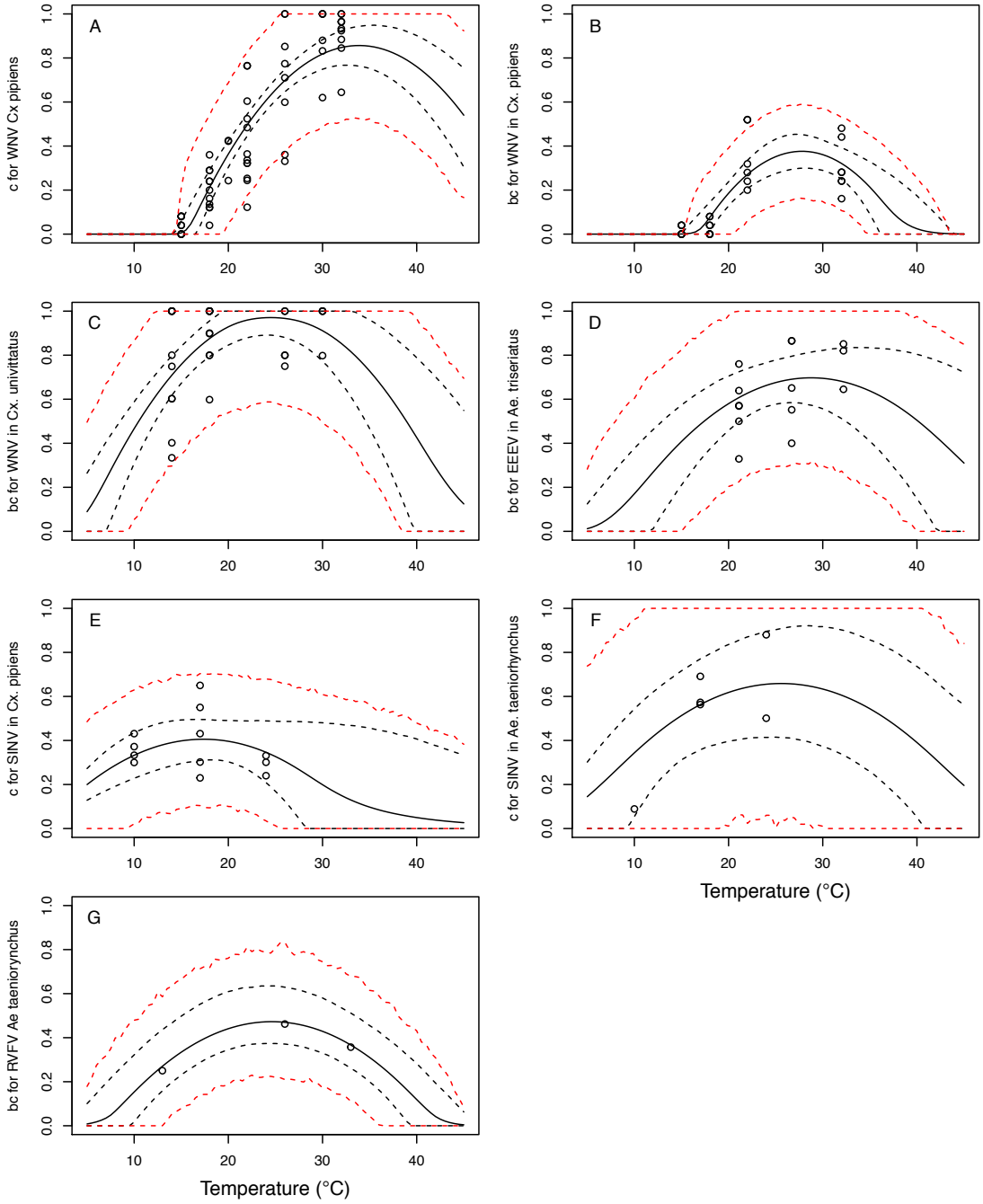

Figure S10: Medians & 95% credible intervals for thermal limits and optima of R_0 models across temperate and tropical mosquito-borne disease systems. Models in order from top to bottom: Eastern Equine Encephalitis virus (EEEV) in *Aedes triseriatus* (dark purple; this paper), Western Equine Encephalitis virus (WEEV) in *Culex. tarsalis* (light purple; this paper), Sindbis virus (SINV) in *Cx. pipiens* (dark blue; this paper), West Nile virus (WNV) in *Cx. univittatus* (medium blue; this paper), WNV in *Cx. tarsalis* (light blue, this paper), St. Louis Encephalitis virus (SLEV) in *Cx. tarsalis* (dark teal; this paper), WNV in *Cx. pipiens* (light teal; this paper), WNV in *Cx. quinquefasciatus* (dark green; this paper), *Plasmodium falciparum* malaria in *Anopheles* spp. (light green; [3]), Rift Valley Fever virus (RVFV) in *Ae. taeniorhynchus* (yellow; this paper), SINV in *Ae. taeniorhynchus* (light orange; this paper), Ross River virus (RRV) in *Cx. annulirostris* (medium orange, [5]), dengue virus (DENV) in *Ae. albopictus* (dark orange; [4]), Murray Valley Encephalitis virus (MVEV) in *Cx. annulirostris* (light red, [5]), Zika virus (ZIKV) in *Ae. aegypti* (medium red; [6]), DENV in *Ae. aegypti* (dark red; [4]). Figure modified from [53].

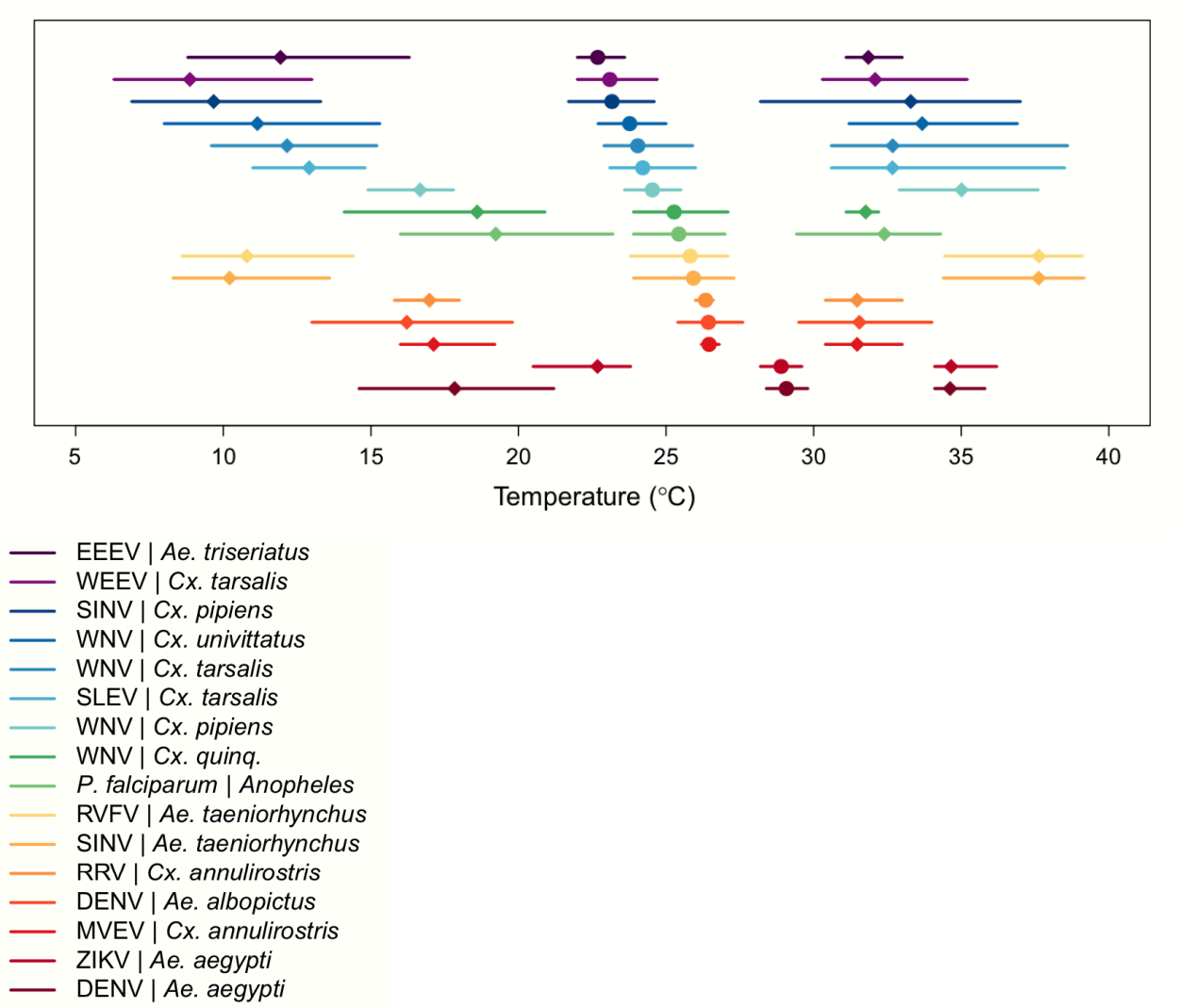

Figure S11: Temperature-dependent R_0, sensitivity analyses, and uncertainty analysis for model of West Nile Virus (WNV) in *Culex pipiens*. (A) Median temperature-dependent R_0 (black line) with 95% credible intervals (dashed red lines). (B) Sensitivity analysis #1: derivative with respect to temperature for R_0 (black) and partial derivatives with respect to temperature for each trait. (C) Sensitivity analysis #2: relative R_0 calculated with single traits held constant. (D) Uncertainty analysis using highest posterior density (HPD) interval widths: the proportion of total uncertainty due to each trait. (B-D) Trait colors: biting rate (*a*, red), vector competence (*bc*, orange), adult lifespan (*lf*, green), parasite development rate (*PDR*, cyan), fecundity (*EFGC*, light blue), egg viability (*EV*, dark blue), larval survival (*pLA*, purple), and mosquito development rate (*MDR*, pink). All traits from *Cx. pipiens*.

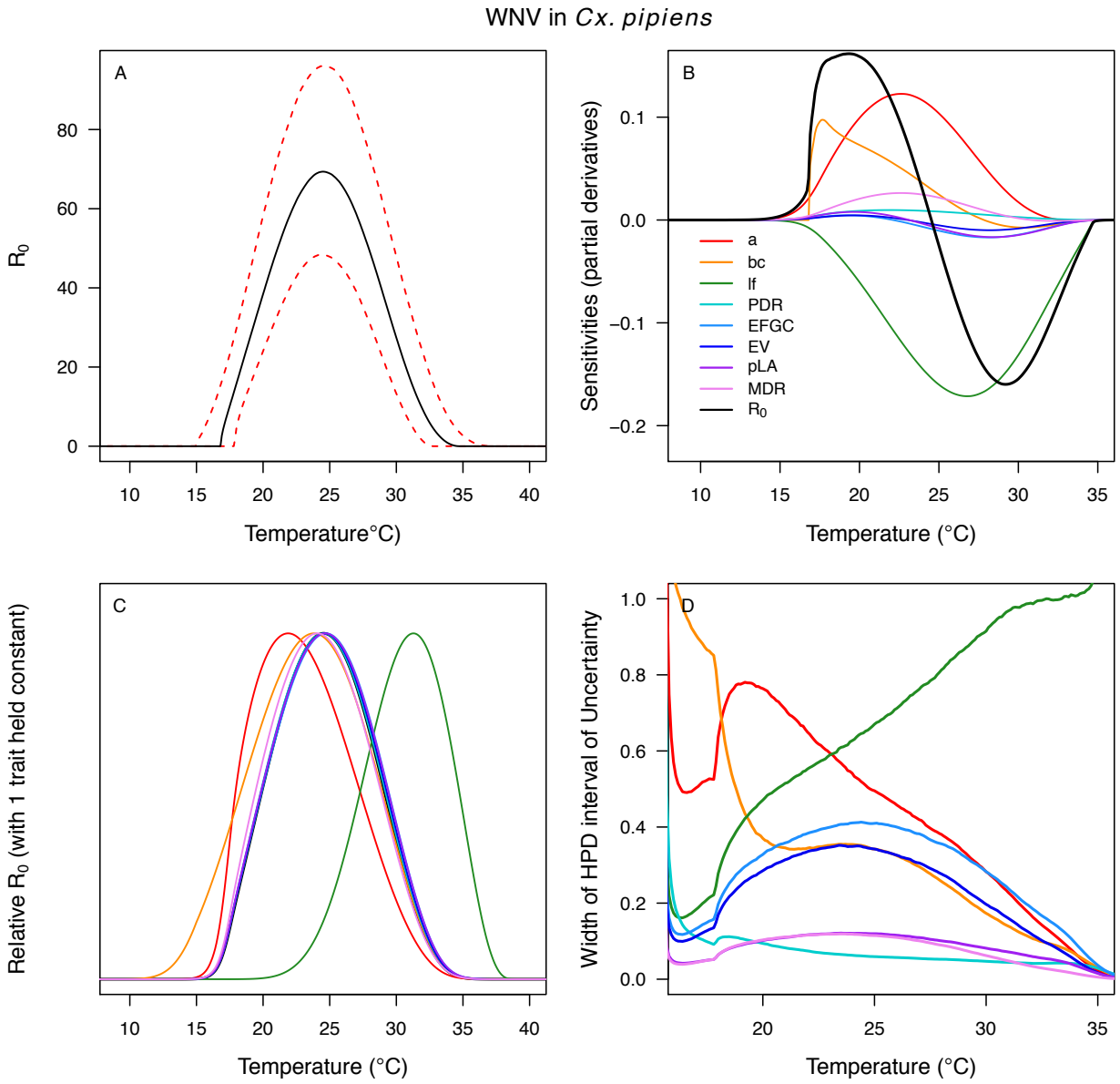

Figure S12: Temperature-dependent R_0, sensitivity analyses, and uncertainty analysis for model of West Nile Virus (WNV) in *Culex quinquefasciatus*. (A) Median temperature-dependent R_0 (black line) with 95% credible intervals (dashed red lines). (B) Sensitivity analysis #1: derivative with respect to temperature for R_0 (black) and partial derivatives with respect to temperature for each trait. (C) Sensitivity analysis #2: relative R_0 calculated with single traits held constant. (D) Uncertainty analysis using highest posterior density (HPD) interval widths: the proportion of total uncertainty due to each trait. (B-D) Trait colors: biting rate (*a*, red), vector competence (*bc*, orange), adult lifespan (*lf*, green), parasite development rate (*PDR*, cyan), fecundity (*EFGC*, light blue), egg viability (*EV*, dark blue), larval survival (*pLA*, purple), mosquito development rate (*MDR*, pink), and proportion ovipositing (*pO*, grey). Vector competence (*bc*) from *Cx. univitattus*; all other traits from *Cx. quinquefasciatus*.

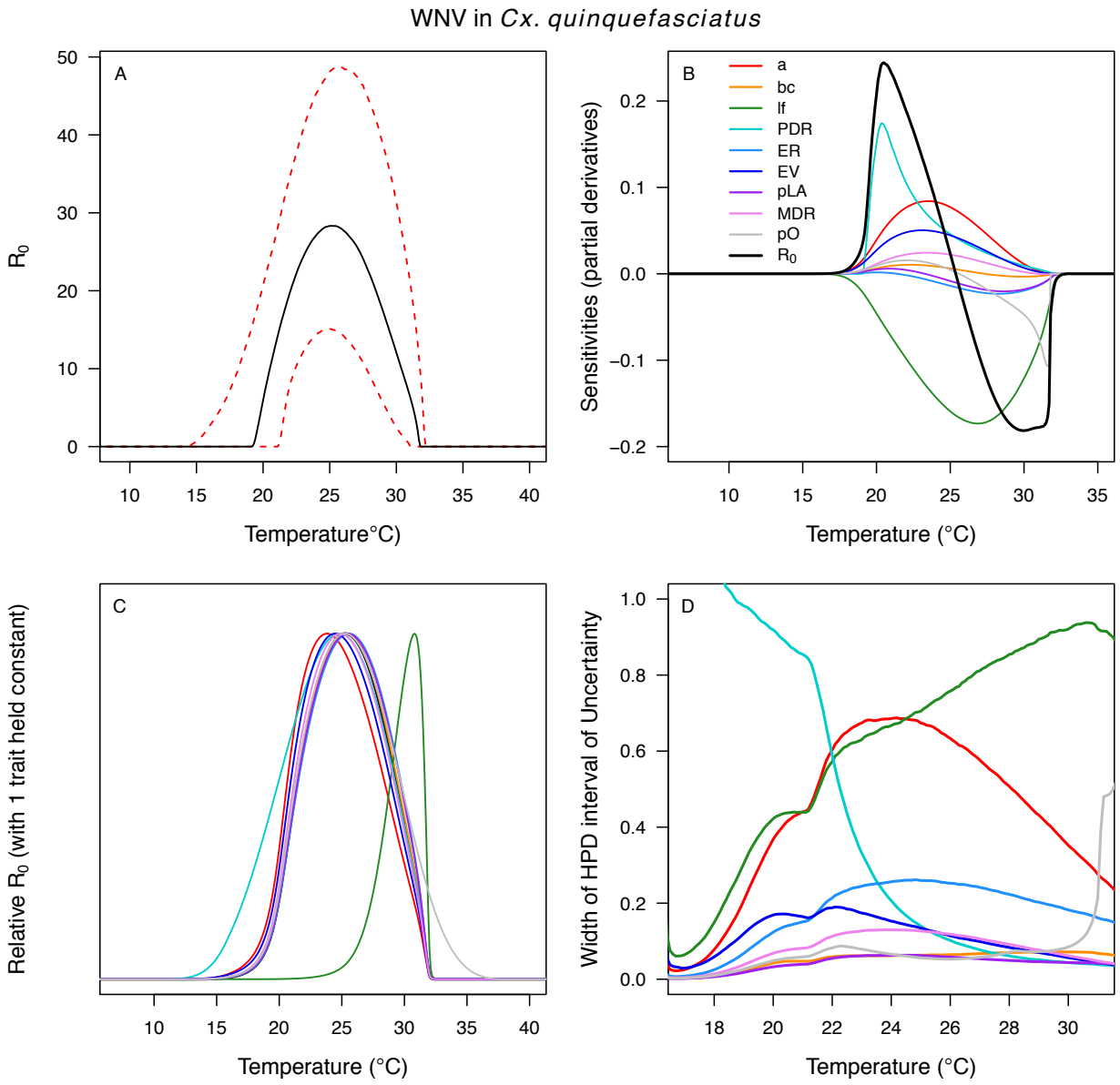

Figure S13: Temperature-dependent R_0, sensitivity analyses, and uncertainty analysis for model of West Nile Virus (WNV) in *Culex tarsalis*. (A) Median temperature-dependent R_0 (black line) with 95% credible intervals (dashed red lines). (B) Sensitivity analysis #1: derivative with respect to temperature for R_0 (black) and partial derivatives with respect to temperature for each trait. (C) Sensitivity analysis #2: relative R_0 calculated with single traits held constant. (D) Uncertainty analysis using highest posterior density (HPD) interval widths: the proportion of total uncertainty due to each trait. (B-D) Trait colors: biting rate (*a*, red), transmission efficiency (*b*, orange), adult lifespan (*lf*, green), parasite development rate (*PDR*, cyan), fecundity (*EFGC*, light blue), egg viability (*EV*, dark blue), larval survival (*pLA*, purple), and mosquito development rate (*MDR*, pink). Fecundity (*EFGC*) and egg viability (*EV*) from *Cx. pipiens*; all other traits from *Cx. tarsalis*.

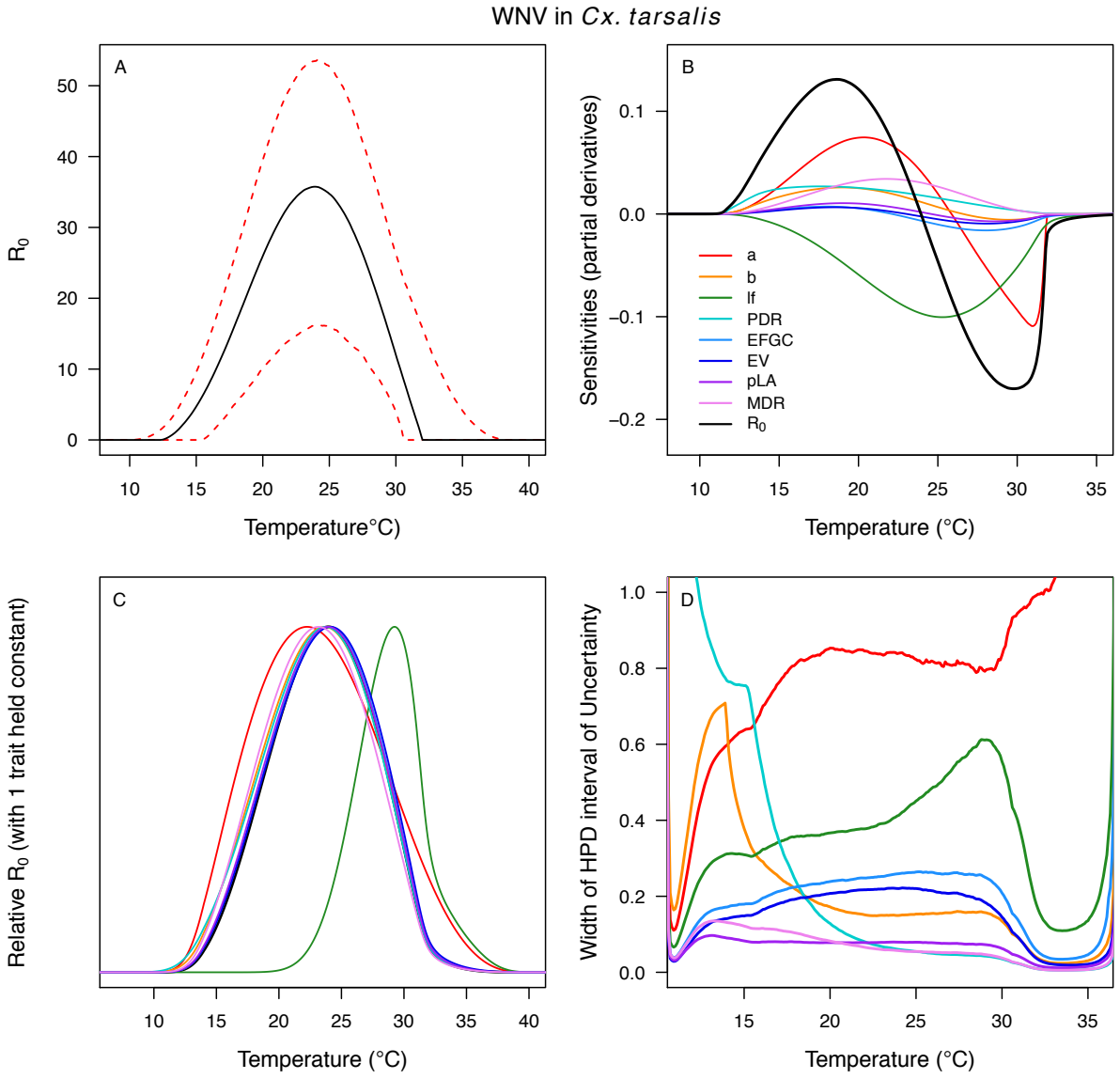

Figure S14: Temperature-dependent R_0, sensitivity analyses, and uncertainty analysis for model of West Nile Virus (WNV) in *Culex univittatus*. (A) Median temperature-dependent R_0 (black line) with 95% credible intervals (dashed red lines). (B) Sensitivity analysis #1: derivative with respect to temperature for R_0 (black) and partial derivatives with respect to temperature for each trait. (C) Sensitivity analysis #2: relative R_0 calculated with single traits held constant. (D) Uncertainty analysis using highest posterior density (HPD) interval widths: the proportion of total uncertainty due to each trait. (B-D) Trait colors: biting rate (*a*, red), vector competence (*bc*, orange), adult lifespan (*lf*, green), parasite development rate (*PDR*, cyan), fecundity (*EFGC*, light blue), egg viability (*EV*, dark blue), larval survival (*pLA*, purple), and mosquito development rate (*MDR*, pink). Infection traits (*bc* and *PDR*) from *Cx. univittatus*; all other traits from *Cx. pipiens*.

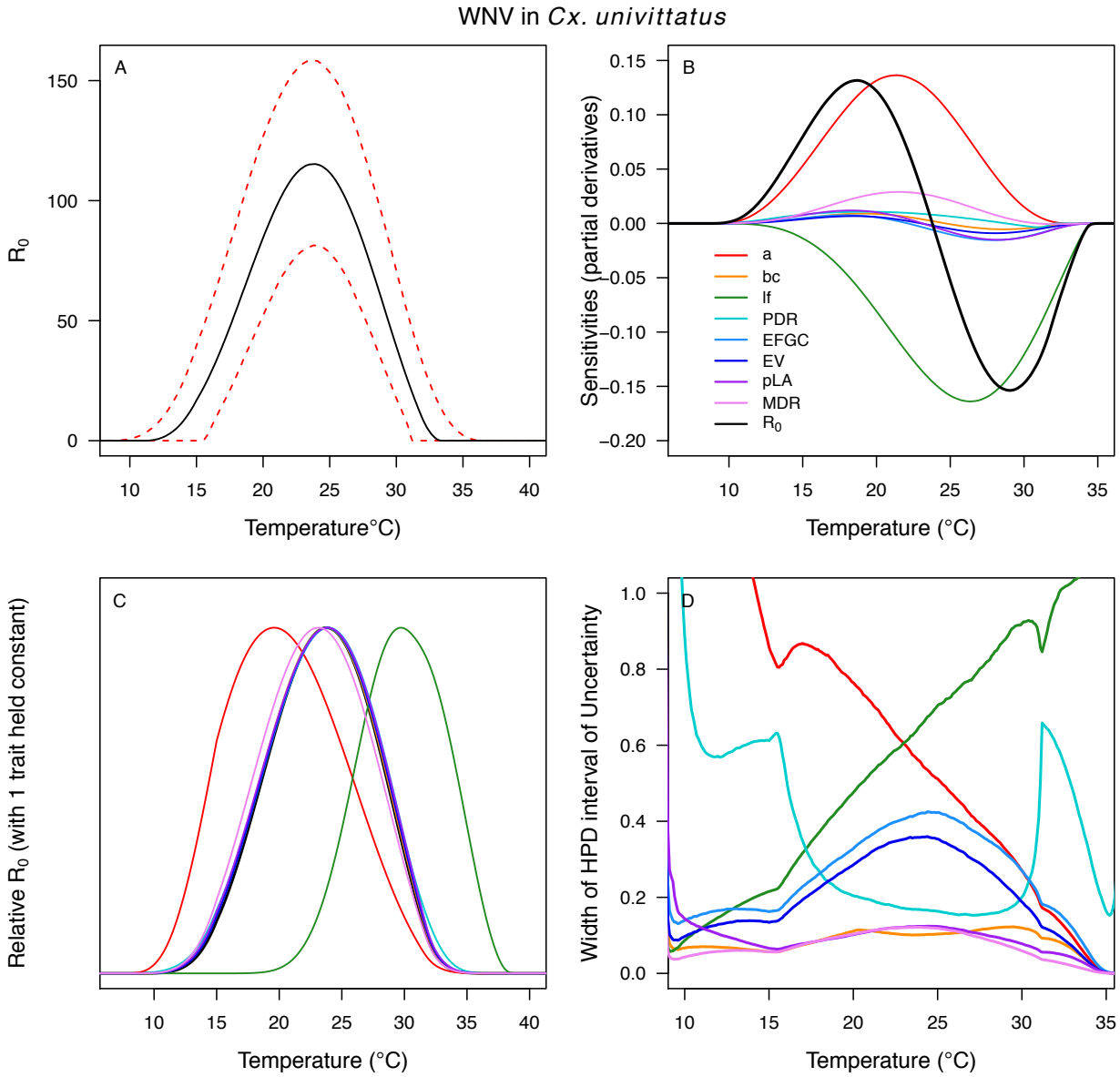

Figure S15: Temperature-dependent R_0, sensitivity analyses, and uncertainty analysis for St. model of St. Louis Encephalitis Virus (SLEV) in *Culex tarsalis*. (A) Median temperature-dependent R_0 (black line) with 95% credible intervals (dashed red lines). (B) Sensitivity analysis #1: derivative with respect to temperature for R_0 (black) and partial derivatives with respect to temperature for each trait. (C) Sensitivity analysis #2: relative R_0 calculated with single traits held constant. (D) Uncertainty analysis using highest posterior density (HPD) interval widths: the proportion of total uncertainty due to each trait. (B-D) Trait colors: biting rate (*a*, red), transmission efficiency (*b*, orange), infection efficiency (*c*, brown), adult lifespan (*lf*, green), parasite development rate (*PDR*, cyan), fecundity (*EFGC*, light blue), egg viability (*EV*, dark blue), larval survival (*pLA*, purple), and mosquito development rate (*MDR*, pink). Fecundity (*EFGC*) and egg viability (*EV*) from *Cx. pipiens*; all other traits from *Cx. tarsalis*.

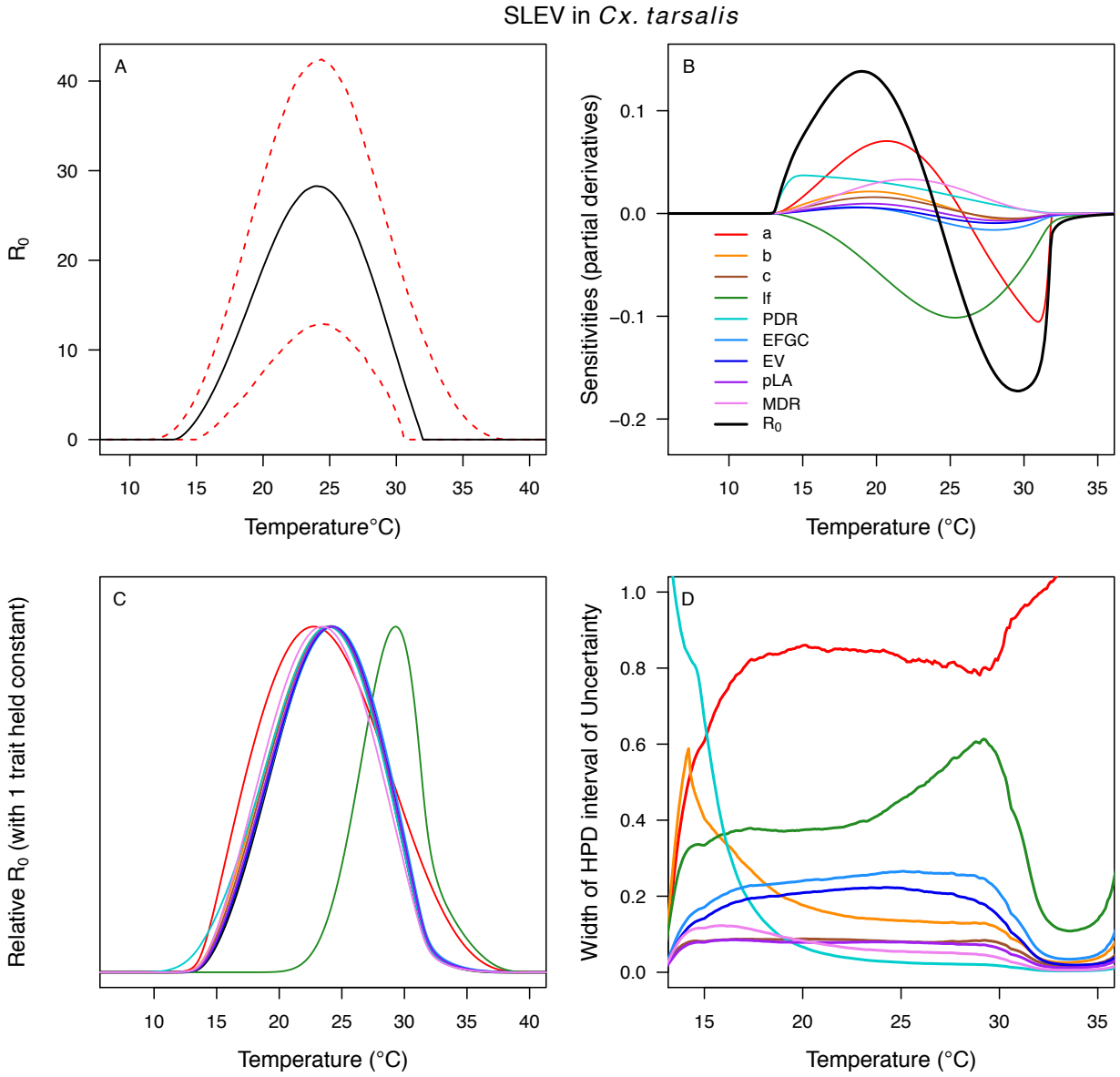

Figure S16: Temperature-dependent R_0, sensitivity analyses, and uncertainty analysis for model of Western Equine Encephalitis Virus (WEEV) in *Culex tarsalis*. (A) Median temperature-dependent R_0 (black line) with 95% credible intervals (dashed red lines). (B) Sensitivity analysis #1: derivative with respect to temperature for R_0 (black) and partial derivatives with respect to temperature for each trait. (C) Sensitivity analysis #2: relative R_0 calculated with single traits held constant. (D) Uncertainty analysis using highest posterior density (HPD) interval widths: the proportion of total uncertainty due to each trait. (B-D) Trait colors: biting rate (*a*, red), transmission efficiency (*b*, orange), infection efficiency (*c*, brown), adult lifespan (*lf*, green), parasite development rate (*PDR*, cyan), fecundity (*EFGC*, light blue), egg viability (*EV*, dark blue), larval survival (*pLA*, purple), and mosquito development rate (*MDR*, pink). Fecundity (*EFGC*) and egg viability (*EV*) from *Cx. pipiens*; all other traits from *Cx. tarsalis*.

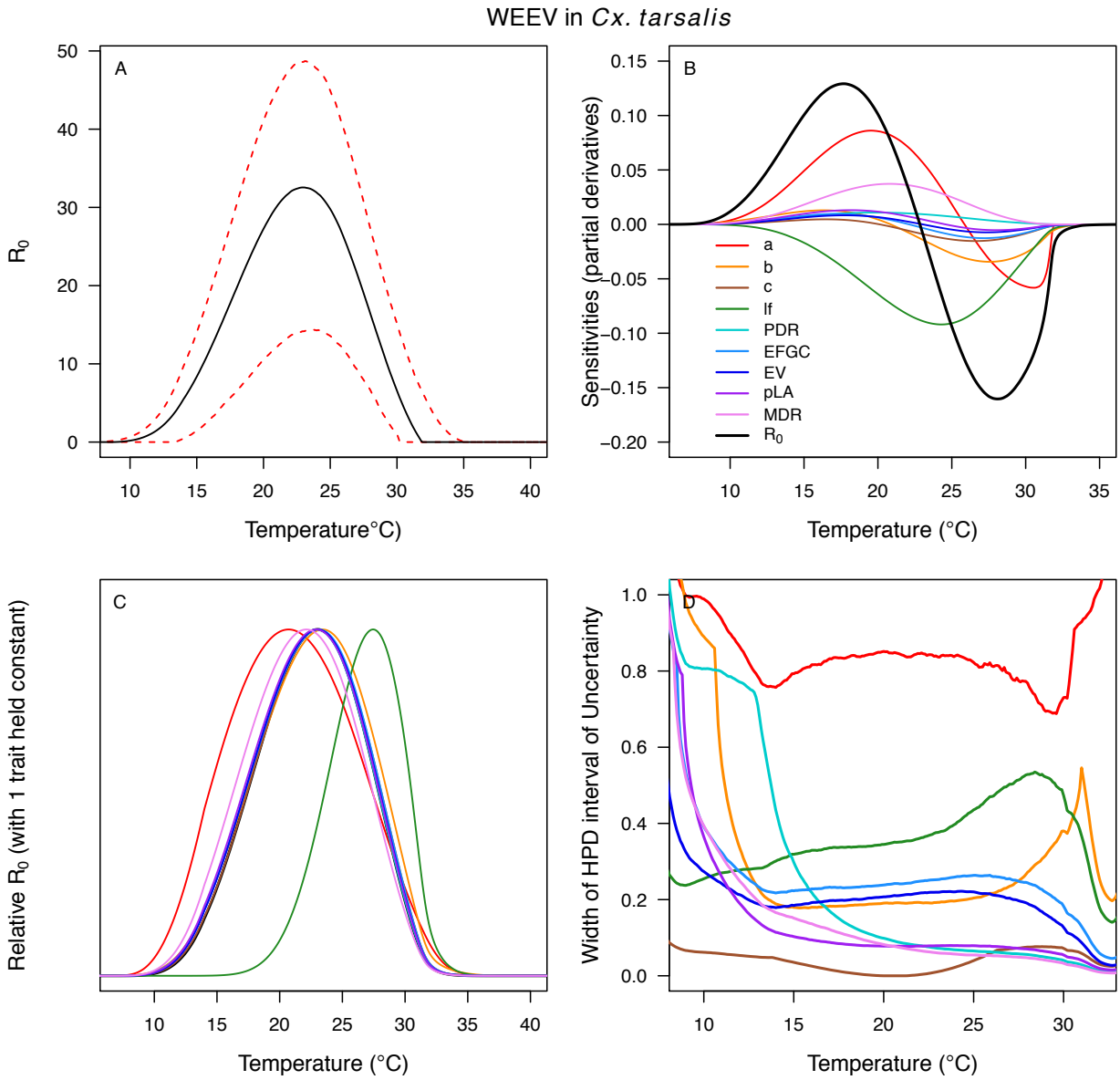

Figure S17: Temperature-dependent R_0, sensitivity analyses, and uncertainty analysis for model of Eastern Equine Encephalitis Virus in *Aedes triseriatus*. (A) Median temperature-dependent R_0 (black line) with 95% credible intervals (dashed red lines). (B) Sensitivity analysis #1: derivative with respect to temperature for R_0 (black) and partial derivatives with respect to temperature for each trait. (C) Sensitivity analysis #2: relative R_0 calculated with single traits held constant. (D) Uncertainty analysis using highest posterior density (HPD) interval widths: the proportion of total uncertainty due to each trait. (B-D) Trait colors: biting rate (*a*, red), vector competence (*bc*, orange), adult lifespan (*lf*, green), parasite development rate (*PDR*, cyan), fecundity (*EFGC*, light blue), egg viability (*EV*, dark blue), larval survival (*pLA*, purple), mosquito development rate (*MDR*, pink), and proportion ovipositing (*pO*, grey). Fecundity (*EFGC*), egg viability (*EV*), and lifespan (*lf*) from *Cx. pipiens*; biting rate (*a*) and proportion ovipositing (*pO*) from *Culiseta melanura*; all other traits from *Ae. triseriatus*. Note: technically fecundity as eggs per female per gonotrophic cycle (*EFGC*) has already accounted for the proportion ovipositing (*pO*). However, we selected this trait fit because it was very similar to the *ER* thermal response from *Cx. quinquefasciatus*, but slightly wider (more conservative).

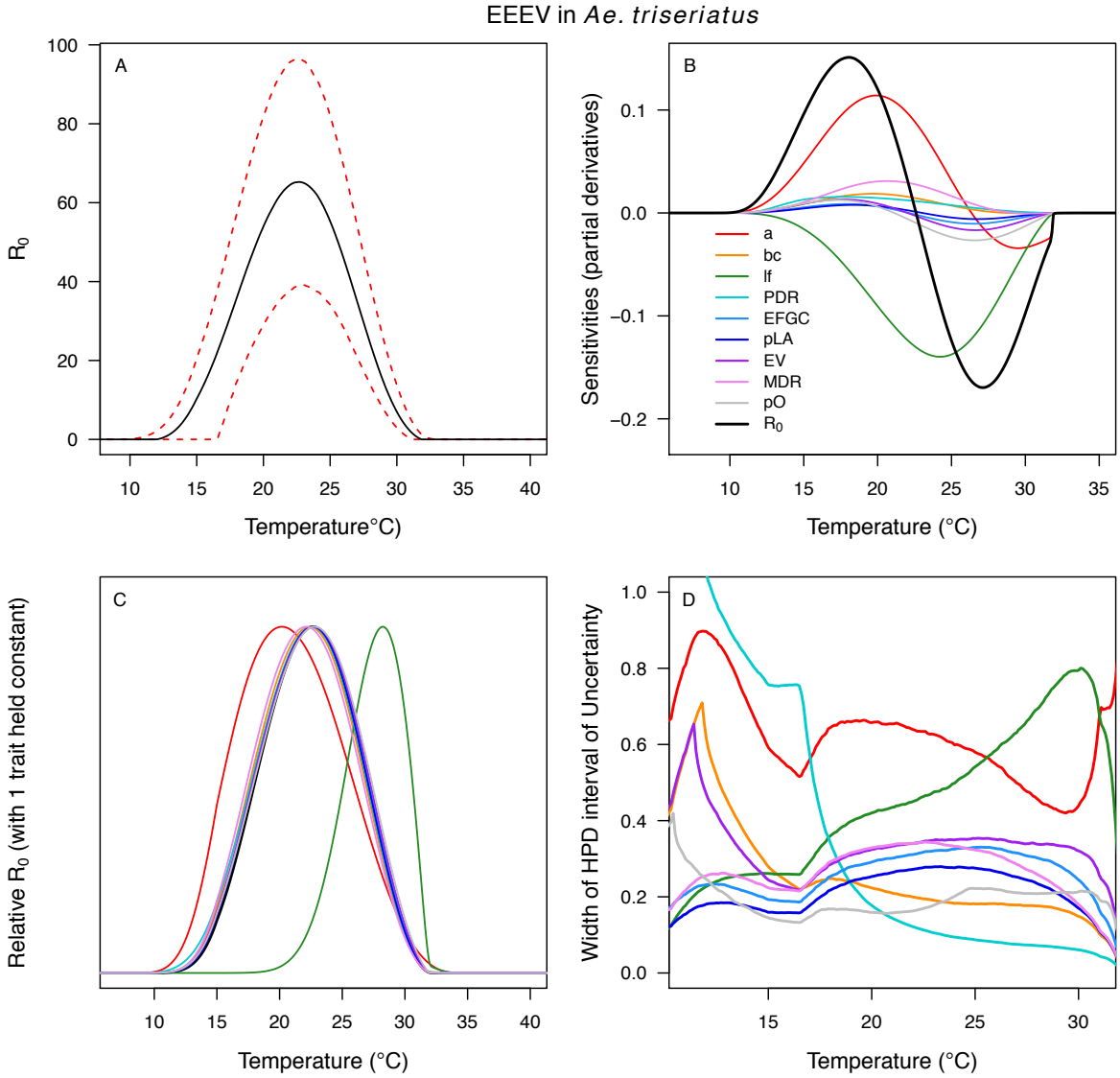

Figure S18: Temperature-dependent R_0, sensitivity analyses, and uncertainty analysis for model of Sindbis Virus in *Culex pipiens*. (A) Median temperature-dependent R_0 (black line) with 95% credible intervals (dashed red lines). (B) Sensitivity analysis #1: derivative with respect to temperature for R_0 (black) and partial derivatives with respect to temperature for each trait. (C) Sensitivity analysis #2: relative R_0 calculated with single traits held constant. (D) Uncertainty analysis using highest posterior density (HPD) interval widths: the proportion of total uncertainty due to each trait. (B-D) Trait colors: biting rate (*a*, red), infection efficiency (*c*, brown), adult lifespan (*lf*, green), fecundity (*EFGC*, light blue), egg viability (*EV*, dark blue), larval survival (*pLA*, purple), and mosquito development rate (*MDR*, pink). All traits from *Cx. pipiens*. NOTE: The raw R_0 calculation used $PDR = 1$, which is not biologically reasonable trait value.

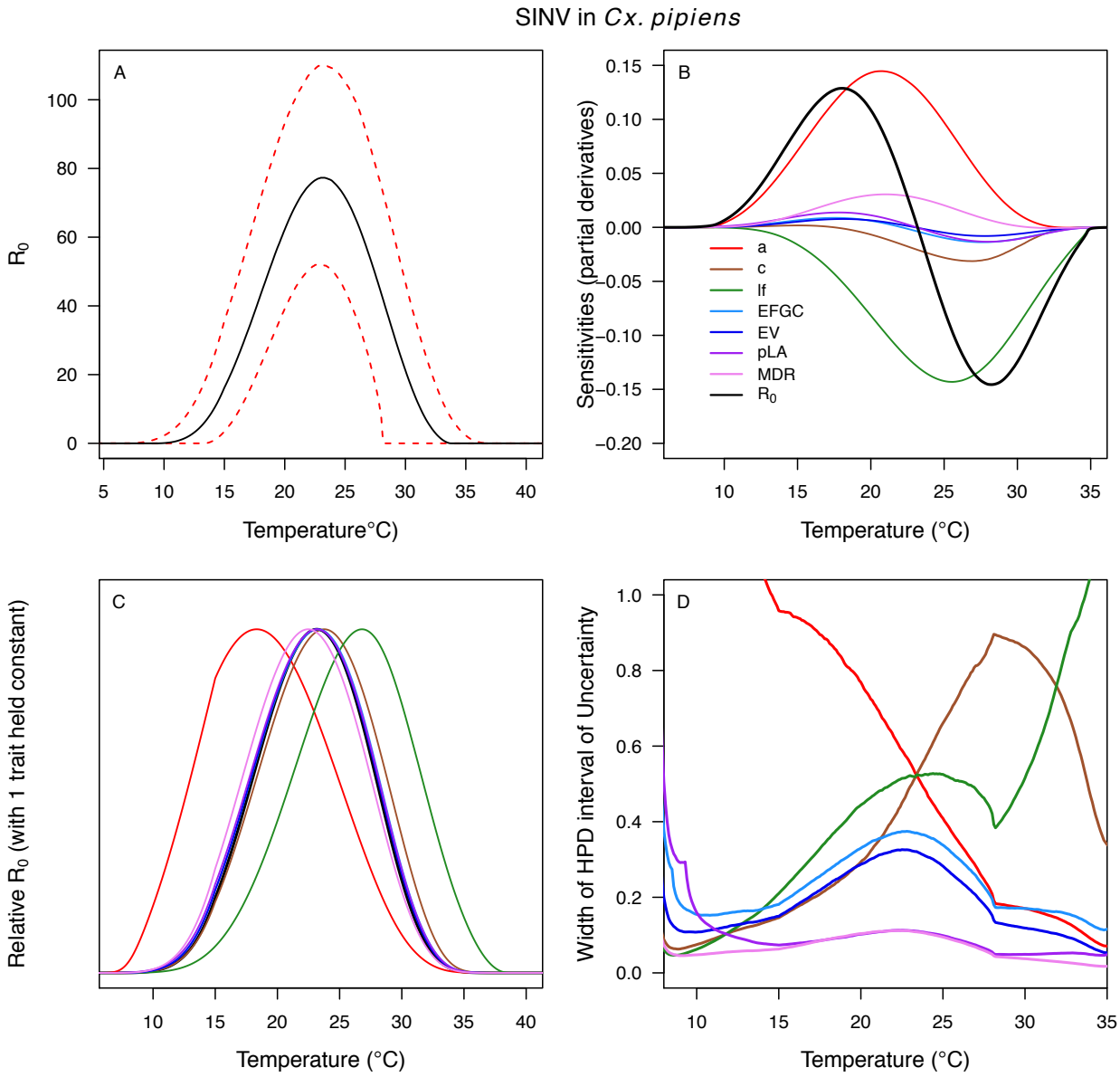

Figure S19: Temperature-dependent R_0, sensitivity analyses, and uncertainty analysis for model of Sindbis Virus in *Aedes taeniorhynchus*. (A) Median temperature-dependent R_0 (black line) with 95% credible intervals (dashed red lines). (B) Sensitivity analysis #1: derivative with respect to temperature for R_0 (black) and partial derivatives with respect to temperature for each trait. (C) Sensitivity analysis #2: relative R_0 calculated with single traits held constant. (D) Uncertainty analysis using highest posterior density (HPD) interval widths: the proportion of total uncertainty due to each trait. (B-D) Trait colors: biting rate (*a*, red), infection efficiency (*c*, brown), adult lifespan (*lf*, green), fecundity (*EFGC*, light blue), egg viability (*EV*, dark blue), larval survival (*pLA*, purple), and mosquito development rate (*MDR*, pink). Fecundity (*EFGC*) and biting rate (*a*) from *Culex pipiens*; egg viability (EV) and larval traits (*pLA* and *MDR*) from *Ae. vexans*; all other traits from *Ae. taeniorhynchus*. NOTE: The raw R_0 calculation used *PDR* = 1, which is not biologically reasonable trait value.

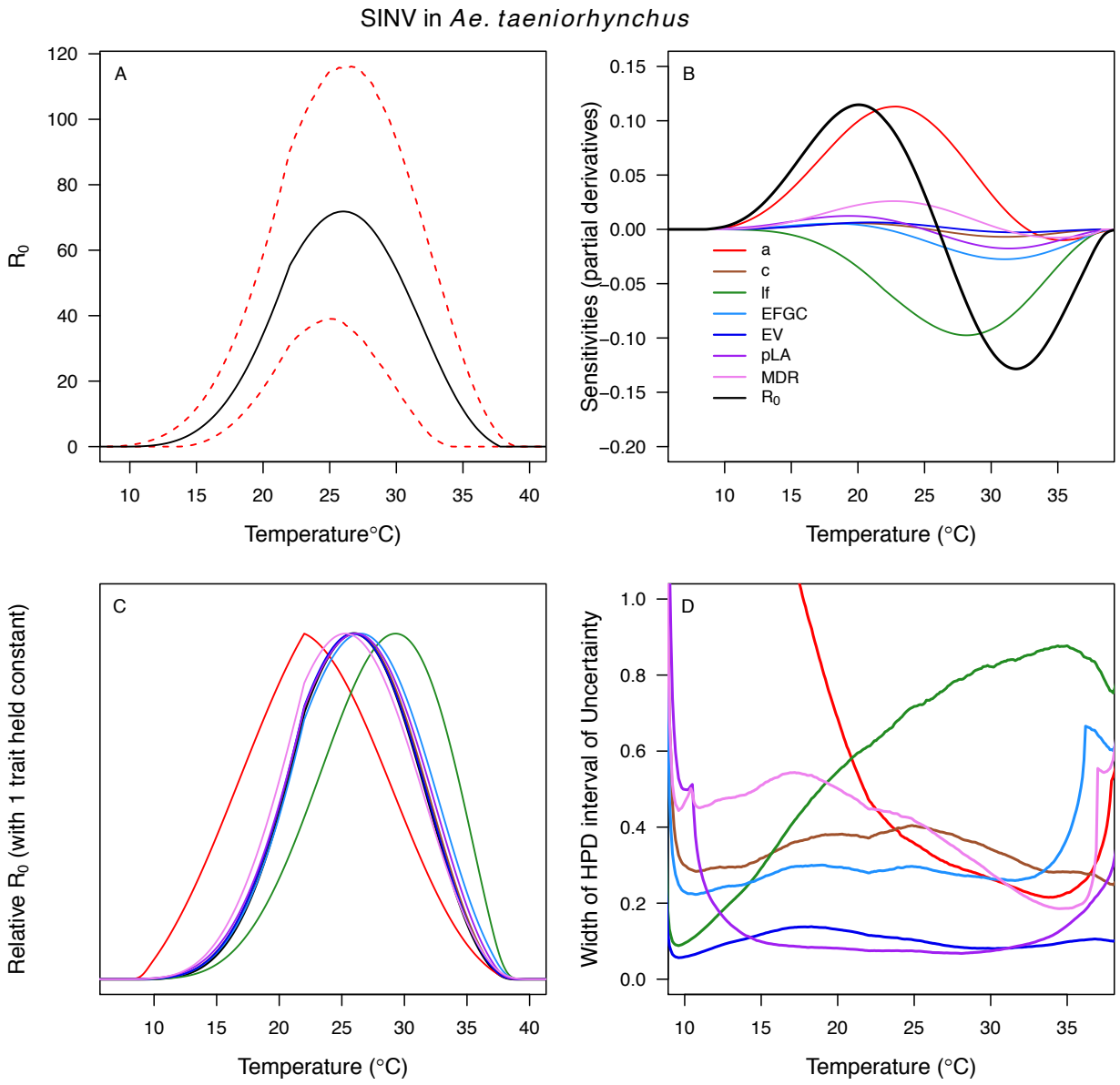

Figure S20: Temperature-dependent R_0, sensitivity analyses, and uncertainty analysis for model of Rift Valley Fever Virus in *Aedes taeniorhynchus*. (A) Median temperature-dependent R_0 (black line) with 95% credible intervals (dashed red lines). (B) Sensitivity analysis #1: derivative with respect to temperature for R_0 (black) and partial derivatives with respect to temperature for each trait. (C) Sensitivity analysis #2: relative R_0 calculated with single traits held constant. (D) Uncertainty analysis using highest posterior density (HPD) interval widths: the proportion of total uncertainty due to each trait. (B-D) Trait colors: biting rate (*a*, red), vector competence (*bc*, orange), adult lifespan (*lf*, green), parasite development rate (*PDR*, cyan), fecundity (*EFGC*, light blue), egg viability (*EV*, dark blue), larval survival (*pLA*, purple), and mosquito development rate (*MDR*, pink). Fecundity (*EFGC*) and biting rate (*a*) from *Culex pipiens*; egg viability (EV) from *Cx. theileri*; larval traits (*pLA* and *MDR*) from *Ae. vexans*; all other traits from *Ae. taeniorhynchus*.

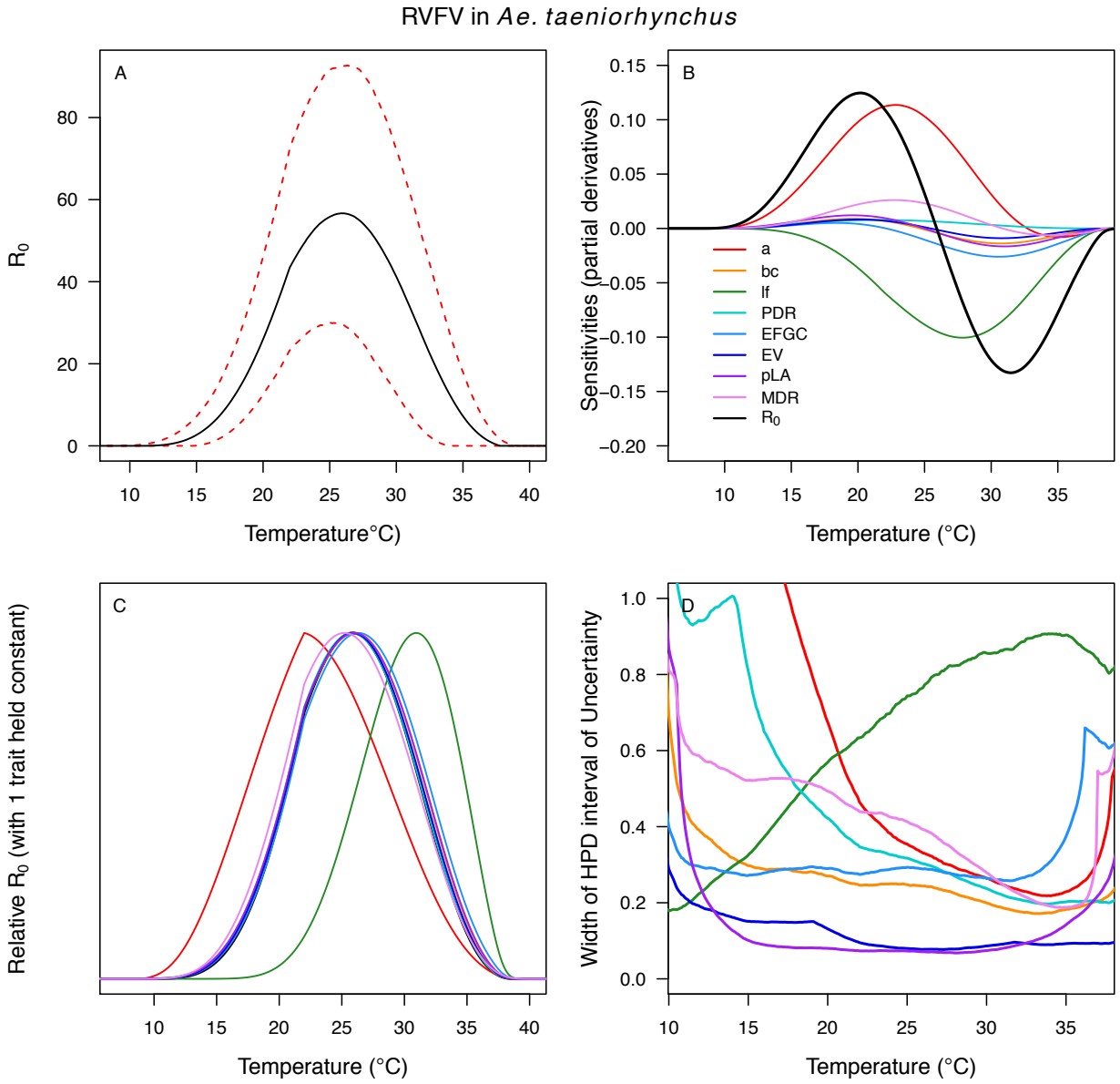

Figure S21: Histograms of T_{min}, optimum, and T_{max} for transmission (R_0) models. T_{min} (left column), optimum (center column), and T_{max} (right column). Top row (A-C): West Nile virus (WNV) in four vectors: *Culex pipiens* (grey), *Cx. quinquefasciatus* (red), *Cx. tarsalis* (blue), and *Cx. univitattus* (orange). Middle row (D-F): three viruses in *Cx. tarsalis*: WNV (same as in top row, bright blue), Western Equine Encephalitis virus (WEEV, light blue), and St. Louis Encephalitis virus (SLEV, dark blue). Bottom row (H-J): Sindbis virus (SINV) in *Aedes taeniorhynchus* (grey), SINV in *Cx. pipiens* (dark green), Rift Valley Fever virus (RVFV) in *Ae. taeniorhynchus* (light green), and Eastern Equine Encephalitis virus (EEEV) in *Ae. triseriatus* (purple).

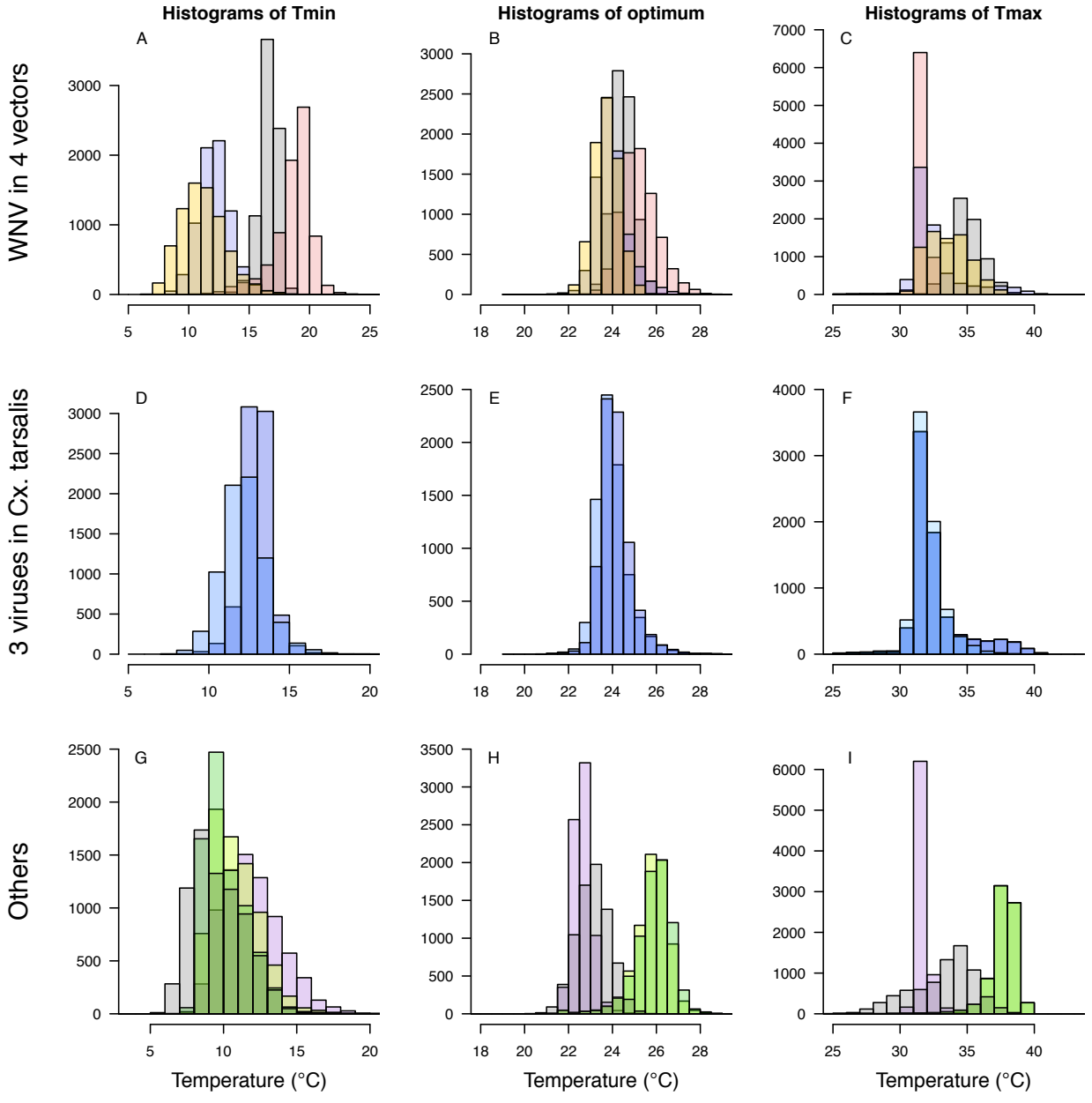

Figure S22: Comparing alternative model parameterizations. Several models had multiple potentially valid choices for traits; we show these alternative models here (dashed lines; base models from main text in solid lines) to show that they make very little difference, except in D. (A) Models for EEEV in *Ae. triseriatus* with larval traits (larval-to-adult survival [*pLA*] and mosquito development rate [*MDR*]) from *Ae. triseriatus* (violet, from the main text) and larval traits from *Cs. melanura* (black). We also show larval traits from *Cs. melanura* without proportion ovipositing (*pO*) in the model (grey), since the thermal responses for *EFCG* (eggs per female per gonotrophic cycle, in *Cx. pipiens*) and *ER* (eggs per raft, in *Cx. quinquefasciatus*) were nearly identical even though the units were different, probably because the ER data were not very informative and the priors strongly shaped the thermal response. (B) Models for WNV in *Cx. quinquefasciatus*, with (light red, from the main text) and without (dark red) the thermal response for fecundity (as eggs per raft, *ER*), for the same reason as in A. (C) Models for WEEV in *Cx. tarsalis* with vector competence estimated by infection efficiency (*c*, Fig 6D) and transmission efficiency (*b*, Fig 6E) measured separately (blue, from the main text) or by vector competence measured as a single trait (*bc*, Fig 6F; light blue). (D) Models for RVFV in *Ae. taeniorhynchus* with lifespan from *Ae. taeniorhynchus* (light green, from the main text) or from *Cx. pipiens* (dark green). We chose the *Ae. taeniorhynchus* version for the main text because it is the same species the infection traits (*PDR*, *bc*) were measured in, and that choice strongly impacted the results.

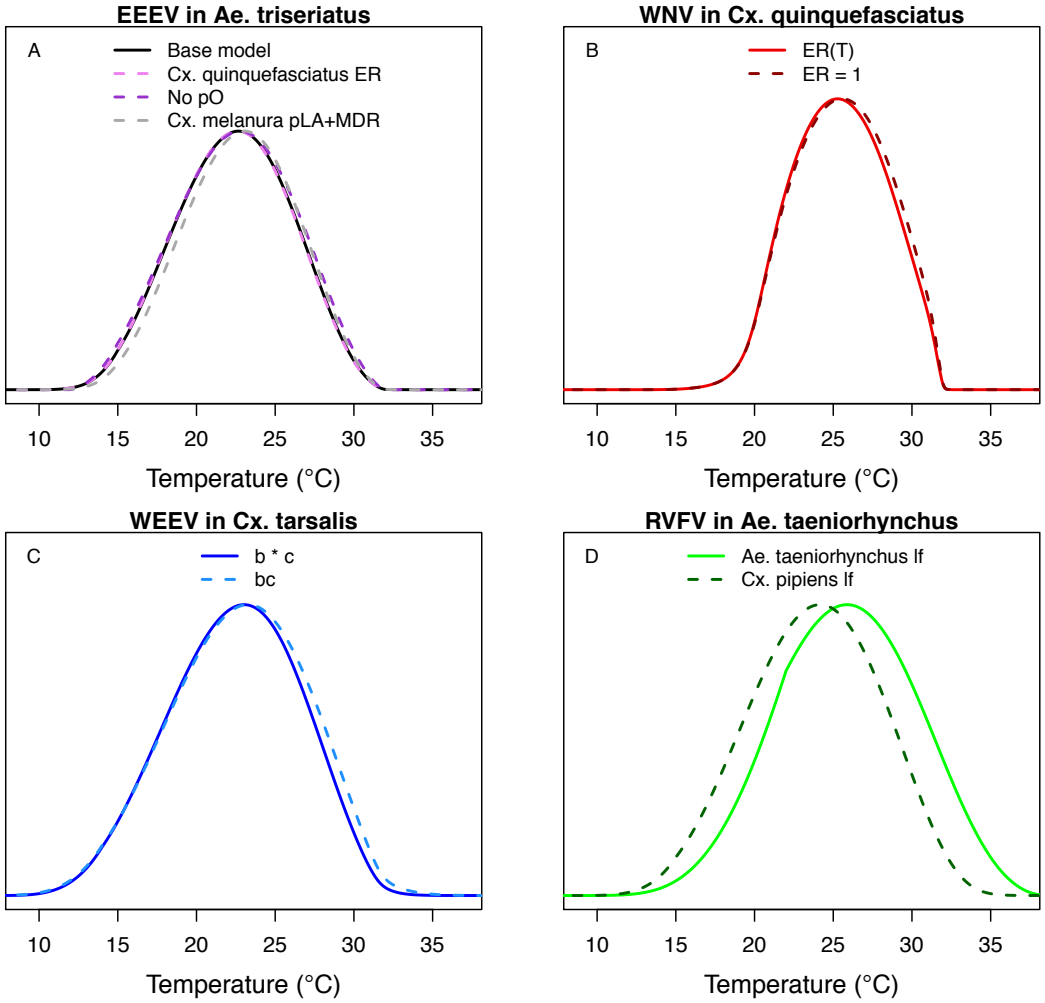

Figure S23: Comparison with previous R_0 models for transmission of West Nile virus. Models taken from this paper (solid lines: *Cx. pipiens* [grey], *Cx. quinquefasciatus* [red], *Cx. tarsalis* [blue], and *Cx. univittatus* [orange]), from Paull et al. 2017 [50] (dashed lines: *Cx. pipiens* [grey], *Cx. quinquefasciatus* [red], and *Cx. tarsalis* [blue]), from Vogels et al. 2017 [54] (*Cx. pipiens* [grey] and *Cx. pipiens molestus* [black]), and from Kushmaro et al. 2015 [55] (not species specific, dot-dashed line [brown]).

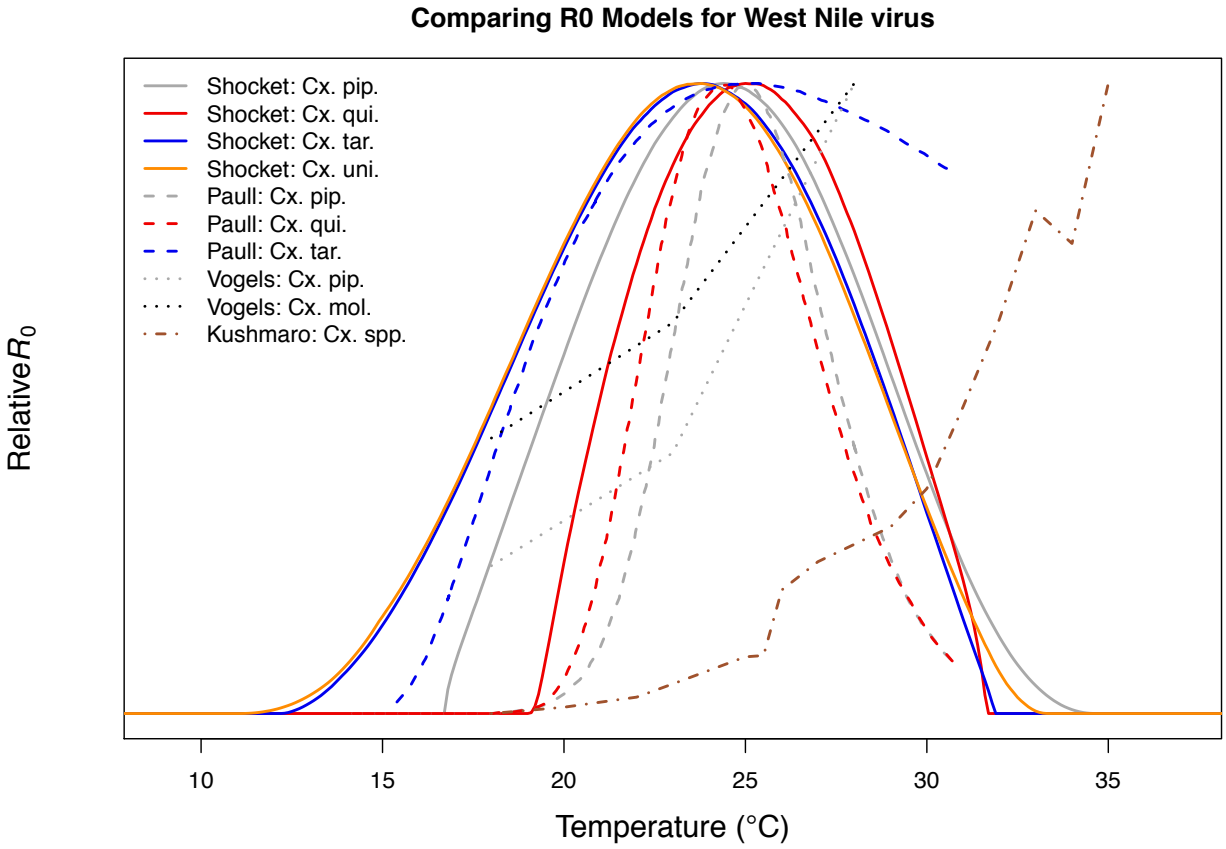

Figure S24: GAM models of mean WNV incidence as a function of average summer temperature. (A-F) Models are fit with differing numbers of knots (4–9). In all models, incidence peaks around 24°C (T_{opt} = 23.5–24.2°C).

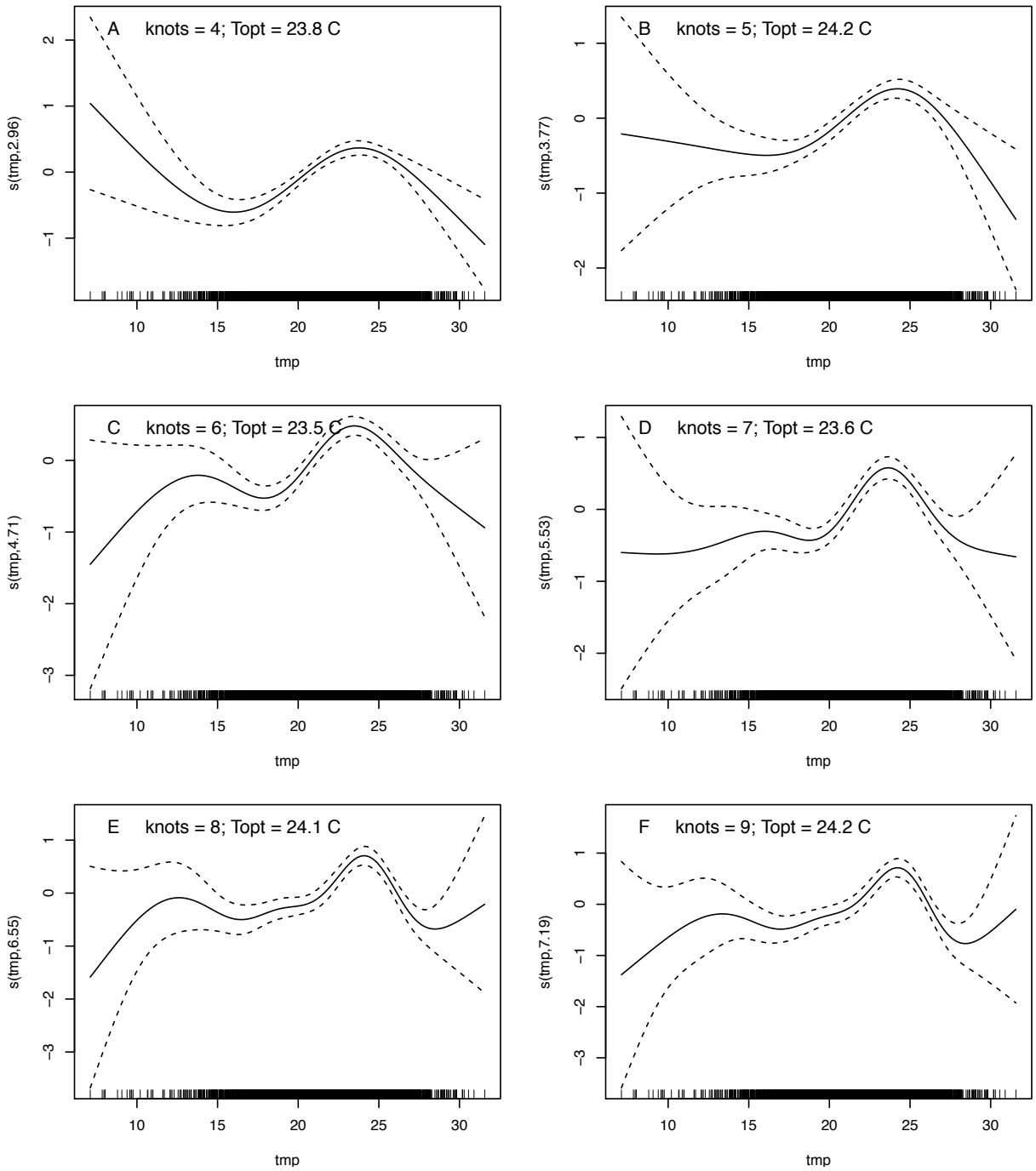

Table S10: GAM models of mean WNV incidence as a function of average summer temperature. Statistics for models fit with differing numbers of knots: edf (estimated degrees of freedom), Ref-df, *F*, and *p*-value refer to the smoothed temperature term (see Fig S24 for plots). Dev. exp. = percent deviance explained. T_{opt} = temperature of peak incidence.

Panel in Fig S24	**# knots**	**edf**	**Ref-df**	***F***	***p*-value**	**Adj. R^2**	**Dev. exp. (%)**	T_{opt}
A	k = 4	2.96	2.99	15.87	$4.03 \cdot 10^{-10}$	0.018	2.33	23.8°C
B	k = 5	3.77	3.97	11.11	$4.64 \cdot 10^{-9}$	0.019	2.44	24.2°C
C	k = 6	4.71	4.96	11.97	$4.77 \cdot 10^{-11}$	0.022	2.85	23.5°C
D	k = 7	5.53	5.92	11.01	$1.31 \cdot 10^{-11}$	0.024	3.11	23.6°C
E	k = 8	6.55	6.93	11.12	$2.73 \cdot 10^{-13}$	0.026	3.62	24.1°C
F	k = 9	7.19	7.80	10.06	$3.17 \cdot 10^{-13}$	0.026	3.67	24.2°C

Figure S25: LOESS models of mean WNV incidence as a function of average summer temperature. Points are means for bins of 42 counties (+/- SE). Lines are locally estimated scatterplot smoothing (LOESS) regression models with different smoothing (span) parameters: 0.1 (red), 0.25 (orange), 0.5 (green), 0.6 (cyan), 0.75 (light blue), 1 (dark blue), and 2 (violet). Models were fit to raw county-level data (n = 3,109, binned for visual clarity). The best model (span = 0.6, which appropriately balances overfitting and underfitting the data) estimates that incidence peaks at 23.9°C.

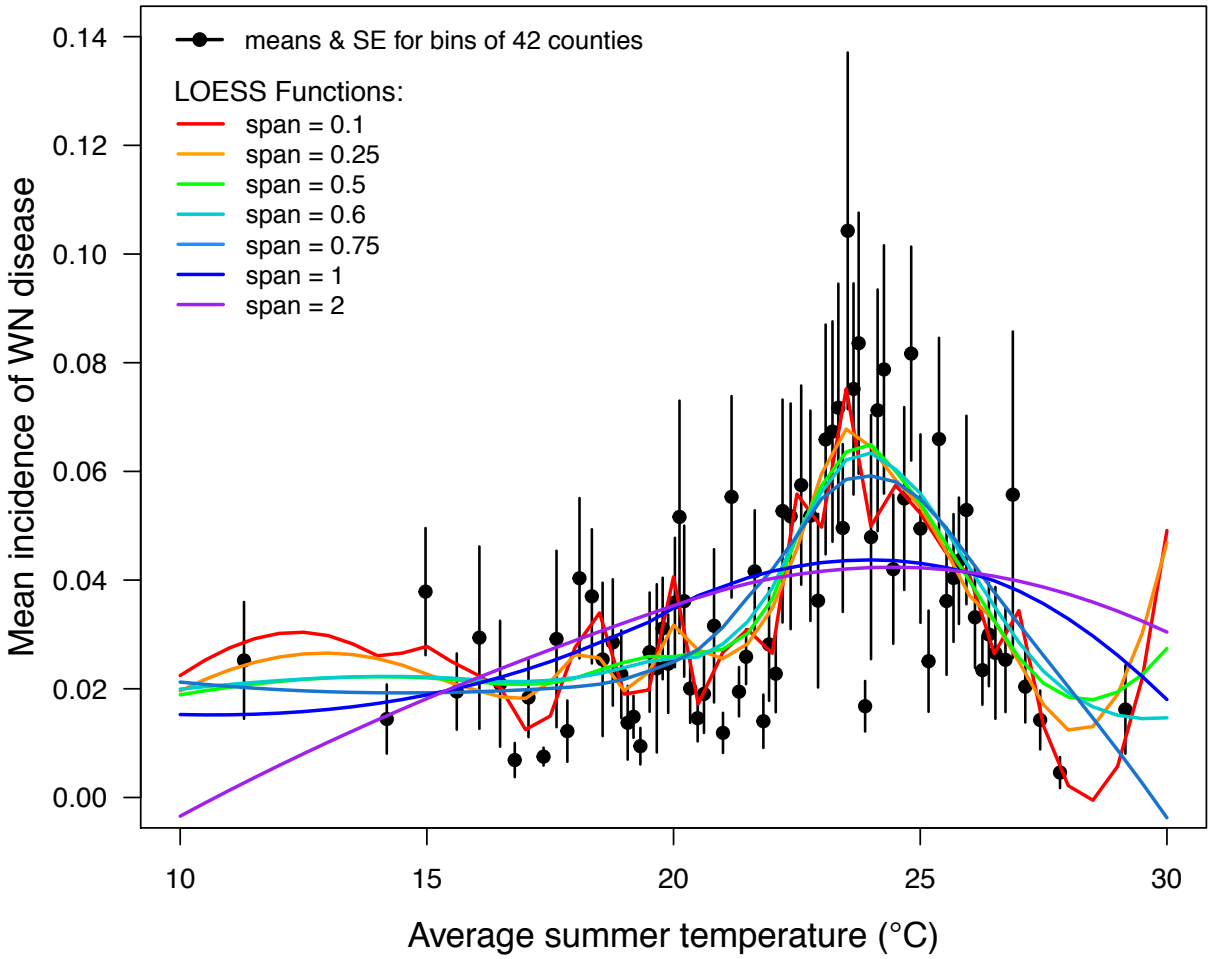

Figure S26: Raw county-level data for mean WNV incidence (2000-2016) as a function of average summer temperature (n = 3,109).

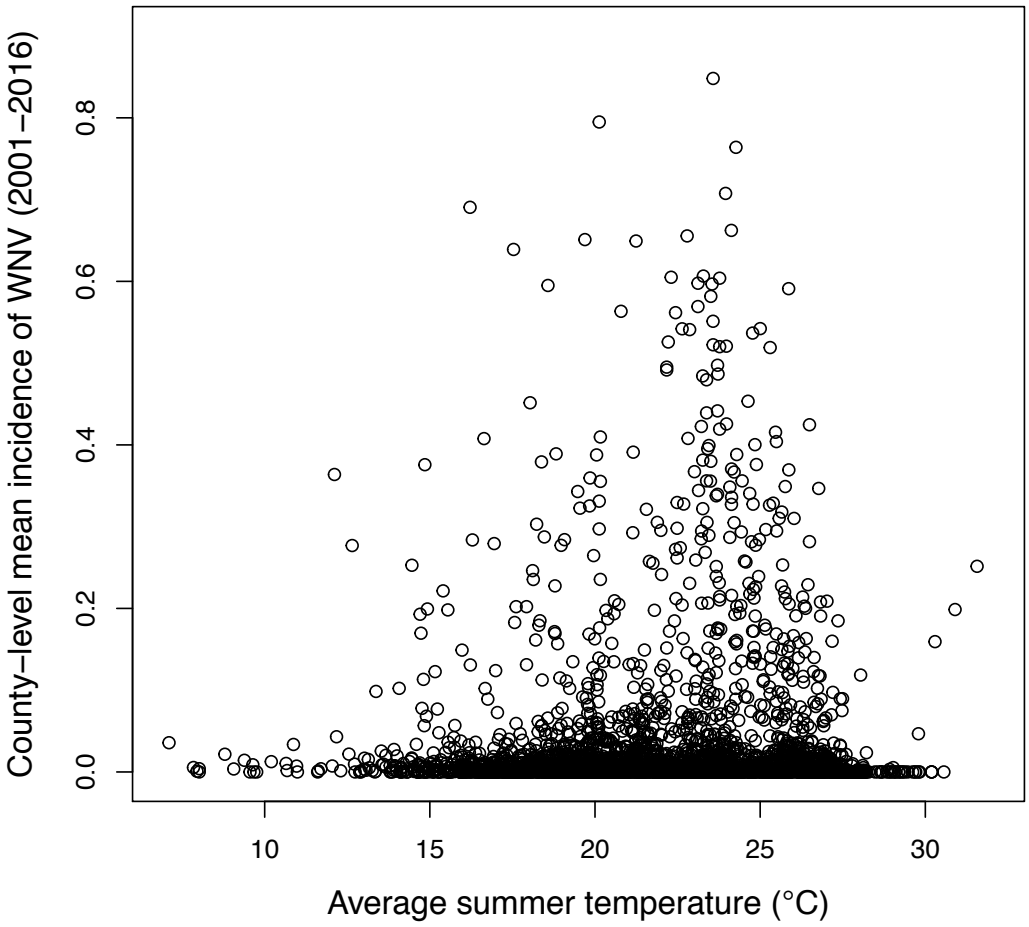

References

1. Parham PE, Michael E. Modeling the effects of weather and climate change on malaria transmission. Environmental Health Perspectives. 2010;118: 620–626. doi:10.1289/ehp.0901256

2. Mordecai EA, Paaijmans KP, Johnson LR, Balzer C, Ben-Horin T, de Moor E, et al. Optimal temperature for malaria transmission is dramatically lower than previously predicted. Ecology letters. 2013;16: 22–30. doi:10.1111/ele.12015

3. Johnson LR, Ben-Horin T, Lafferty KD, McNally A, Mordecai E, Paaijmans KP, et al. Understanding uncertainty in temperature effects on vector-borne disease: A Bayesian approach. Ecology. 2015;96: 203–213. doi:10.1890/13-1964.1

4. Mordecai EA, Cohen JM, Evans MV, Gudapati P, Johnson LR, Lippi CA, et al. Detecting the impact of temperature on transmission of Zika, dengue, and chikungunya using mechanistic models. PLOS Neglected Tropical Diseases. 2017;11: e0005568. doi:10.1371/journal.pntd.0005568

5. Shocket MS, Ryan SJ, Mordecai EA. Temperature explains broad patterns of Ross River virus transmission. eLife. 2018;7. doi:10.7554/eLife.37762

6. Tesla B, Demakovsky LR, Mordecai EA, Ryan SJ, Bonds MH, Ngonghala CN, et al. Temperature drives Zika virus transmission: evidence from empirical and mathematical models. Proceedings of the Royal Society B: Biological Sciences. 2018;285: 20180795. doi:10.1098/rspb.2018.0795

7. Mahmood F, Crans WJ. Effect of temperature on the development of Culiseta melanura (Diptera: Culicidae) and its impact on the amplification of eastern equine encephalomyelitis virus in birds. J Med Entomol. 1998;35: 1007–1012.

8. Weaver SC, Barrett ADT. Transmission cycles, host range, evolution and emergence of arboviral disease. Nature Reviews Microbiology. 2004;2: 789–801. doi:10.1038/nrmicro1006

9. Tekle A. The Physiology of Hibernation and Its Role in the Geographical Distribution of Populations of the *Culex Pipiens* Complex. The American Journal of Tropical Medicine and Hygiene. 1960;9: 321–330. doi:10.4269/ajtmh.1960.9.321

10. Madder DJ, Surgeoner GA, Helson BV. Number of generations, egg production, and developmental time of Culex pipiens and Culex restauns (Diptera: Culicidae) in southern Ontario. J Med Entomol. 1983;20: 275–287.

11. Ruybal JE, Kramer LD, Kilpatrick AM. Geographic variation in the response of *Culex pipiens* life history traits to temperature. Parasites & Vectors. 2016;9. doi:10.1186/s13071-016-1402-z

12. Li J, Zhu G, Zhou H, Tang J, Cao J. Effect of temperature on the development of *Culex pipiens pallens*. Chin J Vector Biol & Control. 2017;28: 35–37.

13. Reisen WK, Milby MM, Presser SB, Hardy JL. Ecology of Mosquitoes and St. Louis Encephalitis Virus in the Los Angeles Basin of California, 1987–1990. Journal of Medical Entomology. 1992;29: 582–598. doi:10.1093/jmedent/29.4.582

14. Mahmood F, Crans WJ. A thermal heat summation model to predict the duration of the gonotrophic cycle of Culiseta melanura in nature. J Am Mosq Control Assoc. 1997;13: 92–94.

15. Oda T, Mori A, Ueda M, Kurokawa K, others. Effects of temperatures on the oviposition and hatching of eggs in *Culex pipiens molestus* and *Culex pipiens quinquefasciatus*. Tropical Medicine. 1980;22: 167–180.

16. Mogi M. Temperature and Photoperiod Effects on Larval and Ovarian Development of New Zealand Strains of *Culex quinquefasciatus* (Diptera: Culicidae). Annals of the Entomological Society of America. 1992;85: 58–66. doi:10.1093/aesa/85.1.58

17. Ciota AT, Matacchiero AC, Kilpatrick AM, Kramer LD. The Effect of Temperature on Life History Traits of *Culex* Mosquitoes. Journal of Medical Entomology. 2014;51: 55–62. doi:10.1603/ME13003

18. McHaffey DG. Photoperiod and temperature influences on diapause in eggs of the floodwater mosquito *Aedes vexans* (Meigen) (Diptera: Culicidae). J Med Entomol. 1972;9: 564–571.

19. Rayah EAE, Groun NAA. Effect of temperature on hatching eggs and embryonic survival in the mosquito Culex quinquefasciatus. Entomologia Experimentalis et Applicata. 1983;33: 349–351. doi:10.1111/j.1570-7458.1983.tb03281.x

20. Van der Linde TCD. Development rates and percentage hatching of Culex (Culex) theileri; Theobald (Diptera: Culicidae) eggs at various constant temperatures. Journal of the Entomological Society of Southern Africa,. 1990;53: 17–26.

21. Parker BM. Temperature and Salinity as Factors Influencing the Size and Reproductive Potentials of *Aedes dorsalis* (Diptera: Culicidae). Annals of the Entomological Society of America. 1982;75: 99–102. doi:10.1093/aesa/75.1.99

22. McHaffey DG, Harwood RF. Photoperiod and Temperature Influences on Diapause in Eggs of the Floodwater Mosquito, *Aedes Dorsalis* (Meigen) (Diptera: Culicidae)1. Journal of Medical Entomology. 1970;7: 631–644. doi:10.1093/jmedent/7.6.631

23. McHaffey DG. Photoperiod and temperature influences on diapause in eggs of the floodwater mosquito *Aedes nigromaculis* (Ludlow) (Diptera : Culicidae). Mosquito News. 1972;32: 51–61.

24. Shelton RM. The effect of temperatures on development of eight mosquito species. Mosquito News. 1973;33: 1–12.

25. Brust RA. WEIGHT AND DEVELOPMENT TIME OF DIFFERENT STADIA OF MOSQUITOES REARED AT VARIOUS CONSTANT TEMPERATURES. The Canadian Entomologist. 1967;99: 986–993. doi:10.4039/Ent99986-9

26. Trpiš M, Shemanchuk JA. EFFECT OF CONSTANT TEMPERATURE ON THE LARVAL DEVELOPMENT OF *AEDES VEXANS* (DIPTERA: CULICIDAE). The Canadian Entomologist. 1970;102: 1048–1051. doi:10.4039/Ent1021048-8

27. Mpho M, Callaghan A, Holloway GJ. Temperature and genotypic effects on life history and fluctuating asymmetry in a field strain of *Culex pipiens*. Heredity. 2002;88: 307–312. doi:10.1038/sj.hdy.6800045

28. Mpho M, Callaghan A, Holloway GJ. Effects of temperature and genetic stress on life history and fluctuating wing asymmetry in *Culex pipiens* mosquitoes. European Journal of Entomology. 2002;99: 405–412. doi:10.14411/eje.2002.050

29. Loetti V, Schweigmann N, Burroni N. Development rates, larval survivorship and wing length of *Culex pipiens* (Diptera: Culicidae) at constant temperatures. Journal of Natural History. 2011;45: 2203–2213. doi:10.1080/00222933.2011.590946

30. Rueda LM, Patel KJ, Axtell RC, Stinner RE. Temperature-dependent development and survival rates of *Culex quinquefasciatus* and *Aedes aegypti* (Diptera: Culicidae). J Med Entomol. 1990;27: 892–898.

31. Mpho M, Holloway GJ, Callaghan A. A comparison of the effects of organophosphate insecticide exposure and temperature stress on fluctuating asymmetry and life history traits in *Culex quinquefasciatus*. Chemosphere. 2001;45: 713–720.

32. Reisen WK. Effect of temperature on *Culex tarsalis* (Diptera: Culicidae) from the Coachella and San Joaquin Valleys of California. J Med Entomol. 1995;32: 636–645.

33. Buth JL, Brust RA, Ellis RA. Development time, oviposition activity and onset of diapause in *Culex tarsalis*, *Culex restuans* and *Culiseta inornata* in southern Manitoba. J Am Mosq Control Assoc. 1990;6: 55–63.

34. Dodson BL, Kramer LD, Rasgon JL. Effects of larval rearing temperature on immature development and West Nile virus vector competence of *Culex tarsalis*. Parasites & Vectors. 2012;5: 199. doi:10.1186/1756-3305-5-199

35. Teng H-J, Apperson CS. Development and Survival of Immature *Aedes albopictus* and *Aedes triseriatus* (Diptera: Culicidae) in the Laboratory: Effects of Density, Food, and Competition on Response to Temperature. Journal of Medical Entomology. 2000;37: 40–52. doi:10.1603/0022-2585-37.1.40

36. Oda T, Uchida K, Mori A, Mine M, Eshita Y, Kurokawa K, et al. Effects of high temperature on the emergence and survival of adult *Culex pipiens molestus* and *Culex quinquefasciatus* in Japan. J Am Mosq Control Assoc. 1999;15: 153–156.

37. Kiarie-Makara MW, Ngumbi PM, Lee D-K. Effects of Temperature on the Growth and Development of *Culex pipiens* Complex Mosquitoes (Diptera: Culicidae). Journal of Pharmacy and Biological Sciences. 2015;10: 1–10.

38. Olejnícek J, Gelbic I. Differences in response to temperature and density between two strains of the mosquito, *Culex pipiens molestus* forskal. J Vector Ecol. 2000;25: 136–145.

39. Muturi EJ, Lampman R, Costanzo K, Alto BW. Effect of Temperature and Insecticide Stress on Life-History Traits of Culex restuans and Aedes albopictus (Diptera: Culicidae). Journal of Medical Entomology. 2011;48: 243–250. doi:10.1603/ME10017

40. Reisen WK, Meyer RP, Presser SB, Hardy JL. Effect of temperature on the transmission of western equine encephalomyelitis and St. Louis encephalitis viruses by *Culex tarsalis* (Diptera: Culicidae). J Med Entomol. 1993;30: 151–160.

41. Reisen WK, Fang Y, Martinez VM. Effects of Temperature on the Transmission of West Nile Virus by *Culex tarsalis* (Diptera: Culicidae). Journal of Medical Entomology. 2006;43: 309–317. doi:10.1603/0022-2585(2006)043[0309:EOTOTT]2.0.CO;2

42. Turell MJ, Lundström JO. Effect of environmental temperature on the vector competence of *Aedes aegypti* and *Ae. taeniorhynchus* for Ockelbo virus. Am J Trop Med Hyg. 1990;43: 543–550.

43. Lundström JO, Turell MJ, Niklasson B. Effect of environmental temperature on the vector competence of *Culex pipiens and Cx. torrentium* for Ockelbo virus. Am J Trop Med Hyg. 1990;43: 534–542.

44. Kilpatrick AM, Meola MA, Moudy RM, Kramer LD. Temperature, viral genetics, and the transmission of West Nile virus by *Culex pipiens* mosquitoes. PLoS Pathogens. 2008;4. doi:10.1371/journal.ppat.1000092

45. Dohm DJ, O'Guinn ML, Turell MJ. Effect of environmental temperature on the ability of *Culex pipiens* (Diptera: Culicidae) to transmit West Nile virus. Journal of Medical Entomology. 2002;39: 221–225. doi:10.1603/0022-2585-39.1.221

46. Kramer LD, Hardy JL, Presser SB. Effect of temperature of extrinsic incubation on the vector competence of *Culex tarsalis* for western equine encephalomyelitis virus. Am J Trop Med Hyg. 1983;32: 1130–1139.

47. Turell MJ, Rossi CA, Bailey CL. Effect of Extrinsic Incubation Temperature on the Ability of *Aedes Taeniorhynchus* and *Culex Pipiens* to Transmit Rift Valley Fever Virus. The American Journal of Tropical Medicine and Hygiene. 1985;34: 1211–1218. doi:10.4269/ajtmh.1985.34.1211

48. Chamberlain RW, Sudia WD. The effects of temperature upon the extrinsic incubation of eastern equine encephalitis in mosquitoes. Am J Hyg. 1955;62: 295–305.

49. Cornel AJ, Jupp PG, Blackburn NK. Environmental Temperature on the Vector Competence of *Culex univittatus* (Diptera: Culicidae) for West Nile Virus. Journal of Medical Entomology. 1993;30: 449–456. doi:10.1093/jmedent/30.2.449

50. Paull SH, Horton DE, Ashfaq M, Rastogi D, Kramer LD, Diffenbaugh NS, et al. Drought and immunity determine the intensity of West Nile virus epidemics and climate change impacts. Proceedings of the Royal Society B: Biological Sciences. 2017;284: 20162078. doi:10.1098/rspb.2016.2078

51. Nayar JK. Effects of constant and fluctuating temperatures on life span of *Aedes taeniorhynchus* adults. Journal of Insect Physiology. 1972;18: 1303–1313. doi:10.1016/0022-1910(72)90259-4

52. Andreadis SS, Dimotsiou OC, Savopoulou-Soultani M. Variation in adult longevity of *Culex pipiens f. pipiens*, vector of the West Nile Virus. Parasitology Research. 2014;113: 4315–4319. doi:10.1007/s00436-014-4152-x

53. Mordecai EA, Caldwell JM, Grossman MK, Lippi CA, Johnson LR, Neira M, et al. Thermal biology of mosquito-borne disease. Ecology Letters. 2019;22: 1690–1078. doi:https://doi.org/10.1111/ele.13335

54. Vogels CBF, Hartemink N, Koenraadt CJM. Modelling West Nile virus transmission risk in Europe: effect of temperature and mosquito biotypes on the basic reproduction number. Scientific Reports. 2017;7. doi:10.1038/s41598-017-05185-4

55. Kushmaro A, Friedlander TA, Levins R. Temperature Effects on the Basic Reproductive Number (R0) Of West Nile Virus, Based On Ecological Parameters: Endemic Vs. New Emergence Regions. Journal of Tropical Diseases. 2015;s1. doi:10.4172/2329-891X.1000S1-001